INFORMATION TO USERS

This manuscript has been reproduced from the microfilm master. UMI films the text directly from the original or copy submitted. Thus, some thesis and dissertation copies are in typewriter face, while others may be from any type of computer printer.

The quality of this reproduction is dependent upon the quality of the copy submitted. Broken or indistinct print, colored or poor quality illustrations and photographs, print bleedthrough, substandard margins, and improper alignment can adversely affect reproduction.

In the unlikely event that the author did not send UMI a complete manuscript and there are missing pages, these will be noted. Also, if unauthorized copyright material had to be removed, a note will indicate the deletion.

Oversize materials (e.g., maps, drawings, charts) are reproduced by sectioning the original, beginning at the upper left-hand corner and continuing from left to right in equal sections with small overlaps.

Photographs included in the original manuscript have been reproduced xerographically in this copy. Higher quality 6" x 9" black and white photographic prints are available for any photographs or illustrations appearing in this copy for an additional charge. Contact UMI directly to order.

Bell & Howell Information and Learning
300 North Zeeb Road, Ann Arbor, MI 48106-1346 USA
800-521-0600

Université d'Ottawa · University of Ottawa

NON-LINEAR FINITE ELEMENT ANALYSIS AND PARAMETRIC INVESTIGATION OF LOW-RISE REINFORCED CONCRETE SHEAR WALLS

by

Nasir Navidpour

A thesis
submitted under the supervision of

Dr. Simon F. Ng
and
Dr. Murat Saatcioglu

In partial fulfillment
of the requirements for the degree of
Master of Applied Science
in
Structural Engineering

Department of Civil Engineering
University of Ottawa
Ottawa, Canada
July 1999

Abstract

A parametric study was carried out on 18 reinforced concrete shear walls to investigate the significance of design parameters on seismic response. The parameters included boundary elements and their reinforcement characteristics, web reinforcement ratios, concrete strength, steel yield strength, and axial load. The investigation was conducted using finite element analyses. Computer program ADINA was used to perform nonlinear analysis of concrete shear walls under axial load and incrementally increasing lateral forces. Material nonlinearities, including those of concrete, were modeled using ADINA material models. Four-node isoparametric plane stress elements were used to model concrete. Steel elements were modeled using two-node nonlinear truss elements. The applicability of the program and the accuracy of finite element models were first validated. This was done by comparing the results of six different shear walls with those obtained experimentally. The walls included three specimens tested by Maier at the Swiss Federal Institute of Technology in Zurich, Switzerland and three shear walls tested by Lefas et al. at Imperial College of Science and Technology, London, England. The analytical and experimental results showed very good agreement.

The results of the parametric investigation indicate that the presence of boundary elements enhanced strength and deformability of shear walls significantly. Wall aspect ratio was also found to be an important parameter dictating the mode of behavior. The longitudinal reinforcement ratio in the boundary elements was found to be a good source of energy dissipation and had much greater influence on ultimate load capacity than the web reinforcement. When confinement of concrete was considered, both the ultimate load capacity and ductility of shear walls improved. The effects of increased axial compression and increased reinforcement yield level were to increase strength but reduce ductility.

To my parents

Acknowledgments

The author wishes to express his sincere gratitude to his supervisors Dr. Simon Ng and Dr. Murat Saatcioglu who provided guidance, advice and encouragement throughout this research project.

The Financial assistance provided by the University of Ottawa and the Natural Sciences and Engineering Research Council of Canada through the research grant of Dr. Simon Ng is gratefully acknowledged.

The author especially would like to thank his parents for their continuous encouragement and support.

Contents

List of tables

List of figures

Notations

$\|A\|$	Euclidean norm of vector A
A_g	The gross area of the section
DNORM	Reference translation defined in ADINA
DTOL	Displacement tolerance defined in ADINA
$\widetilde{E}_0$	Uniaxial initial tangent modulus
${}^{t}E$	Young's modulus
E_s	The modulus of elasticity of steel
$\widetilde{E}_s$	Uniaxial secant modulus
E_{sh}	The modulus of steel in strain-hardening portion
${}^{t}\widetilde{e}$	Uniaxial strain
$\widetilde{e}_c$	Uniaxial maximum compressive strain
$\widetilde{e}_u$	Uniaxial ultimate compressive strain
F	Incremental nodal point forces
${}^{t}F$	Vector of internally nodal force at time *t*

f	The elastic response function
f'c	Compressive strength of concrete
ITEMAX	Maximum number of iterations defined in ADINA
i,j,k	The principal directions for a multiaxial stress condition
K	Tangent stiffness matrix
${}^{t}R$	Vector of externally applied nodal point at time t
U	Vector of incremental nodal point displacement
ν	Poisson's ratio
ϕ	Strain energy density function
ε_D	Displacement convergence tolerance
ε_E	Energy convergence tolerance
ε_F	Force convergence tolerance
${}^{t}\sigma_{pi}$	Stress for the principal direction i
$\tilde{\sigma}_c$	Uniaxial maximum compressive stress
${}^{t}\tilde{\sigma}$	Uniaxial stress
$\tilde{\sigma}_u$	Uniaxial ultimate compressive stress
${}^{0}\sigma_y$	Initial yield stress
Ω	Complimentary energy density function
$\partial\varepsilon_s$	The incremental steel strain

Chapter 1

Introduction

1.1 General

Analysis of reinforced concrete shear walls designed to resist earthquake loads involves considerations of non-linear material and member behavior, and hence often requires a special treatment. One approach that has recently been employed in modeling reinforced concrete shear walls by many researchers is finite element technique. However, obtaining good correlation between experimental and numerical results by the finite element method requires advanced analytical methods and state-of-the-art constitutive models to represent realistic behavior of reinforced concrete members under monotonic or cyclic loading. In nonlinear finite element analysis of reinforced concrete members, post-elastic behavior of materials, load-displacement history, crack patterns, and failure modes all become important considerations.

Finite element method is a numerical procedure for solving continuum mechanics problems with acceptable accuracy. It has been widely used as a research tool during the last three decades. The application of finite element method to structural analysis involves discretization a member or a structure into one or more sets of structural components. Each set, which is referred to as an element group, has a specific geometric pattern. Subsequently, the whole member or structure is discretized into finite number of elements. Each of these finite elements has a specific shape and is connected to adjacent elements by nodal points. An element, either isoparametric or non-isoparametric, may be formed of side nodes or only corner nodes. Nodal forces are then applied on the nodal points as external forces. A set of simultaneous equations can be written for each element to establish a relationship between displacements and nodal forces. After solving the simultaneous equations for a member, displacement of each nodal point under known applied loads may be found. Substituting these displacements to another set of equations yields the stress distribution for each element. Generally, the objective of the analysis is to find the load-displacement relationship of the given member or structure. In other words, displacements may be found when force is known or the force may be found when displacements are prescribed.

The application of the finite element method to the analysis of reinforced concrete structures has become increasingly important. Though difficulties often arise in studying the failure behavior of tall buildings, off shore platforms, reactor vessels and nuclear containment structures, significant advances have been made recently in finite element techniques, especially in the area of material modeling. This is an important development since experimental studies of the behavior of reinforced concrete structures are invariably expensive and time consuming.

The rapid development of the past decade in computer technology has given researchers a great opportunity to apply the finite element method to analyze reinforced concrete structures, while enabling the treatment of nonlinearity in concrete. However, additional research and development effort is required to further enhance capabilities of finite element programs used for reinforced concrete members. Developing an analytical model

for reinforced concrete is a complex matter. Nonlinearity of stress-strain relationship of concrete and reinforcing steel, non-homogeneity of concrete as a composite material, interaction between reinforcing steel and surrounding concrete, post-cracking behavior of concrete, creep and shrinkage of concrete are all complexities that challenge researchers. Recently, a number of general-purpose finite element programs such as DIANA, COSMOS/M, ADINA, ABAQUS, ANSYS have widely been used for analysis, in major structural engineering research projects.

1.2 Literature review

Considerable research has been conducted to examine the behavior of reinforced concrete structures using the finite element method. However, only limited number of this research is relevant to nonlinear finite element analysis of low-rise shear walls. Moreover, most of the previous research was carried out under monotonic loading conditions.

The finite element method was applied to reinforced concrete structures by Ngo and Scordelis [30] in 1967. They conducted a linear elastic analysis on a simple reinforced concrete beam. The crack pattern of the beam was pre-defined and perfect bond was considered between concrete and steel by defining the springs of zero length, known as link elements having constant stiffness.

In 1968, Nilson [31] used the finite element method to perform nonlinear analysis of reinforced concrete. The parameters considered included nonlinear material properties, nonlinear bond-slip relationship between steel reinforcement and concrete, change of geometry due to progressive cracking, and the influence of reinforcement. The cracking of concrete was modeled by considering the separation of concrete element's nodes with nodal connectivity and continuous change in structural geometry.

Rashid [37] modeled material nonlinearity and cracking of concrete through an analytical model in 1968. The material property matrices (elasticity matrices) of individual elements were modified.

In 1970, Franklin [18] introduced his analytical model with concrete cracking within finite elements. In order to account for material nonlinearity and cracking of concrete, the force-control technique was employed with iterations for each load increment. Redistribution of unbalanced forces was also taken into account.

One of the earliest attempts to analyze a reinforced concrete shear wall using finite element method was made by Yuzugullu [48] in 1972. He performed an inelastic finite element analysis of the shear wall-frame system that was tested at the University of Tokyo under monotonic condition.

Mirza and Houde [27] in 1979 carried out an extensive study on bond stress-slip relationship. He tested 62 concentric tension specimens. A bond stress-slip relationship was derived from the experimental data. The parameters considered included concrete strength, load level, and the thickness of concrete cover. A constitutive relationship was derived based on experimental results to idealize the stiffness of spring elements connecting the steel reinforcement and concrete nodes in a finite element formulation of a reinforced concrete member.

In 1991, the Nuclear Power Engineering Corporation's (NUPEC) Tadotsu Engineering Laboratory [42] in Japan tested two identical large-scale reinforced concrete shear walls. These walls were formed of web, two flanges and relatively large and heavy top and bottom slabs. The shear walls were subjected to dynamic excitation up to failure using a high-performance shaking table. These shear walls were considered to be typical shear walls in a reactor building. In order to verify the seismic response analysis, the experimental results were made available to the participants of the Seismic Shear Wall International Standard Problem (SSWIP) workshop. As one of the workshop participants, Brookhaven National Laboratory (BNL) [17], under the supervision of the U.S. Nuclear

Regulatory Commission (USNRC), conducted finite element analyses using the experimental results to study the behavior of these shear walls under monotonic static, cyclic static, and dynamic static loading conditions. In this research the defined constitutive model for concrete was based on orthotropic plasticity theory and the rotating smeared crack model [45, 16]. The 2-D model was defined using triangular 3-node elements. All the rebars in flanges and web were modeled as smeared. No significant difference was observed in the predicted envelope of load-deformation relationship obtained from different types of analyses. The response and timing of sliding shear failure were computed accurately by nonlinear dynamic analysis, as verified by test results. Additional analyses were carried out separately by Vecchio [17] at the University of Toronto, and Filippou [17] at the University of California at Berkeley to investigate the behavior of these shear walls under monotonic static loading. Vecchio, in 1995, performed nonlinear finite element analyses using 3-D and 2-D models subjected to monotonic static loading. Two in-house software were used to conduct the analyses; SPARCS and TRIX for 3-D analyses and 2-D analyses, respectively. The constitutive model used for concrete in these analyses was orthotropic nonlinear elastic, based on the Modified Compression Field Theory [45]. As for the reinforcement, no slip for embedded rebar was assumed. Good correlation was achieved between the analyses and experimental results. Some important results of this investigation may be summarized as follows:

1) The ultimate load capacity from 2-D analysis was about 8% greater than that of 3-D analysis.
2) From 3-D analyses, it was concluded that the wall strength under static monotonic loading was about 12% greater than that of dynamic cyclic loading.
3) Tension softening had a minor effect on the response of shear walls.
4) The effective flange width of the walls tested, established by 2-D analysis, was somewhere between 67% and 100% of the flange width.
5) Response computed by 2-D analysis was stiffer than that computed by 3-D analysis.

Filippou [17], in 1995 conducted a push-over analysis at the University of California at Berkley, on the same shear walls tested by NUPEC's Tadotsu Engineering Laboratory in 1991, employing in-house finite element computer program MIRAG with 2-D models. The concrete model used was a hypo-elastic model, based on a stress-equivalent uniaxial strain relation generalized to account for triaxial stress condition. The out-of-plane normal stress was set to zero in order to simplify the model to biaxial plane stress conditions. In this study, smeared rebar modeling was employed for modeling the steel reinforcement with perfect bond assumption. The analytical results show good agreement with test results.

In 1996, Further research on the shear walls of NUPEC's Tadotsu Engineering Laboratory were carried out in a joint program by Shimizu Corporation and TNO Construction Research [19]. Dynamic nonlinear analysis was conducted using a general-purpose finite element computer program DIANA. The combined cracking-crushing model was used to stimulate the web and the flange material behavior [19.6]. The top slab was modeled with a linear-elastic material model. The bottom slab was not modeled since it was assumed that the bottom slab behaves very stiff and can be presented as fixed supports. The reinforcement in the web and the flange were defined using embedded reinforcement grids. The analytical results show a very good correlation with the test results of the NUPEC's Tadotsu Engineering Laboratory.

Sittipunt and Wood [41] in 1993 at University of Illinois at Urbana-Champain studied the cyclic behavior of slender reinforced concrete shear walls. They developed material models that represent cyclic behavior of concrete and reinforcing steel. In this research, finite element computer program FINITE was used to perform the analyses. Several shear walls that previously were tested by Portland Cement Association were analyzed by implementing these material models in FINITE computer program. Good correlation between analytical and experimental results verified the applicability of the material models. Thereafter, some parametric studies on different walls configuration, reinforcement details, and loading histories were conducted. They concluded that providing distributed diagonal shear reinforcement in the lower part of the walls could

increase the energy dissipation capacity of the wall more effectively than providing additional vertical and horizontal reinforcement in the web.

Two shear walls under monotonic loading condition tested at the University of California at Berkley were modeled by Khatri and Anderson [20] in 1995. In this research, nonlinear concrete material model in ADINA computer program was employed to perform the nonlinear finite element analysis. It was concluded that shear wall response to monotonic loading could be separated as pre-yield and post-yield of reinforcing steel. Consideration of the boundary elements with confined concrete properties and selecting the proper convergence criteria were some of the important results of this investigation.

The University of California at Berkeley has been conducting active research in applying state-of-the-art finite element techniques on reinforced concrete. A number of in-house computer programs such as NON-SAP, STRESS, MIRAGE, etc. have been developed to investigate the nonlinear behavior of reinforced concrete members under static and dynamic loading conditions. Filippou has carried out an extensive investigation on the application of nonlinear finite element method in reinforced concrete structures, and bond-slip implementation into the finite element procedure [29, 22].

1.3 Objectives and scope

The objective of the research program is to study inelastic response of low-rise shear walls analytically to establish significance of design parameters. The scope consists of two tasks. The first task involves the verification of the applicability of finite element techniques to nonlinear analysis of low-rise shear walls under monotonically increasing loading. This task also involves the verification of the constitutive models for concrete and steel used in finite element analysis. The second task consists of a parametric study to observe the sensitivity of selected design parameters on strength and ductility of low-rise shear walls.

The following are the parameters investigated:

- Vertical reinforcement ratio.
- Horizontal reinforcement ratio.
- Compressive strength of concrete.
- Effect of confined concrete in boundary elements.
- Wall aspect ratio.
- Yield strength of reinforcing steel.
- Axial force.

Chapter 2

Behavior of low-rise shear walls

2.1 General

Performance of reinforced concrete buildings during recent earthquakes has shown that properly designed shear walls are effective in resisting lateral loads in the plane of walls. Shear walls provide drift control, reducing structural and non-structural damage during earthquakes significantly.

Shear walls often have a rectangular, barbell, or flanged cross-section. They provide strength and ductility, while also ensuring overall stability and stiffness of the entire structure. The behavior of a shear wall is affected by many parameters, which play important roles on various modes of behavior and resulting failures. It is important to understand these modes of behavior and related mechanisms of failure before the significance of design parameters for earthquake resistant walls can be investigated. This

chapter describes fundamental features of shear wall response, as well as the role of design parameters from the point of view of earthquake resistance.

2.2 Strength, stiffness and ductility of shear walls

Primary factors affecting strength, stiffness and ductility of low-rise shear walls are discussed below. These factors include both material and geometric properties of walls.

2.2.1 Reinforcement

One of the parameters that has an important effect on strength and ductility of shear walls is web reinforcement. The web reinforcement is often expressed in terms of reinforcement ratios in horizontal and vertical directions. The ratio of area of reinforcing steel to gross cross-sectional area of concrete crossed by this reinforcement defines the reinforcement ratio.

The amount of reinforcement dictates the behavior of a wall as ductile or non-ductile. Web reinforcement is distributed in vertical and horizontal directions and often in two parallel layers. The current Canadian Standard (CSA A23.4 – 1994) requires the spacing of web reinforcement in both horizontal and vertical directions to be limited to 500 mm or 3 times of the thickness of the wall, whichever is smaller. The web reinforcement is distributed uniformly over wall height and width, to control shear cracking and improve ductility.

One of the most significant contributions of web reinforcement is to supply shear resistance. Horizontal reinforcement provides partial shear strength. Vertical reinforcement contributes to both flexural and shear resistances because vertical reinforcement stands against opening of horizontal as well as diagonal cracks.

Since most low-rise shear walls are susceptible to brittle shear failure, it is desirable to increase the shear capacity above shear force corresponding to flexural capacity. This

promotes ductile flexure dominant response. The vertical reinforcement also plays a major role on flexural behavior. The minimum reinforcement ratio for horizontal and vertical reinforcement are typically 0.2 % and 0.15 %, respectively.

In addition to horizontal and vertical reinforcement, diagonal reinforcement may be used sometimes, although rarely. The diagonal reinforcement is most effective in resisting shear, and also contributes to flexural strength. It also enhances resistance against sliding shear, when anchored properly into the framing element. All reinforcement expected to function in compression must be prevented against buckling by providing adequate ties with short tie spacing. The latter point becomes especially important for extreme compression reinforcement, as in the case of vertical boundary elements, and diagonal reinforcement forming part of a compression strut.

2.2.2 Aspect ratio of the wall

Structural walls with an aspect ratio (ratio of height-to-width) of less than two are usually referred to as low-rise walls. Aspect ratio of a shear wall is an important parameter that affects strength and ductility of the wall. The stress distribution and crack pattern of low-rise shear walls are different from those of high-rise shear walls. A low-rise shear wall behaves more like a deep beam while a high-rise shear wall behaves like a cantilever. The flexural capacity of a low-rise shear wall is often not attained because of diagonal tension or diagonal compression failure. Conversely, flexure may dominate the behavior in high-rise walls while the shear capacity is never attained.

2.2.3 Wall cross-section

Cross-sectional shape of a shear wall is another factor to be considered when discussing the strength and stiffness of the wall. Generally, there are three types of cross-sections for shear walls; rectangular, barbell, and flanged (Fig. 2.1).

Two flanges at the ends of a rectangular shear wall form flanged shear wall. This type of shear wall is widely used in nuclear power plants, as well as the elevator cores of high-rise buildings. When a flanged shear wall is subjected to in-plane lateral forces, the flanges behave like the flanges of a deep beam, and contribute to the stiffness of the shear wall system. This contribution is considerable for shear walls with aspect ratio of 1.0 and higher. Flexural component of deformations forms a significant fraction of total deflection in flanged walls. The stiffness contribution of flanges depends on the flange thickness and the aspect ratio of shear wall and flanged portion [47].

Rectangular walls in the past have been designed to have uniformly spaced web reinforcement only. This was an acceptable practice for even in earthquake resistant construction. However, current building codes require the walls to provide boundary elements. Boundary elements are formed by four or more longitudinal bars tied with adequate stirrups at the ends of a wall. Since shear walls under cyclic loading are subjected to high compressive stresses near the base, well-confined boundary elements limit the crushing of concrete and buckling of vertical reinforcement. As a result, boundary elements increase the ultimate load capacity and ductility of shear walls.

2.2.4 Type of loading

Shear walls that are subjected to earthquake loading experience dynamic load reversals in both horizontal and vertical directions. This type of loading is simulated in laboratory environment as slowly applied static lateral load reversals, monotonically increasing lateral loads, or dynamic loads provided by a shake table. The monotonic loading tests are often conducted because of its simplicity, and represent the envelope of hysteretic behavior under cyclic loading, providing basic information on force-displacement characteristics of walls (Fig. 2.2). However, for low-rise shear walls, a good correlation may not be achieved between the monotonic curve and the envelope of cyclic curves at later stages of loading, due to faster degradation of strength in the latter case. Under reversed cyclic loading, two sets of diagonal cracks criss-cross each other, reducing the compressive strength of concrete. It was found that the amount of degradation primarily

depends on the aspect ratio of wall. The ultimate load capacity under reversed cyclic loading is generally observed to be approximately 10% below that attained under monotonic loading [1, 8].

The effect of axial compression on walls is to increase strength but decrease deformability. However, these effects are often ignored since low-rise walls are subjected to small gravity loads.

2.2.5 Material Properties

Modulus of elasticity and modulus of shear are two parameters that affect the stiffness of shear walls in flexure and shear, respectively. The wall stiffness is usually considered to be proportional to the elastic modulus of concrete.

Compressive strength of concrete is another material property that has a direct effect on strength and ductility of shear walls. It is well recognized that concrete with higher compressive strength behaves in a more brittle manner though it shows higher strength. Fig. 2.3 shows typical stress-strain relationships for normal density concrete [32].

The source of ductility in reinforced concrete is based on the properties of concrete as well as reinforcing steel. After the formation of diagonal cracks, reinforcing steel plays a major role in dissipating energy. When a shear wall is subjected to lateral forces, inelastic deformations, including yielding of vertical reinforcement, especially at the base of the wall, dissipate energy. Thus, reinforcing steel plays an important role on strength and ductility of walls.

2.3 The mechanism of shear resistance

The mechanism of shear resistance in reinforced concrete walls is a complex phenomenon. Shear stress in low-rise shear walls is sustained through diagonal tension and compression. Diagonal tension capacity of concrete is much less than that under

direct shear. Therefore, the inclined cracks make their appearance first. After the formation of diagonal cracks, several mechanisms sustain shear stresses. A considerable fraction of shear forces is transferred to the bottom beam or foundation through diagonal compression struts. Diagonal compression struts are formed between the inclined tension cracks. The inclinations of these compression diagonal struts are governed by the aspect ratio of the wall. The diagonal struts, however, may be formed only if adequate diagonal tension is provided by web reinforcement.

The components of diagonal compression and tension must always be in equilibrium. This requirement of equilibrium is maintained by vertical and horizontal reinforcement forming a truss mechanism. The characteristics of this mechanism of shear resistance, however, depend on the aspect ratio of the wall, reinforcement ratio, and reinforcement configuration. In walls with rectangular cross-section, web reinforcement is often the only member that resists tensile stresses.

A small portion of shear stress is resisted by vertical reinforcement through dowel action. A more significant contribution comes from the mechanism of aggregate interlock, which is maintained through the control of web cracking by reinforcement. The relative movement of cracked surfaces is subjected to contacts of coarse aggregate. Roughness and irregularity of course aggregates limit further movement of the surfaces, activating the aggregate interlock. The amount of shear resisted by aggregate interlock is highly dependent on the aggregate size, web reinforcement, and presence of externally applied axial load.

2.4 Energy dissipation mechanism

Ductility is defined as the ratio of deformation at any specific stage of loading to the deformation at yield point (Fig. 2.4). Ductility is a useful quantitative index to describe the hysteretic energy dissipation capability of the wall.

It is well recognized that greater energy is dissipated if a wall experiences inelastic response. It is not cost effective if the shear wall is intended to resist seismic induced forces within the elastic range. The ultimate inelastic deformation may be defined as the limit deformation when the load capacity of the wall decreases to 80% of the maximum strength, permitting some strength decay within the inelastic range [24].

Since concrete is a brittle material, its inelastic deformation is not a good source for energy dissipation under reversed cyclic loading. Yielding of flexural reinforcement under reversed cyclic loading, especially at the base of the wall, is a major source of energy absorption for the shear wall system. If advanced failure is inhibited in reinforced concrete shear walls (such as diagonal compression or tension failure, and sliding shear failure), significant amount of energy can be dissipated. The amount of dissipated energy by shear wall is the area under the load-displacement curve. Fig. 2.5 depicts desired well-rounded load-displacement hysteresis loops under reversed cyclic loading. An unsuitable energy dissipation mechanism is shown in Fig. 2.6 when hysteresis loops are pinched due to shear distortions. In this case, significant degradation in stiffness is observed. Consequently, the diagonal crack would open more and more with progressive reversed cyclic loading. It is clear now that shear deformation of shear walls should be suppressed to enhance energy dissipation capability of the walls.

2.5 Failure modes

The ultimate load capacity of a wall under sever earthquake may be achieved if the foundation is well designed to provide adequate resistance against overturning. Eventually, low-rise shear walls fail in one of the following failure modes:

2.5.1 Diagonal tension failure

Shear walls develop principal tensile stresses with approximately 45° inclination when subjected to shear forces. Since the tensile strength of concrete is very low, it cracks at early stages of loading. After the formation of diagonal cracks, horizontal reinforcement,

which is usually known as shear reinforcement, resists opening of diagonal cracks. Diagonal tension failure occurs when the horizontal reinforcement is insufficient to sustain diagonal tension stress (Fig. 2.7). However, walls with top and bottom beams develop corner-to-corner diagonal crack because the lateral load is distributed along the rest of the wall through the top beam as shown in Fig. 2.8.

2.5.2 Diagonal compression failure

If the diagonal tension failure is controlled by sufficient shear reinforcement, shear wall sustains higher shear stresses. Consequently, an increase in average compressive stress is experienced in diagonal compression struts. If compressive stresses in diagonal struts exceed the compressive strength of concrete, crushing of concrete occurs. This mode of failure is referred to as diagonal compression failure.

Under reversed cyclic loading, opening and closing of diagonal cracks in two opposite directions reduces the compressive strength of concrete (Fig. 2.9). As a result, diagonal compression failure takes place sooner and drastic degradation of strength and stiffness is observed.

2.5.3 Sliding shear failure

Sliding shear failure may be triggered after the formation of a horizontal crack along the interface of wall and its foundation due to flexure. It usually occurs after a few cycles of inelastic deformations, producing a natural plane for sliding. Another underlining condition is to have adequate shear capacity to preclude premature diagonal tension or compression failures. This mode of failure is responsible for significant degradation of stiffness and pinching of hysteresis loops. Sliding shear is recognized by sliding displacement of the wall along the construction joint at the base, as depicted in Fig. 2.10. Walls with low aspect ratios are likely to develop considerable shear sliding. This failure mode can be limited by providing appropriate details in reinforcement crossing the construction joint. Sufficiently high axial load is another factor to limit sliding shear failure [34, 38, 46].

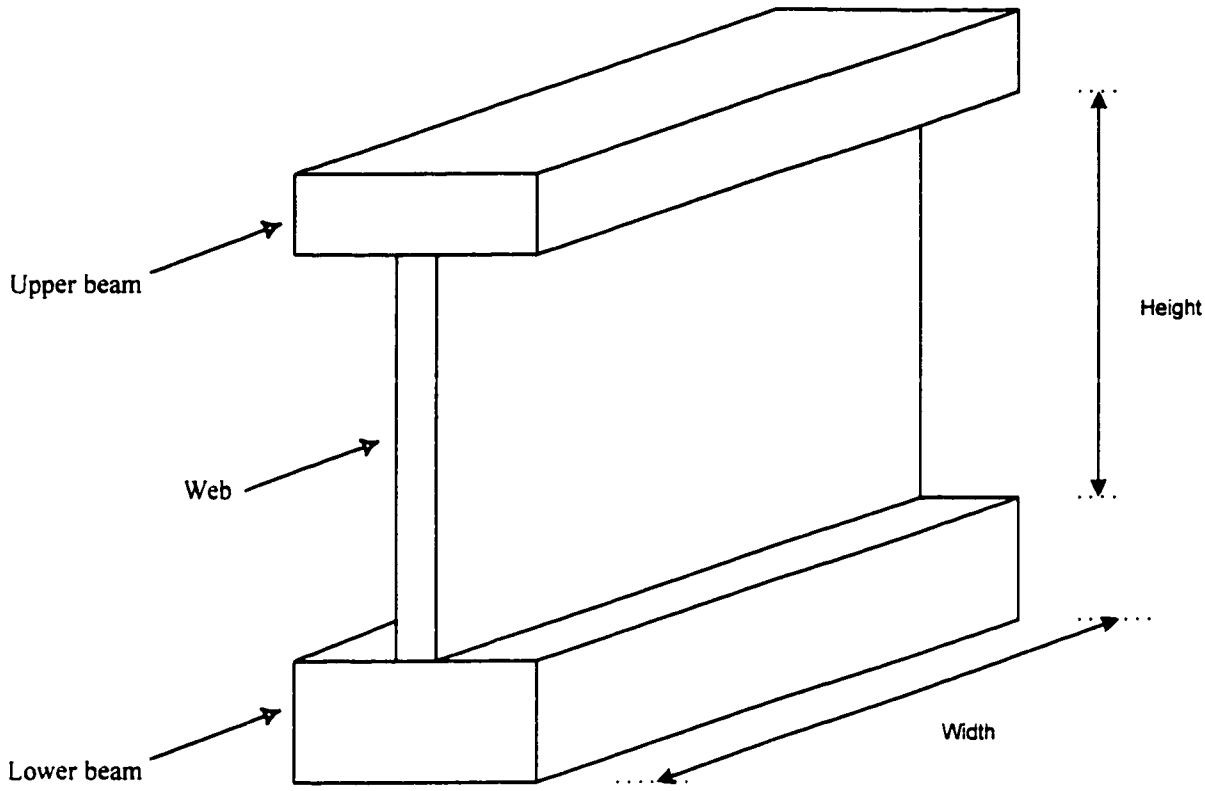

Typical shear wall

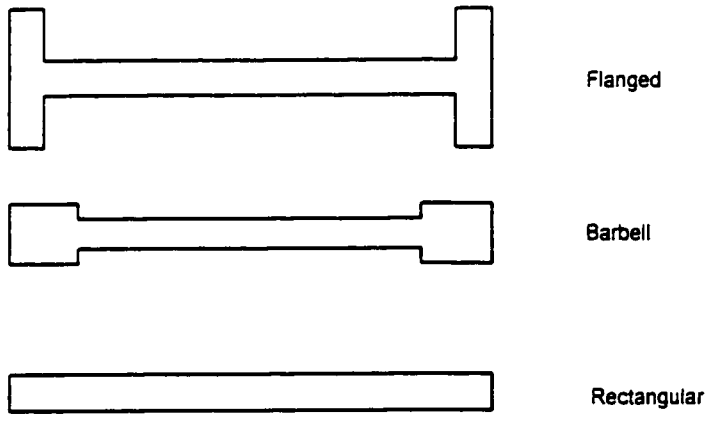

Fig. 2.1 Typical cross-sections of shear walls

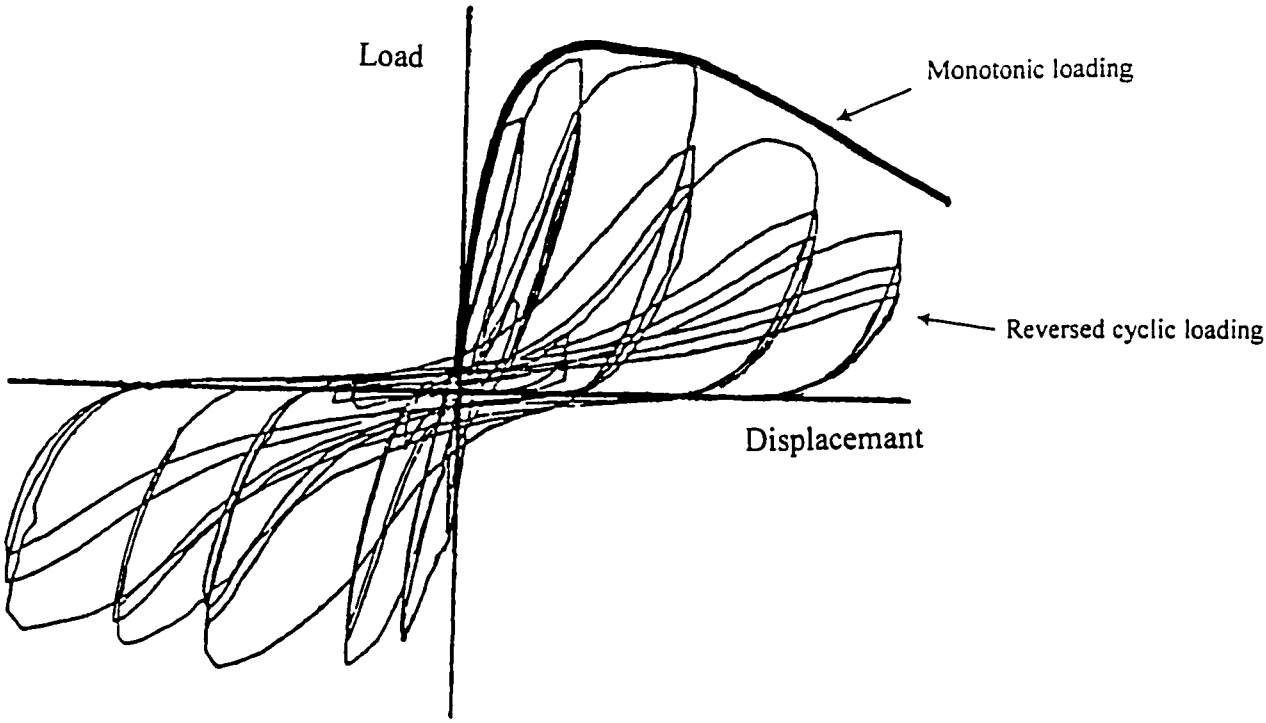

Fig. 2.2 Monotonic envelope for hysteresis loops in flexural dominent members

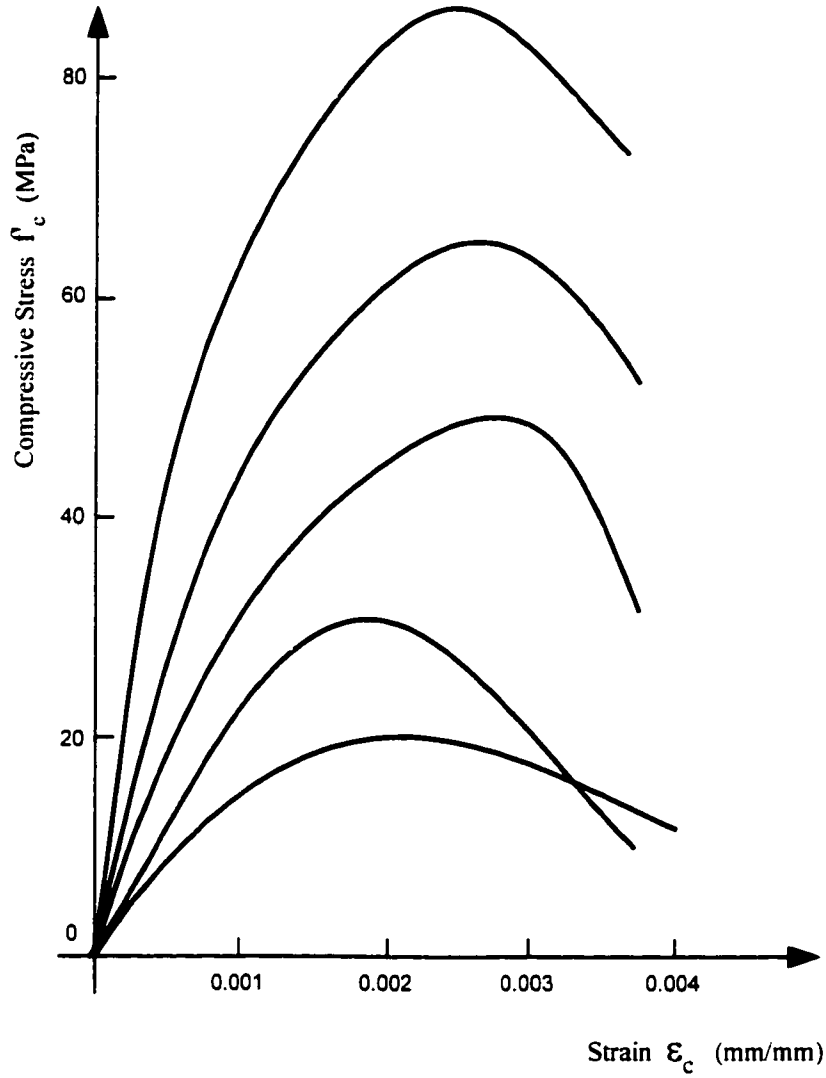

Fig. 2.3 Compressive stress-strain relationship of concrete

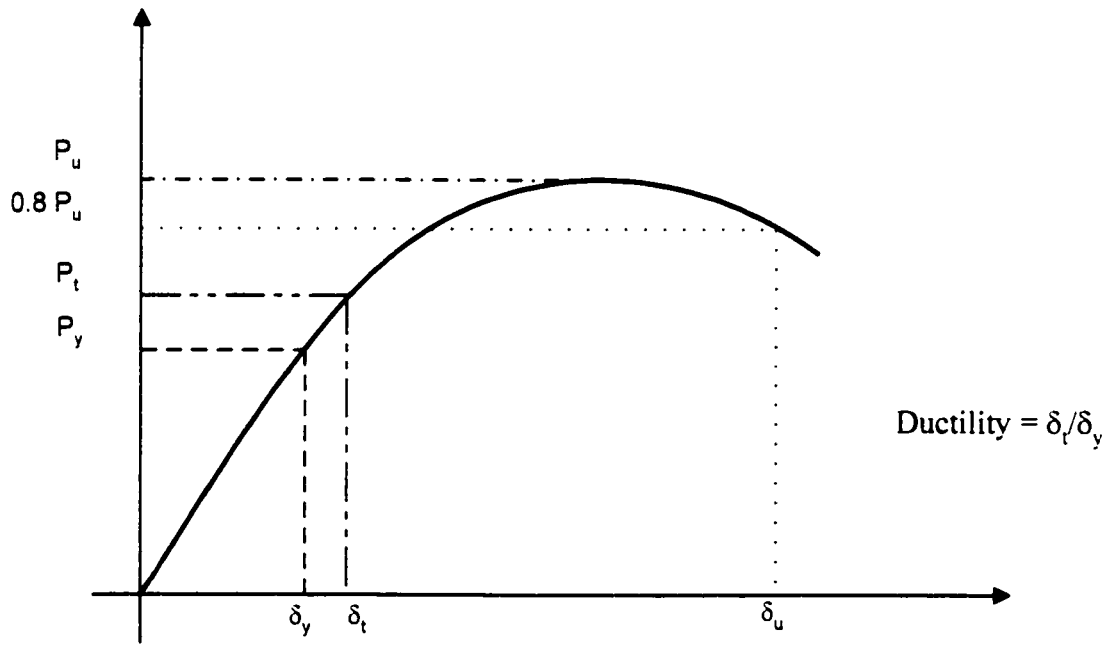

Fig. 2.4 Definition of ductility

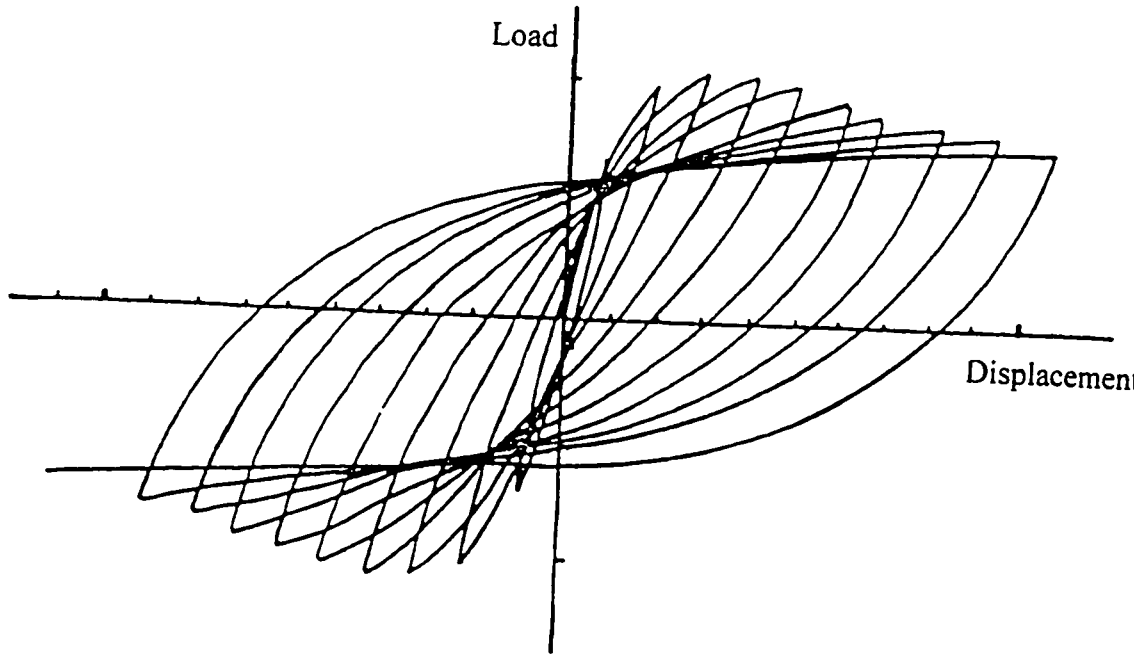

Fig. 2.5 Ductile load-displacement response to reversed cyclic loading

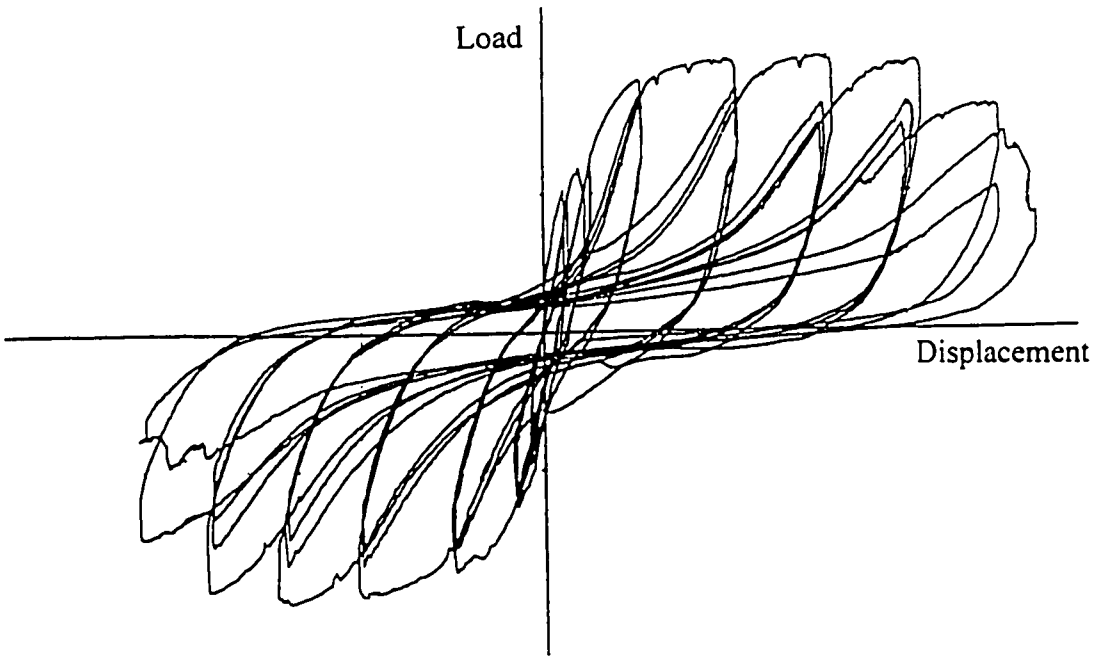

Fig. 2.6 Pinched hysteresis loops due to shear distortion

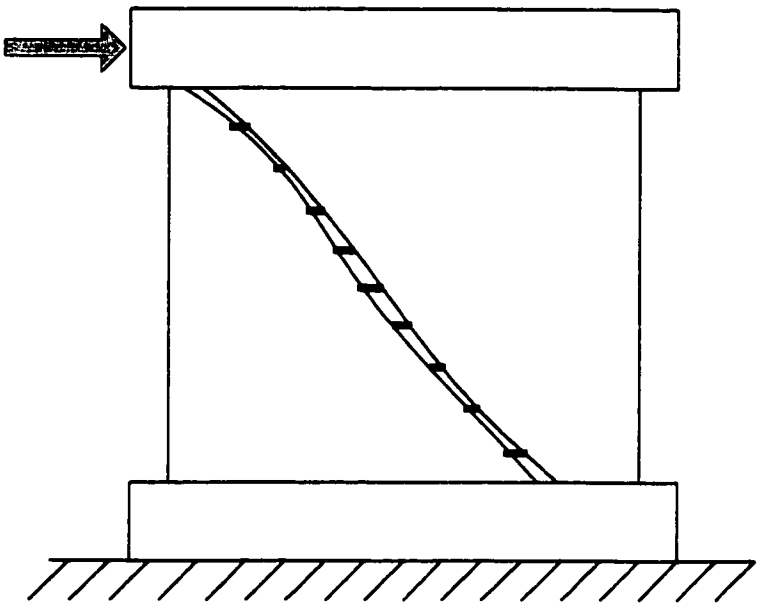

Fig. 2.7 45° diagonal tension failure

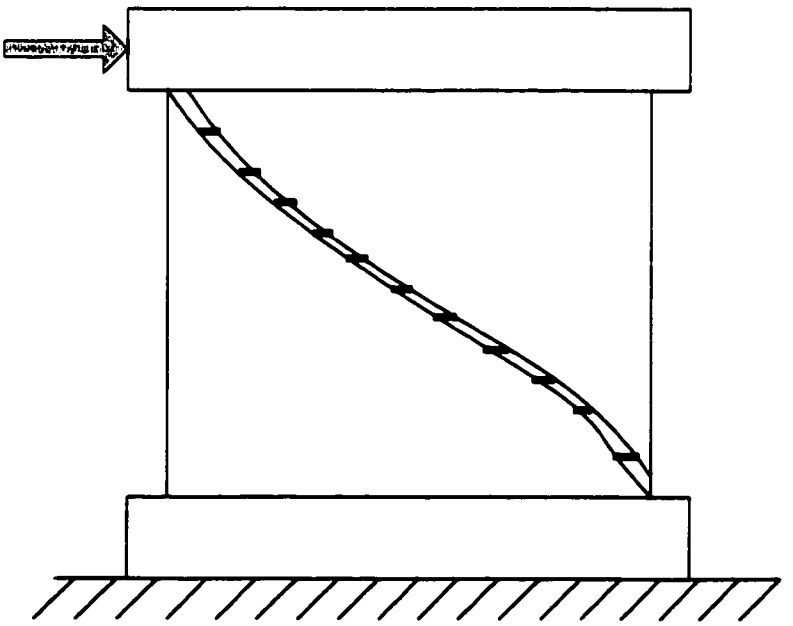

Fig. 2.8 Corner-to-corner diagonal tension failure

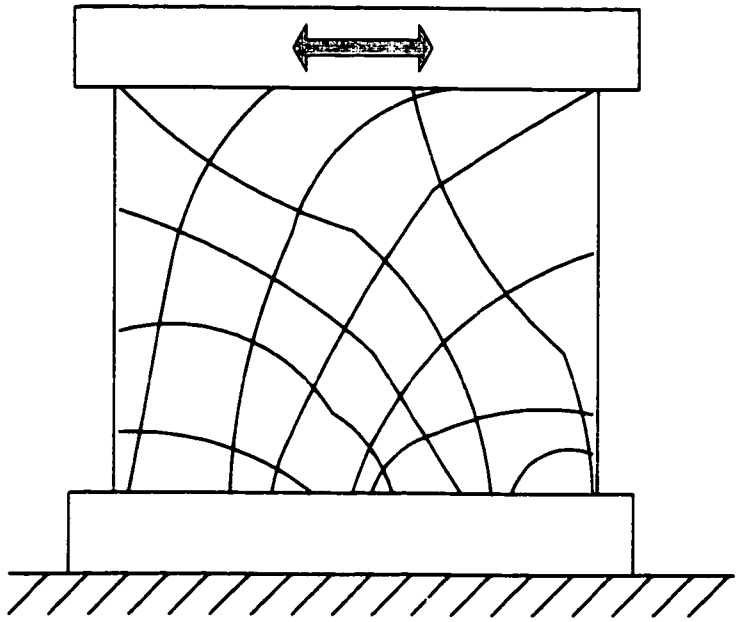

Fig. 2.9 Diagonal compression failure

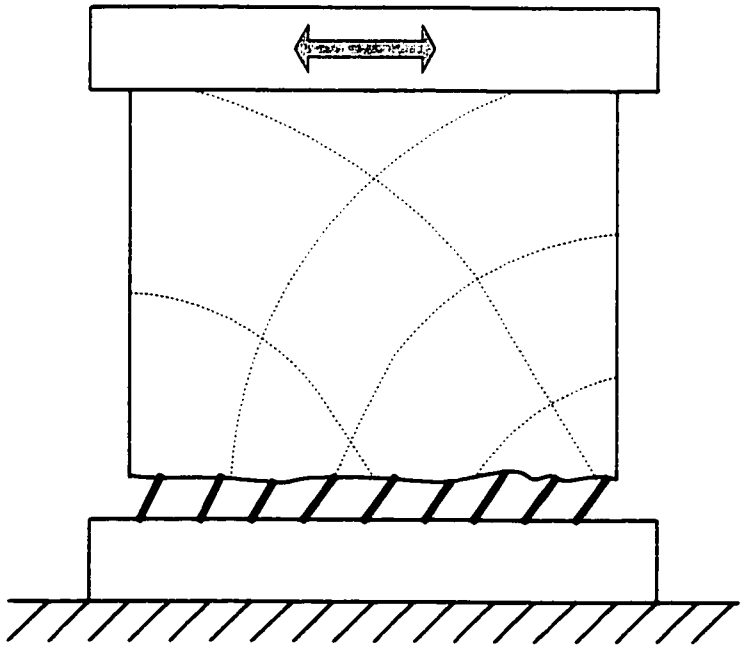

Fig. 2.10 Sliding shear failure

Chapter 3

Nonlinear finite element procedure

3.1 General

Structures and materials in routine daily application are often considered to behave within small-deflection linear elastic range. Nevertheless, almost every structure experiences nonlinear behavior especially during a severe earthquake. Shear walls as earthquake resistant members, would dissipate more energy if their response to lateral forces were relied upon nonlinear inelastic range.

Different behaviors are referred to as nonlinear. Stress-strain relationship may be nonlinear as time-dependent or time-independent. The magnitude or distribution of applied loads may change due to nonlinear deformations. Structural nonlinearity, however, can be categorized as material nonlinearity, geometric nonlinearity, and boundary nonlinearity. Nonlinearity can be slight or severe. The analysis result of a

slightly nonlinear problem is close enough to linear response that very often linear analysis is employed instead of nonlinear analysis. Nonlinear analysis is more difficult to treat and more expensive to perform. However, with the advent of personal computers and dramatic increase in computing capabilities, nonlinear analyses are now used frequently.

In general, the objective of nonlinear analysis is to find nonlinear load-displacement relationship. A good understanding of the problem and the analytical tools are essential to have the right choice of computer software and analytical models. Several types of analyses are usually needed in order to obtain acceptable results. Nonlinear analyses often are performed using different step length and convergence criteria to validate the results. A series of linear steps are taken to solve nonlinear equations. Many solution procedures have been proposed to overcome the nonlinearity problems.

This chapter is intended to cover basic concepts of structural analysis and to glance over different solution algorithms for nonlinear problems.

3.2 Structural nonlinearities

3.2.1 Material nonlinearity

One of the important sources of nonlinearity in structural analyses arises from the nonlinear relationship between stress and strain characteristics of materials. Reinforced concrete, in particular shows this type of nonlinearity of material both in concrete and reinforcing steel.

If stress-strain relationship is elastic and linear or even nonlinear, there is a unique relationship between stress and strain. But if plastic deformations are encountered, the relationship between stress and strain is not unique, but path dependent. Several reasons may cause material nonlinearity. Plasticity, creep, and thermo-plasticity are phenomena

that result in material nonlinearity. Fig. 3.1 illustrates examples of nonlinear stress-stain relationships.

3.2.2 Geometric nonlinearity

In nonlinear finite element analysis, nonlinearity due to the effects of large displacements on geometry is known as geometric nonlinearity. If displacements are to be determined accurately, geometric nonlinearity should be considered in structural analysis. In this type of nonlinearity, considerable decrease of deformation may be observed compared with small-displacement solution, even though displacements are still small (stiffening). Conversely, displacements may increase more rapidly than small-displacement solution, or in other words, load-carrying capacity of the structure decreases rapidly with progressing displacements (softening). Fig. 3.2 depicts these effects of geometric nonlinearity in structures.

Load-induced deformations can cause significant changes in the geometry of structures even though actual strains may remain small. The definition of small strain differs among researchers. In this research the criteria used in Reference 3 was adopted for small strains. Accordingly, if the element experiences strains greater than 0.04, the analysis lies on large-displacement large-strain condition.

In practice, it is important to identify the type of non-linearity that may be encountered. This dictates the formulation to be used in the analysis. The consideration of all types of non-linearities may be a safe approach to follow. However, this may be costly and slow.

There are two approaches introduced for large-displacements, regardless of small or large-strain condition. These include; i) total Lagrangian and, ii) updated Lagrangian. In the total Lagrangian approach, the original reference frame remains stationary. All displacements are calculated with respect to the original frames, regardless of how big or small the strains are. In the updated Lagrangian approach, a local coordinate system is joined to each element. The local coordinate system moves with the element and the

current state of deformation is the reference state for the next incremental step. The local coordinate system is updated at each state and then displacements are calculated.

In small-displacement analysis, the deformations due to applied loads are assumed small enough to ignore the change in element stiffness. However, in large-displacement analysis, the element stiffness changes due to the change in the geometry of element; i.e., length, thickness or area of the element. Fig. 3.3 illustrates the geometric changes in elements with large-displacement conditions.

3.2.3 Boundary nonlinearity

This type of nonlinearity arises in situations where the nature of the boundary condition changes during the motion of the structure. The degrees of freedom of nodes may become restrained after contact, though they may be free to move or rotate beforehand. This mode of nonlinearity is encountered in contact analysis. The contact problems are nonlinear because the contact (boundary) area grows as applied loads increase. A simple contact problem is shown in Fig. 3.4.

The change of boundary conditions may occur in either materially nonlinear or geometrically nonlinear problems. Pounding of structures during earthquakes is an example where boundary nonlinearity may have to be included in structural analysis.

3.3 Incremental-iterative algorithm

3.3.1 Control techniques

In nonlinear analysis, a control technique is required to control the progress of nonlinear solution along the equilibrium path. Several incremental control techniques such as force-control technique, displacement-control technique, and arc-length technique are proposed.

In force-control technique, the externally applied loads are taken as prescribed variables. In this strategy, the corresponding deformation for each specified force is obtained by the intersection of the surface of constant value of the force with the path (Fig. 3.5a). In finite element analysis, the external loads are incrementally applied with respect to the time-curve of the load case.

In displacement-control technique, each state on the equilibrium path is found by intersection of the surface of constant deformation with the equilibrium path (Fig. 3.5b). In this technique, the externally applied load is increased proportionally, to establish equilibrium according to the time-curve of the controlled degree of freedom.

Generally, force-control technique as well as displacement-control technique fail to find the equilibrium path in the case of sudden turning points. Arc-length control will get over this type of a problem [15]. In arc-length control technique, the applied loads are incremented proportionally to establish equilibrium by considering a determined arc-length on the path (Fig. 3.5c).

3.3.2 Solution procedure

A major problem in nonlinear analysis is to find the state of equilibrium with the applied load at each step, which is an unknown to start with. For nonlinear problems, the stiffness of structure may be affected by large displacements of structure. An iterative method is required in nonlinear analysis to solve a set of simultaneous equations at each step. Various strategies have been proposed to conduct nonlinear analyses. In many cases, the problem requires to be analyzed with different solution schemes. Some iterative methods may fail to converge when others succeed in obtaining the correct answers. The choice of method is dependent on several parameters. Type of nonlinearity (materially nonlinear, geometrically nonlinear), mild or severe nonlinearity, formulation, problem size and intended accuracy are all the factors that can influence the choice of the solution method.

Assuming that the externally applied loads are defined as a function of time, t, equilibrium of a finite element system can be written as follows:

$$^{t}\mathbf{R} - {}^{t}\mathbf{F} = 0 \tag{3.1}$$

where

$^{t}\mathbf{R}$ = Vector of externally applied nodal point at time t

$^{t}\mathbf{F}$ = Vector of internally nodal forces at time t

In incremental solution, it is assumed that the solution at time t is known and the solution for distinct time $t + \Delta t$ is desired, where Δt is the time increment usually defined by the analyst. Therefore, Eq. (3.1) can be rewritten as follows:

$$^{t+\Delta t}\mathbf{R} - {}^{t+\Delta t}\mathbf{F} = 0 \tag{3.2}$$

Since the solution at time t is known, the following equation can be stated:

$$^{t+\Delta t}\mathbf{F} = {}^{t}\mathbf{F} + \mathbf{F} \tag{3.3}$$

where

$\mathbf{F}$ = The incremental nodal point force

On the other hand, vector $\mathbf{F}$ can be expressed using the tangent stiffness matrix, which corresponds to the material and geometry of the element at discrete time t.

$$\mathbf{F} = {}^{t}\mathbf{K}\mathbf{U} \tag{3.4}$$

where

$\mathbf{K}$ = Tangent stiffness matrix

$\mathbf{U}$ = Vector of incremental nodal point displacement

Substituting (3.3) and (3.4) into (3.2) yields following equation:

$$^{t}\mathbf{K}\mathbf{U} = {}^{t+\Delta t}\mathbf{R} - {}^{t}\mathbf{F} \tag{3.5}$$

Finally, the element displacement at time $t + \Delta t$ is found by solving Eq. (3.5) for U and then substituting in the following equation:

$$^{t+\Delta t}\mathbf{U} = {}^{t}\mathbf{U} + \mathbf{U} \tag{3.6}$$

Different schemes have been proposed to perform the above iteration. The most frequently used iteration scheme is Newton-Raphson iteration. In this method, the tangential stiffness matrix is formed and decomposed at each iteration (Fig. 3.6). The Newton-Raphson iteration has a high convergence rate. However, it is expensive for large problem since the tangential stiffness matrix is decomposed at each iteration.

Since the Newton-Raphson scheme is not suitable in some cases, the modified Newton-Raphson iteration has been proposed. In the modified Newton-Raphson, the tangential stiffness matrix is formed and decomposed at each solution step. It should be noticed that the maximum number of iteration at each step is defined by analyst in the program.

3.3.3 Convergence criteria

In incremental solution methods based on an iterative strategy, a practical convergence criterion is needed to terminate the iteration process. The solution obtained at the end of each iteration should be compared with a realistic convergence tolerance to determine if the iteration should be terminated. A very loose tolerance would cause inaccurate results while a very tight tolerance requires more computational time but does not necessarily more accurate results. A number of termination schemes such as displacement convergence, force convergence, and energy convergence are discussed briefly below.

In the displacement convergence criterion, incremental displacement is compared at the end of each iteration with a defined tolerance as follows:

$$\varepsilon_D \geq \frac{|\mathbf{U}^{(i)}|}{|{}^{t+\Delta t}\mathbf{U}^{(i)}|} \tag{3.7}$$

where

ε_D = Displacement convergence tolerance

$\mathbf{U}^{(i)}$ = Vector of incremental nodal point displacement at iteration (i)

$|\mathbf{A}|$ = Euclidean norm of vector A

In the force convergence criterion, the out-of-balance load vector at the end of each iteration is compared with the force tolerance specified by the analyst as follows:

$$\varepsilon_F \geq \frac{|{}^{t+\Delta t}\mathbf{R} - {}^{t+\Delta t}\mathbf{F}^{(i)}|}{|{}^{t+\Delta t}\mathbf{R} - {}^{t}\mathbf{F}|} \tag{3.8}$$

where

ε_F = Force convergence tolerance

In the energy convergence criterion, both displacement and force are used to express the energy tolerance. In this criterion, the work done by the out-of-balance loads through the incremental displacement is checked with the initial internal energy increment.

$$\varepsilon_E \geq \frac{(\mathbf{U}^{(i)})^T({}^{t+\Delta t}\mathbf{R} - {}^{t+\Delta t}\mathbf{F}^{(i-1)})}{(\mathbf{U}^{(1)})^T({}^{t+\Delta t}\mathbf{R} - {}^{t}\mathbf{F})} \tag{3.9}$$

where

ε_E = Energy convergence tolerance

The initial conditions are defined as:

${}^{t+\Delta t}\mathbf{U}^{(0)} = {}^{t}\mathbf{U}$

${}^{t+\Delta t}\mathbf{F}^{(0)} = {}^{t}\mathbf{F}$

The convergence criterion (ε_D, ε_F, or ε_E) is defined by analyst in the program and its value depends on the type and level of nonlinearity of the problem. In some cases, the convergence tolerance should be defined very small value to obtain accurate result [2].

3.3.4 Concept of time-curve

In nonlinear analysis, a non-unique solution will be obtained if one-step operation for full load is accomplished. Therefore, it is desired to proceed with an incremental approach to obtain a nonlinear solution. In static analysis, when time-dependent effects such as creep are not included, time is a non-real variable. The time step represents the intensity of applied loads at that specific step. Same results will be obtained if the time step is incremented to double or even reduced to half. However, in dynamic analysis or in static analysis when time-dependent effects are considered as material nonlinearity, the time step represents the real value of actual time. In this case, time step increment is used to calculate the actual integration of the equation of motion.

3.4 Implementation of the finite element method

Finite element analysis would be quite difficult to be performed if high-speed digital computers were not available to solve the large number of simultaneous equations induced by discretization of the model. A number of general-purpose finite element programs have been developed to perform nonlinear finite element analysis. The rapid development of new generations of computers has made it possible to analyze finite element models with hundreds of thousands of degrees of freedoms in a short time. Consequently, more engineers are using finite element analysis than before.

A typical general-purpose finite element computer program consists of several modulus, which may have different implementation in different contexts. One of the important issues in this regard is to recognize the limitation of the finite element computer programs for some specific applications. In this research, since the behavior of reinforced concrete

shear walls is of interest, the concrete constitutive material model is quite important. In this regard, finite element computer program ADINA has been chosen for the purpose of successive parametric study. ADINA has formulated an effective nonlinear constitutive material model for concrete for two- and three-dimensional applications. This program has the capability of performing linear and nonlinear stress analysis, heat transfer of solids, compressive and incompressible flows, and more. A complete description of the capabilities of the concrete model and the program is given in detail in the following chapter.

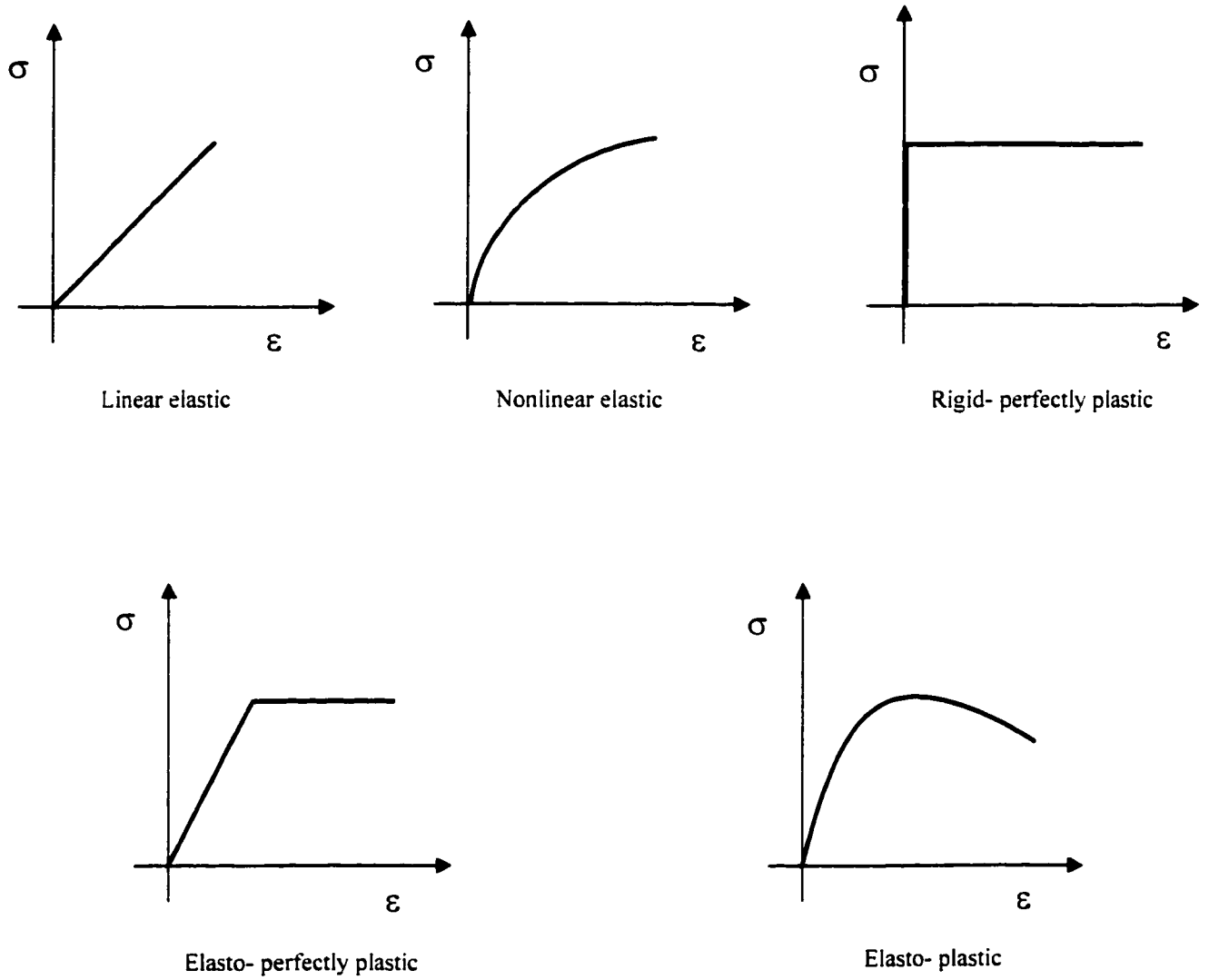

Fig. 3.1 Materially nonlinear stress-strain relationships

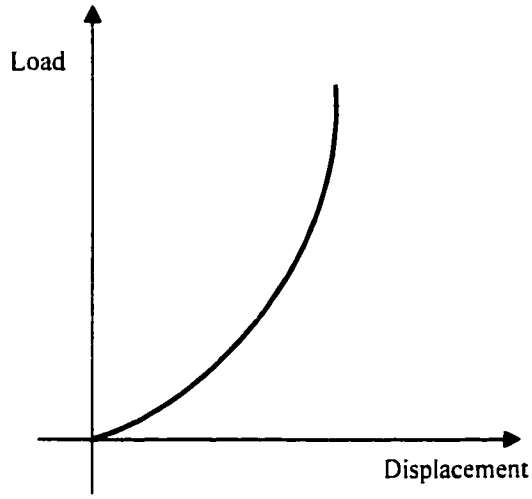

(a) Stiffening problem

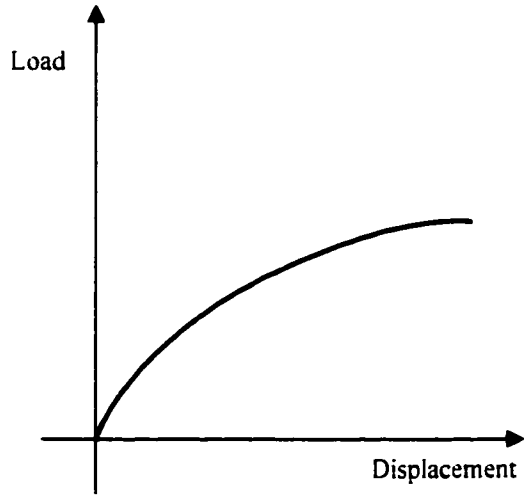

(b) Softening problem

Fig. 3.2 Stiffening and softening effects due to geometric nonlinearity

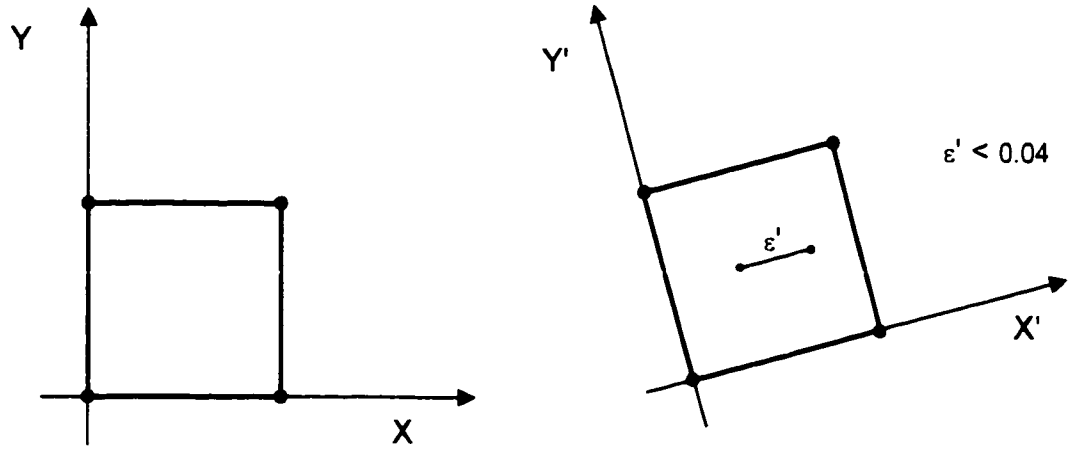

(a) Large displacements, large rotations but small strains

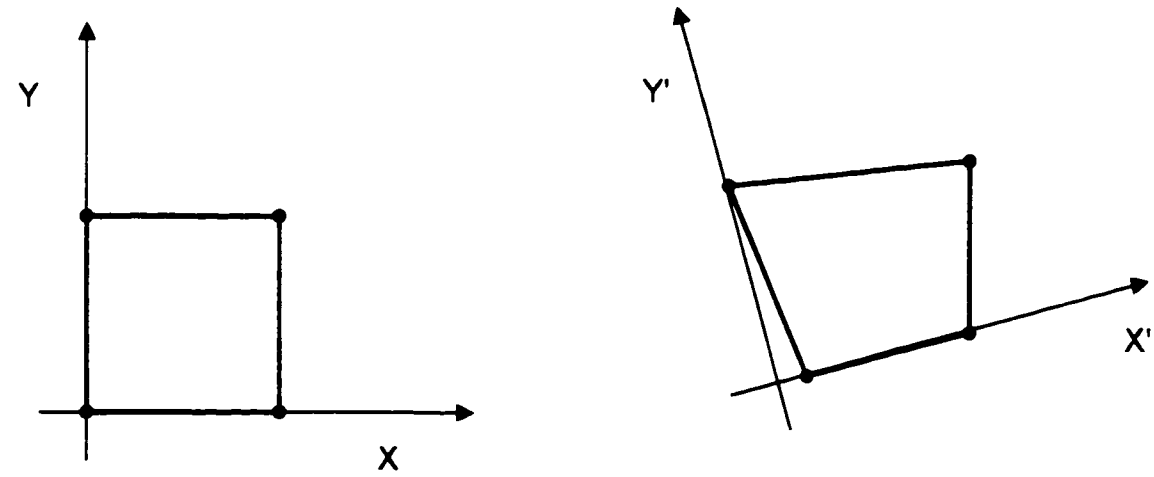

(b) Large displacements, large rotations and large strains

Fig. 3.3 Geometric nonlinearities

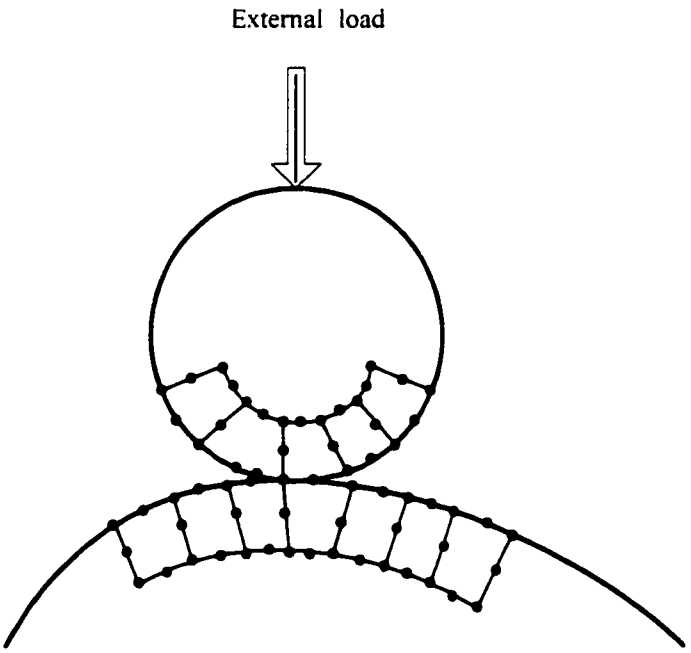

Fig. 3.4 Boundary (contact) nonlinearity problem

(a) Force-control

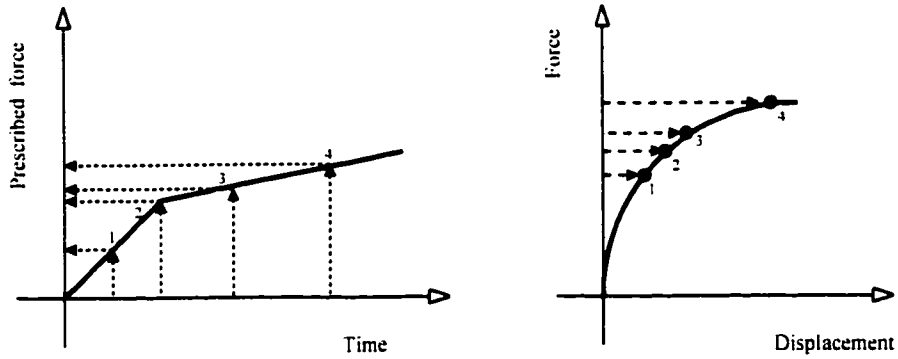

(b) Displacemant-control

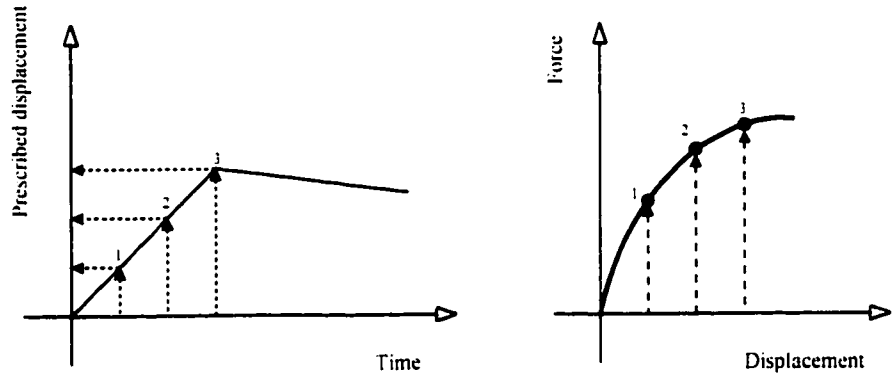

(c) Arc-length control

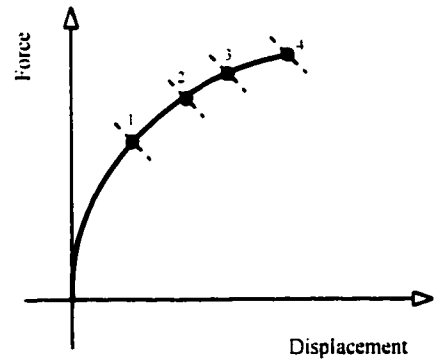

Fig. 3.5 Incremental control techniques

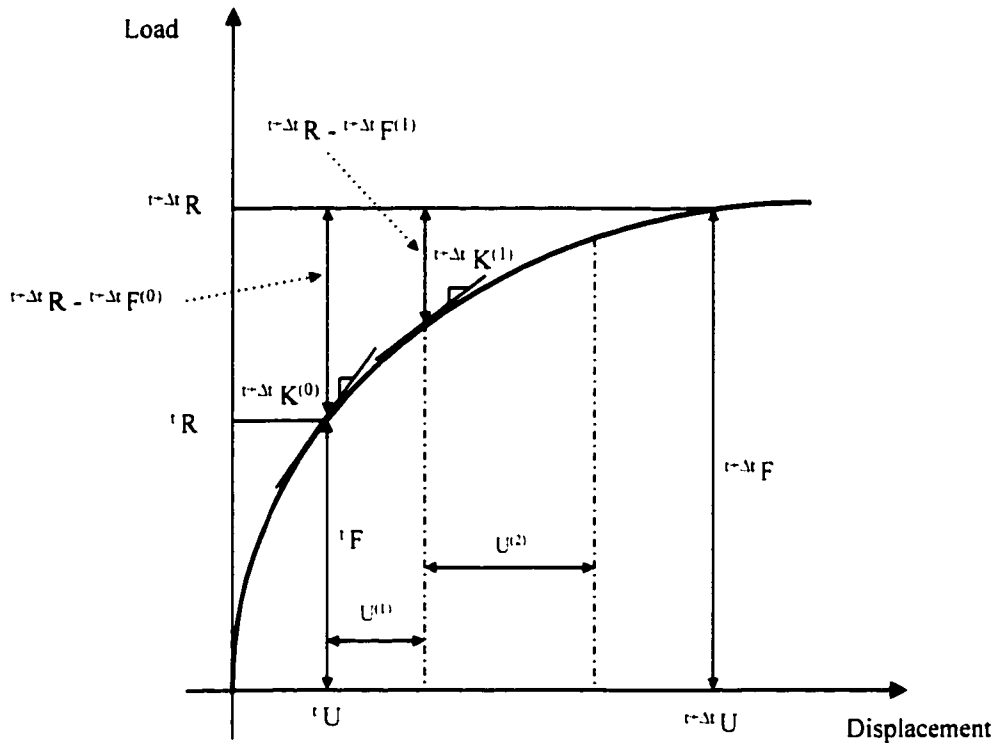

Fig. 3.6 Newton-Raphson iteration method

Chapter 4

Modeling of reinforced concrete structures for finite element analysis

4.1 Constitutive model for concrete

4.1.1 General

In recent years, significant efforts have been made to establish a profound understanding of nonlinear behavior of concrete. It is well recognized that concrete has very complex characteristics, and developing a mathematical model that covers the entire behavior of concrete is quite laborious. Considerable progress has been accomplished and relatively large numbers of constitutive models have been proposed by researchers. Nonlinear stress-strain behavior, progressive cracking caused by tensile stress, crushing of concrete, strain softening, and time-dependent effects are some characteristics of concrete which

should be reflected in a rigorous constitutive model. Hence, developing a state-of-the-art constitutive model that covers all conditions is a very challenging task. Generally, the constitutive models have been categorized as elasticity-based models, plasticity-based models, and endochronic models.

4.1.2 Elasticity-based theory

The elasticity-based model, in general, describes the material behavior as either secant stress-strain approach or linear step incremental technique. In the past few years, different models such as isotropic linear elastic model, Cauchy elastic model, hyperelastic model, and hypoelastic model have been proposed by researchers.

The isotropic linear model is a secant stress-strain formulation that characterizes the behavior of concrete under uniaxial or multiaxial tensile stress. This model can also approximate the behavior of concrete under low compressive stress. Young's modulus E and Poisson's ratio ν are the constants required for the formulation of this model as follows:

$$\sigma_{ij} = \frac{E}{1+\nu}\varepsilon_{ij} + \frac{\nu . E}{1+\nu}\varepsilon_{kk} . \delta_{ij} \tag{4.1}$$

where

i, j and k = The principal direction for a multiaxial stress condition

Cauchy model was proposed and then completed by Saenz [40], Popovics [36] and Carreina and Chu [9]. In this model, when concrete is under compressive stress, the current state of stress σ is described as a function of current strain ε as follows:

$$\sigma = f(\varepsilon) \tag{4.2}$$

where

f = The elastic response function

Hyperelastic or Green elastic model is based on the assumption of the existence of a strain energy density function Φ or a complimentary energy density function Ω such that:

$$\sigma_{ij} = \frac{\partial \Phi}{\partial \varepsilon_{ij}}$$
$$or \qquad (4.3)$$
$$\varepsilon_{ij} = \frac{\partial \Omega}{\partial \sigma_{ij}}$$

The behavior of Green elastic and Cauchy approach is described as path independent. There is a unique relationship between total strain and total stress at any state, which is independent of deformation. Since the behavior of concrete is load-path dependent, this type of formulation is not suitable for modeling of concrete and the application of this model is restricted to monotonic loading conditions.

The hypoelastic model describes the material behavior with an incremental stress-strain relationship. In this approach the tangent stiffness is used to establish the stress-strain relationship. Since the tangent stiffness changes with current stress state, the hypoelastic model relies on the deformation history of the material.

4.1.3 Plasticity-based theory

Plasticity-based model was originally developed to characterize the behavior of metals. Consequently, it has been modified considerably to model the behavior of concrete through classical plasticity-based theory or plastic-fracturing theory. In classical plastic-based modeling, the theory deals with micromechanism of plastic slip in crystals which is defined by the strain increment while the stress remain constant without change in the modulus of elasticity. In plastic-fracturing modeling, however, in addition to plastic slip, microcracking effects are considered in the model to regulate the inelastic behavior of concrete [5]. The modulus of elasticity decreases as concrete gets into the plastic region.

Classical plasticity-based models may be categorized as elastic perfectly plastic model [10], and elastic-strain hardening plastic model [11]. The classical theory of plasticity is based on three assumptions: an initial yield surface, a hardening rule, and a flow rule. The initial yield surface defines the stress level at which beyond this level material deforms inelastically. The hardening rules set the succeeding loading surfaces and a flow rule establishes an incremental plastic stress-strain relationship. Figures 4.1a and 4.1b illustrate the initial yield, loading surfaces, and yield surfaces for an isotropic hardening plasticity model [11].

In concrete, unlike metals, fracture takes place at early stage of loading. Therefore, the plasticity theory by itself cannot characterize the inelastic behavior of concrete adequately, especially in multiaxial stress condition and under high stress levels. Plastic-fracturing models are an extension of classical plasticity theory. Besides the loading surfaces, this theory defines a cracking loading surface in strain space to calculate cracking stress relaxation. Plastic-fracturing theory, in general, is capable of representing an extensive range of inelastic behavior including strain-softening and hysteretic loops under cyclic loading condition. This model, however, needs much more computational time because of the nonsymmetrical stiffness matrix.

4.1.4 Endochronic theory

Endochronic model is based on endochronic theory of viscoplasticity in which inelastic strains are calculated from a development of irreversible damage in material instead of loading surfaces as in plastic-fracturing models [4]. Since this model is capable of characterizing the irreversibility in unloading conditions, it is quite appropriate for modeling the behavior of concrete under cyclic loading condition. The required computational time for the endochronic model is quite considerable because the theory is not based on an incremental procedure approach. In recent years, considerable research have been conducted to develop an elastic-plastic-damage theory, as an extension of endochronic theory [12, 13]. In this approach the failure of concrete is related to the progressive propagation and concentration of microcracks. This is expressed as the

damage of material. Since the elastic-plastic-damage model combines the plasticity theory with continuum damage theory, it describes the behavior of concrete quite well.

4.2 ADINA concrete model

4.2.1 General

ADINA has formulated a comprehensive nonlinear model for two and three-dimensional applications. The concrete model in ADINA is a hypoelastic model with good flexibility in establishing the stress-strain curve and other material properties. Various parameters such as strength and ductility as well as failure envelopes can be calibrated within the program. ADINA concrete model accounts for two and three-dimension stress states based on uniaxial stress-strain relationship, since biaxial or triaxial loading condition changes the overall behavior of the reinforced concrete member drastically. Another interesting feature of the program is to provide the crack configuration under the applied loads at each step. By this means, the analyst can easily locate the critical areas of the reinforced concrete member under the applied loads. Moreover, the analytical mode of failure may be compared with the experimental one using this feature.

Three important aspects of this concrete model can be highlighted as nonlinear stress-strain relationship, tension and compression failure envelopes, and post-cracking and crushing behavior of the concrete.

4.2.2 Stress-strain relationship

The uniaxial stress-strain relationship of concrete in ADINA has been illustrated in Fig. 4.2. This curve shows materially nonlinear characteristics of concrete under compressive and tensile stresses. Under tensile stress, uniaxial strain is positive and the linear relation between stress and strain for this region can be expressed as follows:

$$ {}^{t}\tilde{\sigma} = E_0 .\ {}^{t}\tilde{e} \tag{4.4} $$

where

${}^{t}\tilde{\sigma}$ = Uniaxial stress

$\tilde{E}_0$ = Uniaxial initial tangent modulus

${}^{t}\tilde{e}$ = Uniaxial strain

When concrete is under compressive stress (${}^{t}\tilde{e} \le 0$) the stress-strain relationship is formulated as follows [14]:

$$ \frac{{}^{t}\tilde{\sigma}}{\tilde{\sigma}_c} = \frac{\left[\frac{\tilde{E}_0}{\tilde{E}_s}\right]\left[\frac{{}^{t}\tilde{e}}{\tilde{e}_c}\right]}{1 + A\left[\frac{{}^{t}\tilde{e}}{\tilde{e}_c}\right] + B\left[\frac{{}^{t}\tilde{e}}{\tilde{e}_c}\right]^2 + C\left[\frac{{}^{t}\tilde{e}}{\tilde{e}_c}\right]^3} \tag{4.5} $$

and

$$ {}^{t}\tilde{E} = \frac{\tilde{E}_0\left[1 - B\left(\frac{{}^{t}\tilde{e}}{\tilde{e}_c}\right)^2 - 2C\left(\frac{{}^{t}\tilde{e}}{\tilde{e}_c}\right)^3\right]}{\left[1 + A\left(\frac{{}^{t}\tilde{e}}{\tilde{e}_c}\right) + B\left(\frac{{}^{t}\tilde{e}}{\tilde{e}_c}\right)^2 + C\left(\frac{{}^{t}\tilde{e}}{\tilde{e}_c}\right)^3\right]^2} \tag{4.6} $$

where

$$A=\frac{\left[\frac{\tilde{E}_0}{\tilde{E}_u}+\left(p^3-2p^2\right)\frac{\tilde{E}_0}{\tilde{E}_s}-\left(2p^3-3p^2+1\right)\right]}{\left[\left(p^2-2p+1\right)p\right]}$$

$$B=\left[\left(2\frac{\tilde{E}_0}{\tilde{E}_s}-3\right)-2A\right] \qquad C=\left[\left(2-\frac{\tilde{E}_0}{\tilde{E}_s}\right)+A\right]$$

$$p=\frac{\tilde{e}_u}{\tilde{e}_c}$$

$$\tilde{E}_s=\frac{\tilde{\sigma}_c}{\tilde{e}_c}$$

$$\tilde{E}_u=\frac{\tilde{\sigma}_u}{\tilde{e}_u}$$

Eqs. (4.5) and (4.6) are derived based on monotonic loading condition. During unloading stage in a reversed cyclic condition, the material is assumed to behave as isotropic with the initial Young's modulus E_0 , and when reloading the stress σ_{pi} is calculated for each principal direction with respect to ε_{pi} using Eqs. (4.4) and (4.6) with the Young's modulus E_{pi}.

In this model, Poisson's ratio of concrete remains constant under tension, while under compressive stress the Poisson's ratio may change as the stress increases. The thermal effects also could be included in this model. In this case, the material properties are considered temperature-dependent.

4.2.3 Failure envelopes

Failure envelope of concrete is an envelope that defines the maximum load carrying capacity of the concrete under given loading condition. A precise prediction of concrete failure at different stages is a complicate issue. Failure of concrete depends upon the nature of loading as well as the material properties of concrete.

There are two predefined failure envelopes in ADINA: Sadina and Kupfer [14, 21]. The failure envelopes, however, could be defined or modified by the analyst. Fig 4.3 illustrates compressive failure envelope of concrete under biaxial compressive stress condition. The rate of the increase in compressive stress, however, depends on the principal stress ratio σ_{p1}/σ_{p2}. Under triaxial stress condition, ADINA employs the failure envelope shown in Fig 4.4 to identify whether the concrete is crushing.

The tensile failure envelope of concrete model in ADINA is shown in Fig. 4.5. As it is depicted, the principal stresses are used to calculate the stress state at each step. Failure of concrete under tensile stress takes place when tensile stress in any principal direction exceeds the tensile capacity of concrete specified in the tensile failure envelope. It is assumed that the plane of cracking is normal to the direction of corresponding principal stress. The configuration of cracking and crushing of concrete can be shown by the program at each loading step using these failure envelopes.

4.2.4 Post-failure behavior

Post-failure behavior of concrete is one of the most important aspects of the concrete material model. Post-failure characteristics affect the finite element results quite significantly. Complex nature of concrete such as opening and closing of cracks, shear transfer mechanism and aggregate interlock, tension stiffening, and compression softening make it difficult to model the post-failure behavior of concrete accurately.

When principal tensile stress reaches the maximum tensile stress, tensile failure occurs perpendicular to the corresponding principal direction. After the formation of a crack, a discontinuous linear unloading branch represents the stress-strain relationship of concrete as depicted in Fig. 4.2. As shown in this figure, tensile stress of concrete drops immediately from maximum tensile stress σ_t to a lower stress σ_{tp}. Afterward, as tensile strain increases, the tensile stress decreases linearly. In ADINA, post-tensile cracking behavior is checked at each solution step after formation of the failure plane. The failure is either active, which is referred to as open crack, or inactive referred to as closed crack condition. The failure is inactive if normal strain along the plane of a crack is less than the strain from previous solution step. Therefore, more accurate results are predicted under cyclic loading by considering the effect of opening and closing of cracks.

When concrete is under low compressive stress, the uniaxial stress-strain relationship of concrete is almost linear. As compressive stress in concrete increases, the uniaxial stress-strain curve begins to soften gradually until it reaches the maximum compressive stress σ_c. At this stage, concrete starts crushing. In the descending branch of uniaxial stress-strain relationship, compressive stress decreases as strain increases until it reaches the ultimate compressive stress σ_u. Then, stresses are released to zero linearly using following modulus:

$$\tilde{E}_u = \frac{\tilde{\sigma}_u - \tilde{\sigma}_c}{\tilde{e}_u - \tilde{e}_c} \tag{4.7}$$

4.3 Constitutive model for reinforcing steel

4.3.1 General

A typical monotonic stress-strain curve under tension is shown in Fig. 4.6. The monotonic curve for reinforcing steel consists of three distinct portions: the linear region, the yield plateau, and the strain-hardening region. Elasto-plastic behavior of

reinforcing steel is represented in the linear region and the yield plateau. The linear region characterizes the elastic behavior of reinforcing steel up to the yield stress σ_y with the slope of E_s. In this region, the incremental stress $\partial\sigma_s$ can be defined as follows:

$$\partial\sigma_s = E_s \cdot \partial\varepsilon_s \tag{4.8}$$

where

$\partial\varepsilon_s$ = The incremental steel strain

E_s = The modulus of elasticity of steel

Beyond yield stress σ_y, steel shows plastic behavior until it reaches the strain-hardening strain, ε_{sh}. Since zero slope of this portion often causes numerical difficulties in the finite element method, usually a small value of tangent stiffness is assumed for this portion. The strain-hardening region starts when strain of steel exceeds ε_{sh}. In the finite element method, it is usually preferable to idealize the stress-strain curve of reinforcing steel into a bilinear or trilinear curve. When bilinear idealization is employed, the strain-hardening portion can be determined as follows:

$$\partial\sigma_s = E_{sh} \cdot \partial\varepsilon_s \tag{4.9}$$

where

E_{sh} = The modulus of elasticity of steel in strain-hardening portion

4.3.2 ADINA steel model

In ADINA, reinforcing steel can be modeled using a linear or nonlinear truss element. Von Mises plasticity model with isotropic hardening is employed to represent the material behavior of reinforcing steel in this research. Figs. 4.7a and 4.7b illustrate the von Mises model for bilinear or multilinear stress-strain curve, where E is the Young's

modulus, E_T is the strain-hardening modulus and $^{o}\sigma_y$ is the initial yield stress.

This model can be used in small displacement - small strain analysis, large displacement - small strain analysis (strain approximately less than 4%), and large displacement – large strain analysis. However, the definition of reinforcing steel should agree with that of the concrete model in the finite element analysis.

In this model, the rupture of the reinforcing steel can be identified. In the case of bilinear curve, a maximum allowable plastic strain is defined as an input to the program to recognize the element rupture. When rupture takes place, the corresponding element is removed from the finite element model.

4.4 Steel reinforcing representation

There are basically three approaches in finite element analyses to model the reinforcing steel in reinforced concrete: discrete steel model, embedded steel model, and smeared steel model as shown in Figures 4.8a, 4.8b and 4.8c.

The discrete steel approach was first introduced by Ngo and Scordelis [30]. The discrete steel model can be represented either as a truss element, which is assumed to be pin-connected with two degrees of freedom at each nodal point, or as a beam element to represent the axial, bending and shear stiffness of the reinforcing steel. The significant advantages of this model are its simplicity to model and its capability to represent bond-slip relation of reinforcing bar and surrounding concrete. On the other hand, the disadvantage of the discrete model is its mesh dependency. In this case the location of bar elements is dependent on the mesh layout of the model.

In embedded steel approach, the reinforcing steel is represented as a two or three dimensional truss element. The nodes of the truss element do not necessarily coincide with those of the isoparametric concrete element. The displacements of the embedded

steel element are assumed to be consistent with the concrete element. Perfect bond between concrete and steel bar is assumed in this model.

In smeared model, reinforcing steel is distributed over the concrete uniformly. Perfect bond between reinforcing steel and surrounding concrete must be considered in this model. The constitutive matrix of reinforced concrete is a superimposed result of the constitutive matrix of reinforcing steel and the constitutive matrix of concrete.

4.5 Verification of the finite element results

4.5.1 General

In order to perform the finite element analysis, the reinforced concrete structure is discretized into finite number of elements. This transformation from a real reinforced concrete structure to an analytical model causes some approximation regarding structural behavior and material properties. Complexities of characteristics of concrete make it difficult to define a perfect constitutive material model. Idealization of the behavior of reinforcing steel to a bilinear curve, and the assumption of perfect bond are other sources of approximations. Moreover, the computational technique can have a significant impact on the results. Selecting an inappropriate solution algorithm, especially in problems with high nonlinearity, yields diverging answers. Therefore, the applicability of the finite element computer program as well as the accuracy of the defined finite element model for reinforced concrete should be verified before it can be confidently used for further parametric study. In this regard six shear walls, which are identified as series I and II in this research have been studied in the following sections. The defined parameters in the finite element model for each shear wall are also discussed in detail.

4.5.2 Shear wall series I

Lefas et al. [23] tested 13 shear walls with the aspect ratios between 1.0 and 2.0. Shear walls SW14, SW15, and SW16 with rectangular cross-section were chosen for the purpose of verification of the finite element program ADINA.

The nominal dimensions of chosen shear walls were 750 mm wide, 750 mm high, and 70 mm thick. Fig. 4.9 shows the geometric details and reinforcement layout of these shear walls. Each shear wall consists of an upper beam, web and lower beam. The role of the upper beam is to transfer the lateral load over the top portion of the web. The lower beam is used to clamp down the shear wall to the laboratory floor. Shear walls SW15 and SW16 were subjected to axial loads of 185 kN and 460 kN, respectively. No axial load was applied on SW14. Constant axial load was first applied in the center of the boundary elements and then the monotonic horizontal load was applied at the top corner of the upper beam.

These walls were heavily reinforced with high-tensile deformed steel bars. The vertical and horizontal reinforcing bars were placed in two layers. The nominal diameters of vertical and horizontal bars were 8 mm and 6.25 mm, respectively, with yield strength of 470 MPa for vertical bars and 520 MPa for horizontal bars. The horizontal and vertical reinforcement ratios were designed according to the ACI building code recommendations. The ratios of main flexural reinforcement to the gross concrete area of boundary elements was 3.1%, the horizontal reinforcement to the gross concrete area of vertical section of the web was 1.1%, and the vertical reinforcement to the gross concrete area of horizontal section of the web was 2.4% for all specimens. The modulus of elasticity of reinforcing steel was 210,000 MPa and the strain-hardening modulus of reinforcing bars was assumed to be 5% of the modulus of elasticity.

The cube strength of concrete was 42.1 MPa, 43.3 MPa, and 51.7 MPa for shear walls SW14, SW15 and SW16, respectively. The cylinder strength of concrete is usually assumed to vary between 0.85 to 0.90 of the cube strength [33]. In this research, cylinder

strength is assumed to be 89% of the cube strength for chosen shear walls. The Poisson's ratio for concrete was 0.15 and the modulus of elasticity of concrete was 30720 MPa, 31023 MPa, and 33183 MPa for SW14, SW15, and SW16, respectively.

4.5.3 Shear wall series II

Maier [25], at Swiss Federal Institute of Technology tested 10 square shear walls. Three of these shear walls had rectangular cross-section and the remaining walls had a flanged section. Among them, specimens S2, S3, and S6, with a flanged cross-section, were chosen to investigate the applicability of the computer program ADINA.

Fig 4.10 shows the geometry and reinforcement details of the selected specimens. These shear walls had a length of 1.18 m, height of 1.20 m, and thickness of 0.10 m. They were firmly attached to the test-floor through a heavily reinforced lower slab to simulate the fixed boundary condition while the thick upper slab was used to transfer the load to the flanged wall.

The reinforcing bars were arranged on both sides of the walls in vertical and horizontal directions with 100 mm spacing. Minimum concrete cover of 10 mm was provided for the specimens. The nominal diameters of bars were 8 mm in horizontal and vertical directions for S2, 8 mm and 12 mm in horizontal and vertical direction for S3, and 6 mm and 8 mm for S6. The reinforcement was made of hot-rolled steel with a modulus of elasticity of 200,000 MPa. The strain-hardening modulus was assumed to be 10,000 MPa, which forms 5% of the modulus of elasticity. For specimens S2, S3, and S6, the yield strengths of web horizontal reinforcement were 574 MPa, 574 MPa, and 537 MPa, and for web vertical reinforcement and flange vertical reinforcement these values were 574 MPa, 530 MPa, and 575 MPa, respectively. The web horizontal reinforcement ratios were 1.03% for S2 and S3, and 0.57% for S6. Web vertical reinforcement had ratios of 1.05%, 2.23%, and 1.02%, and the flanges had 1.29%, 2.74%, and 1.26% for S2, S3, and S6, respectively.

The cylinder strength of concrete for specimens S2, S3 and S6 were 34.6 MPa, 36.7 MPa, and 35.6 MPa, with modulus of elasticity of 26470 MPa, 30474 MPa, and 30132 MPa, respectively. The Poisson's ratio of concrete was 0.15. The normal force was kept constant throughout the test while the shear force monotonically increased until failure. The constant normal forces for specimens S2, S3, and S6 were 1689 kN, 460 kN, and 452 kN, respectively.

4.5.4 Defined finite element model

Fig. 4.11 depicts the defined finite element model in this research. Each concrete element was surrounded by four steel elements. Perfect bond between reinforcing steel and concrete was assumed for all shear walls in both series I and II. Shear walls SW14, SW15 and SW16 were modeled using 386 four-node isoparametric elements to represent concrete elements. The reinforcing steel was modeled using 825 two-node nonlinear truss element. Fig. 4.12 shows the layout of the finite element mesh for shear walls series I. Shear walls S2, S3 and S6 were discretized into 800 four-node isoparametric concrete elements and 1671 two-node nonlinear truss elements for reinforcing steel. Fig. 4.13 depicts the defined finite element mesh for shear walls series II.

Several finite element mesh configurations were employed to investigate the sensitivity of mesh size. The mesh size that gave more accurate results with less required solution time was then chosen for this research. The effect of concrete confinement is also considered for shear walls series I and II. In order to achieve accurate results, stress-strain relationship for boundary elements are defined on the basis of the confined concrete model proposed by Saatcioglu and Razvi model [39]. The overall load-displacement relationship shows a premature failure when the effect of confined concrete is neglected.

The convergence criterion and iteration method also have significant impact on the results of the finite element analysis. Newton-Raphson and BFGS iterations have demonstrated a powerful convergence behavior in many nonlinear structural analyses [2]. For all shear walls in series I and II, the specified iteration method was full-Newton

method with the line searching option. In these walls, the displacement convergence criterion was used with DTOL=0.5 and DNORM=1.0 as the input to the program and the maximum number of iterations was set to ITEMAX=150 for each solution step. A small load increment of 10 kN per step was considered for all shear walls.

4.5.5 Comparison between analytical and experimental results

The analytical results from the finite element program contain variety of results including reactions, nodal forces, nodal displacements, and stresses and strains at each integration point. The ultimate load capacity and the load-displacement characteristics of walls between computed and experimental values are compared in this section, in order to verify the applicability of finite element program ADINA and the accuracy of defined models for reinforced concrete.

Load-displacement characteristic of a shear wall is an important aspect that describes the strength, lateral stiffness and energy dissipation characteristics of the wall. The experimental response of shear wall series I and II are illustrated in Figs. 4.14 and 4.18 in term of applied lateral load versus top displacement of the wall. Figs. 4.15 to 4.17 and 4.19 to 4.21 compare the load-displacement response of ADINA results with experimental data for each series. As can be seen in these figures, there is an excellent correlation between ADINA analysis and experimental results for walls SW15, SW16 and S2. Load-displacement curves for specimens SW14, S3, and S6 show minor overestimation relative to the experimental curve. Overall, ADINA has demonstrated very good results compared to the experimental values.

The ADINA results for specimen SW14 were 290 kN for horizontal load and 13 mm for ultimate deflection. The same quantities recorded during testing were 265 kN and 11.2 mm. This comparison indicates 9% and 14% higher values for force and deflection quantities when ADINA was employed. Experimental results for shear wall SW15 show 315 kN as ultimate horizontal load and 8 mm maximum deflection, compared to 290 kN and 7.42 mm from ADINA analysis. The difference is 9% and 8% in force and

displacement capacities, respectively. Shear wall SW16 had 355 kN lateral load capacity at 5.78 mm deflection during testing. ADINA results show 340 kN force capacity at 5.69 mm deflection, which are 4% and 2% below those measured in the laboratory, respectively. Ultimate lateral load for shear wall S2 was 883 kN with 8.15 mm top corner deflection, when computed by ADINA. During testing, the same wall resisted 928 kN shear force, deflecting a maximum of 10.41 mm. The difference appears to be 5% in strength and 27% in ductility.

As Fig. 4.20 depicts the comparison of experimental and analytical results for shear wall S3, the experiment produced 977 kN force capacity with 14.72 mm top deflection. The corresponding ADINA results are 900 kN and 13.36 mm, indicating a discrepancy of about 8% in load capacity and 10% in ductility. Finally, the flanged wall S6 failed when the applied shear force reached 667 kN at a deflection of 18.69 mm. ADINA results indicate a failure load of 701.25 kN at 16 mm top displacement. The analytical results for this wall show 5% increase in ultimate load capacity and 16% decrease in ductility.

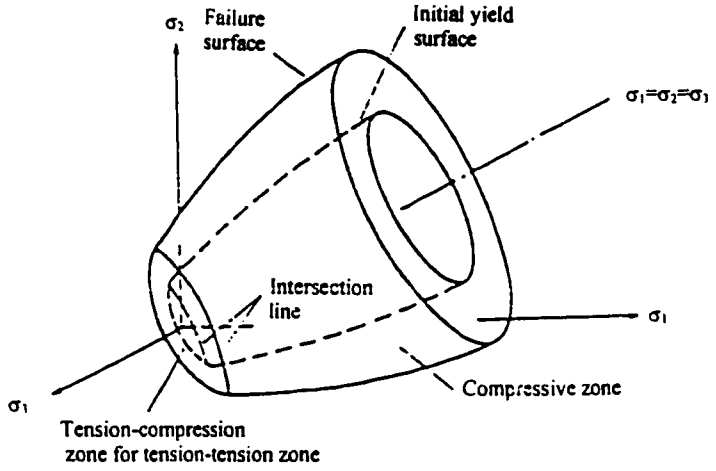

Fig.4.1a Initial yield and failure surfaces of Chen-Chen Model [33]

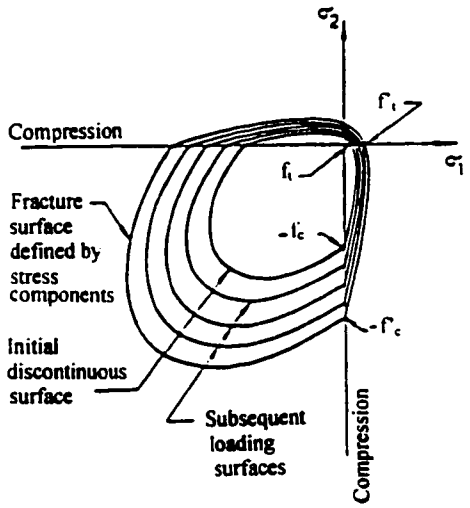

Fig.4.1b Evolution of loading surfaces of Chen-Chen Model [33]

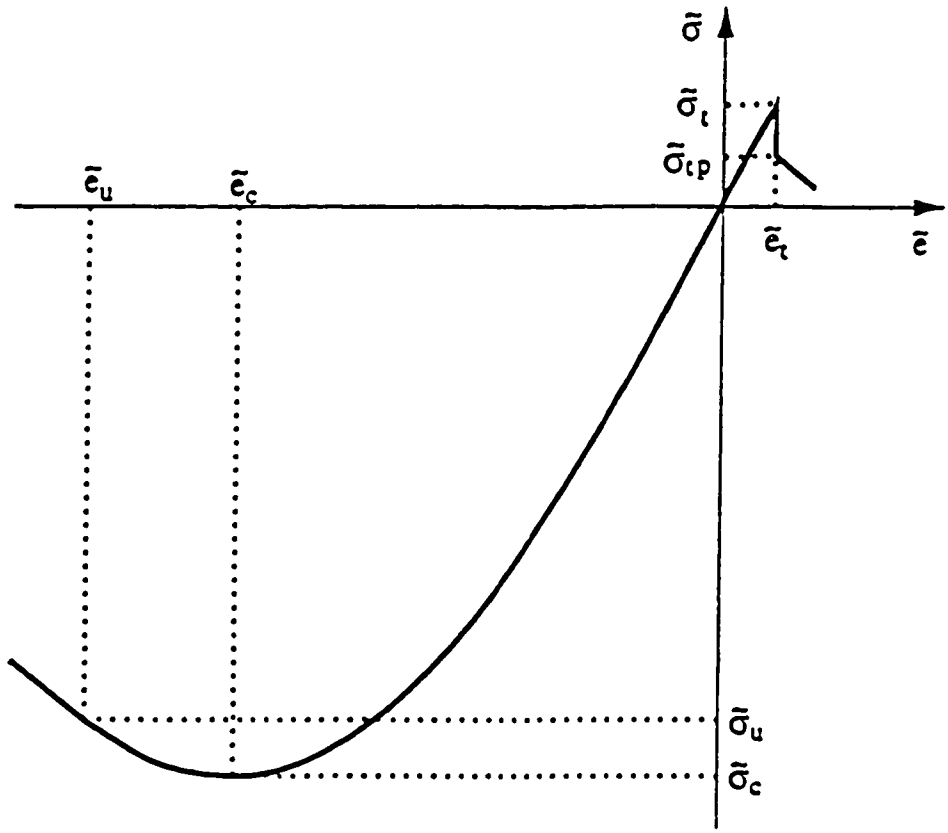

Fig.4.2 ADINA uniaxial stress-strain relationship for concrete

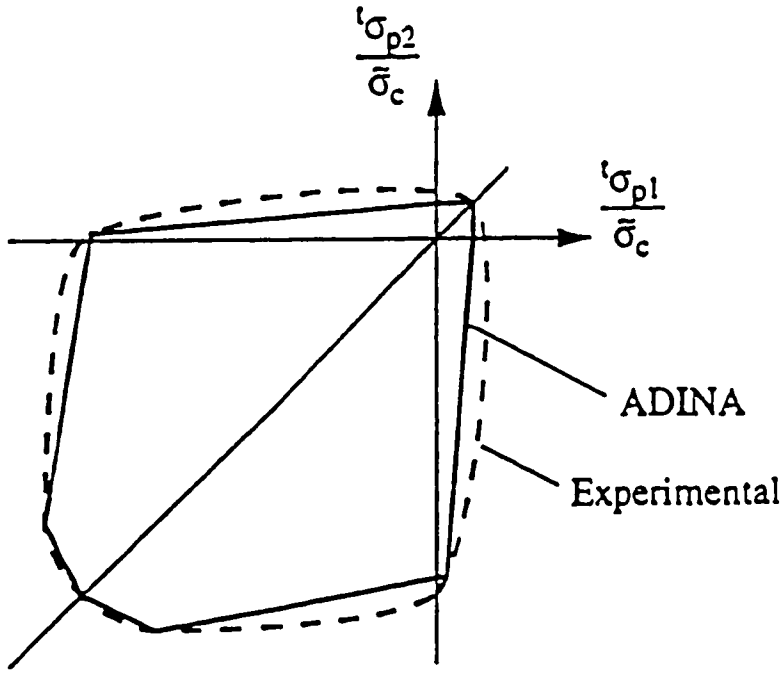

Fig.4.3 Compressive failure envelope of concrete under biaxial stress condition

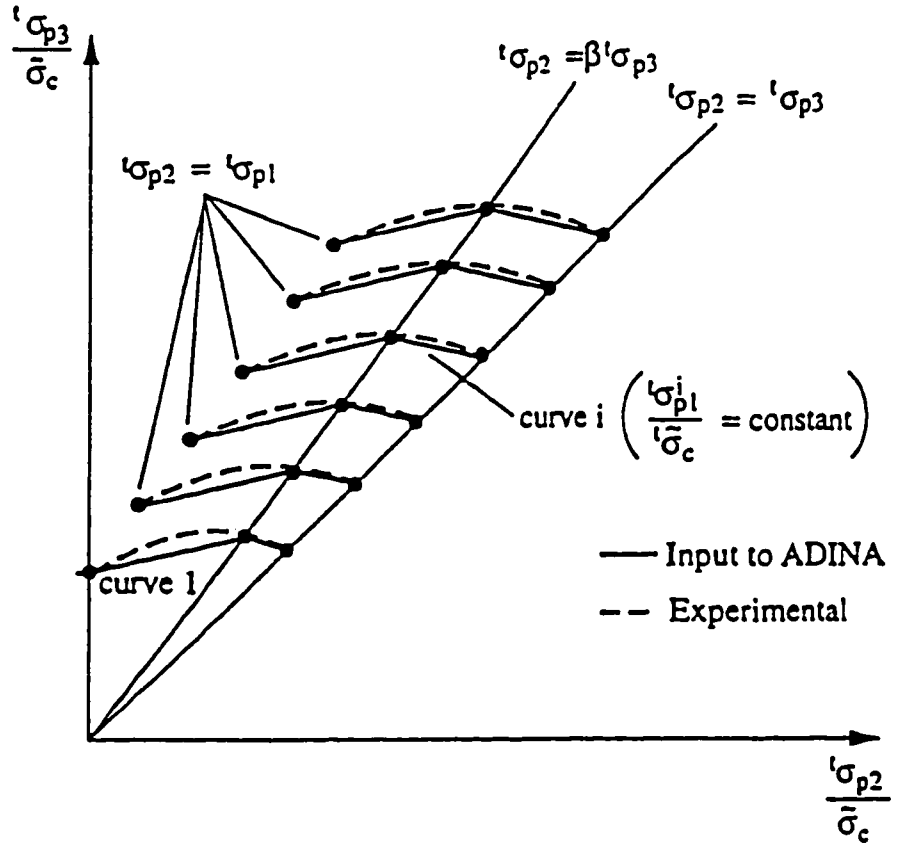

Fig.4.4 Compressive failure envelope of concrete under triaxial stress condition

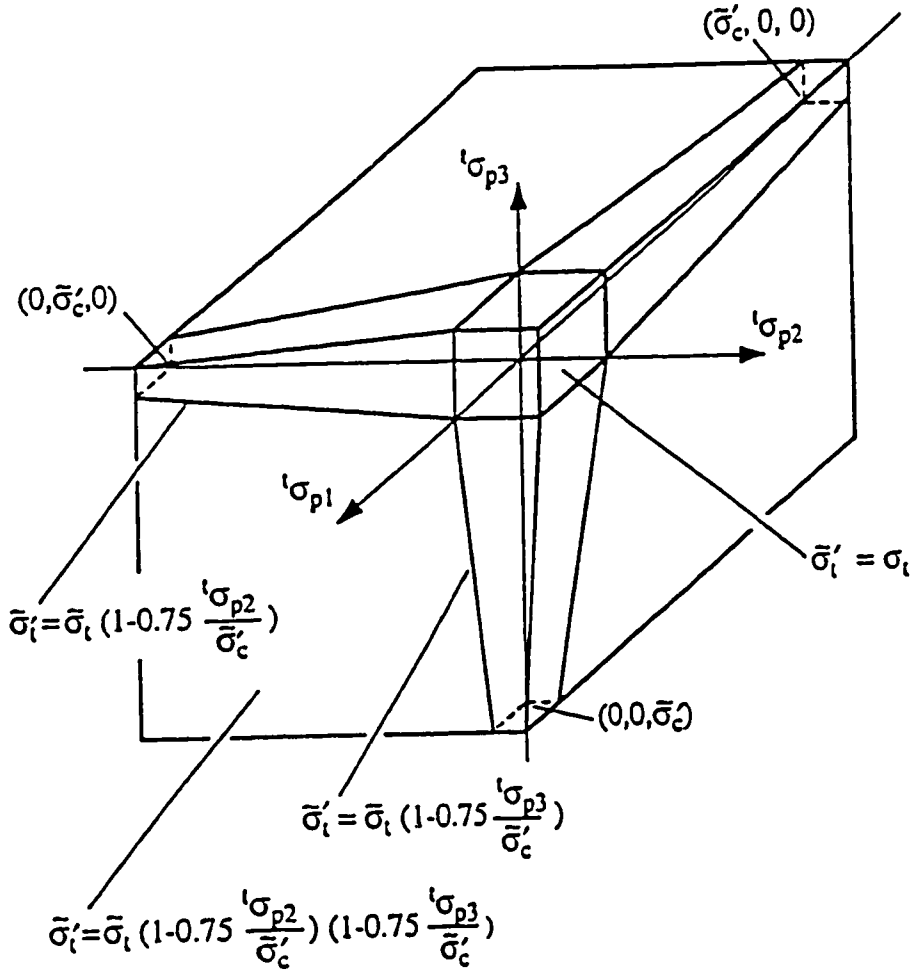

Fig 4.5 Three dimensional tensile failure envelope of concrete used in ADINA

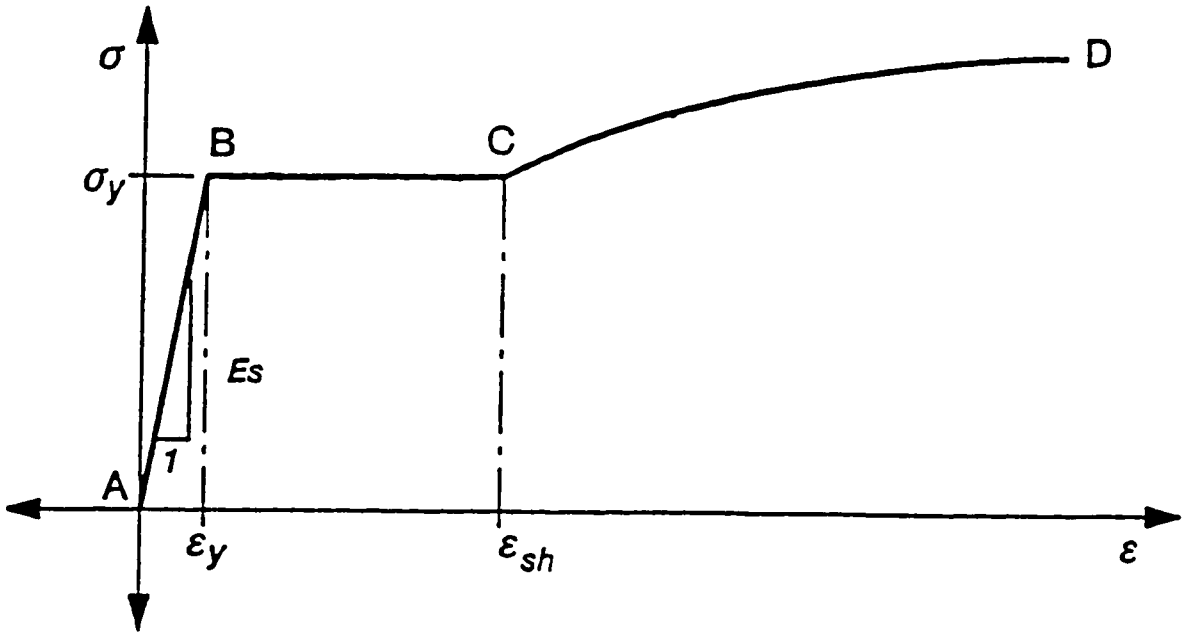

Fig 4.6 Monotonic stress-strain relationship for reinforcing steel

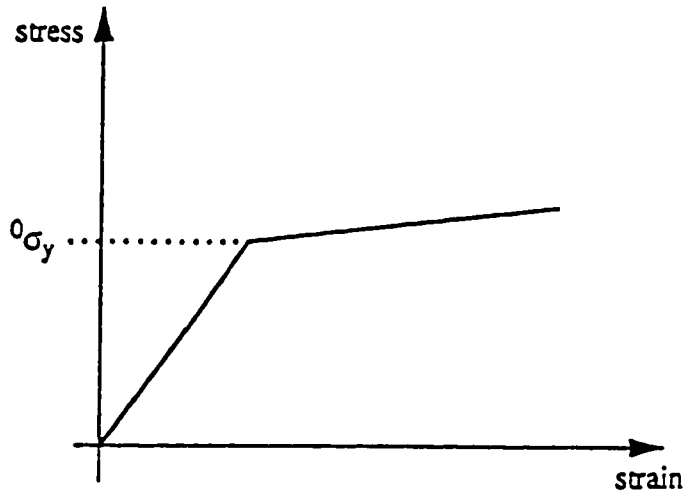

(a) Bilinear curve

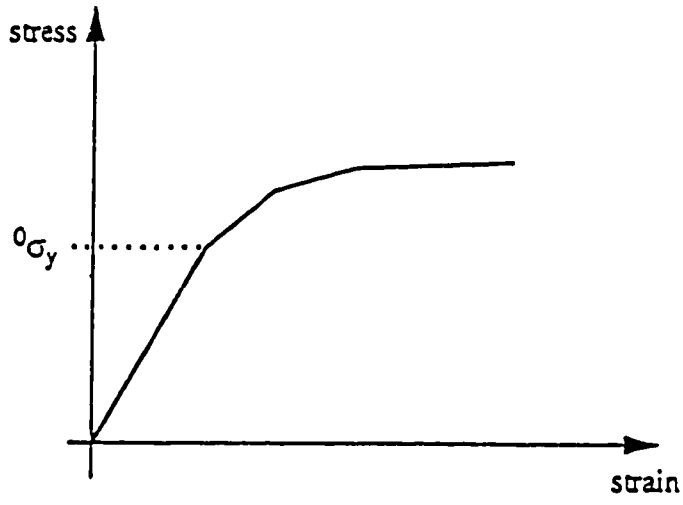

(b) Multilinear curve

Fig. 4.7 von Mises stress-strain model for reinforcing steel

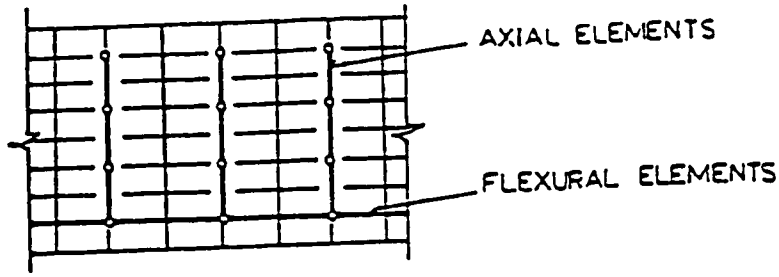

(a) Discrete steel model

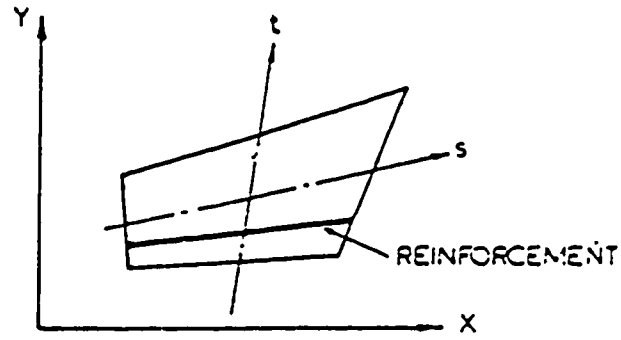

(b) Embedded steel model

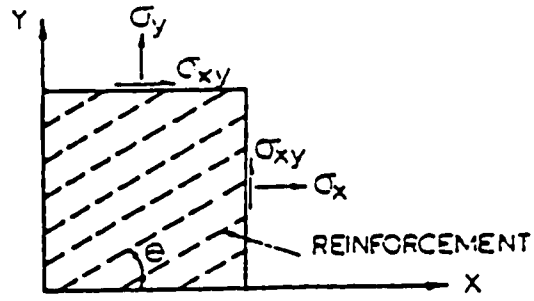

(c) Smeared steel model

Fig. 4.8 Steel representation in finite element method

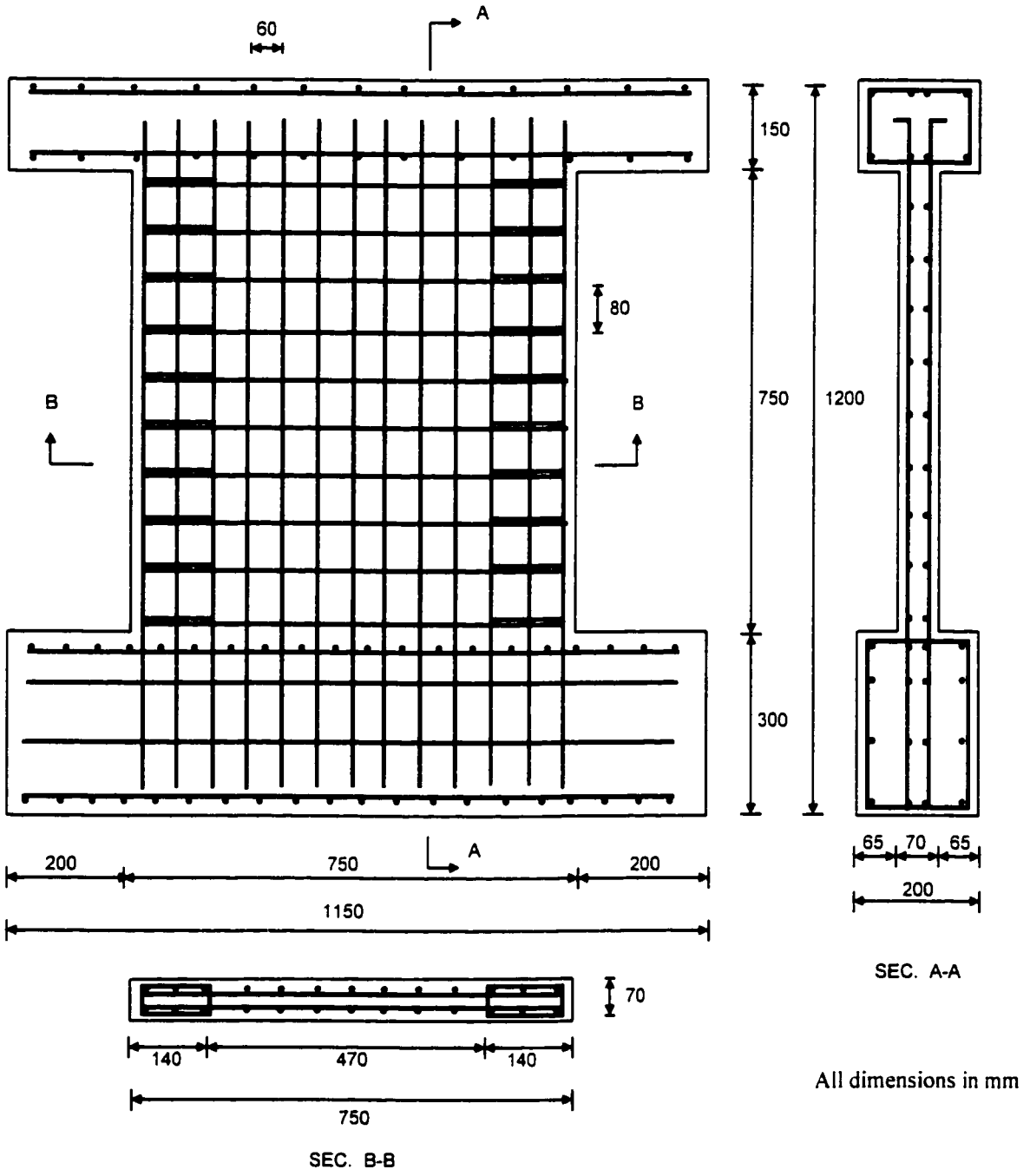

Fig. 4.9 Geometry and reinforcement details of shear walls SW14, SW15, and SW16 tested by Lefas et al [23]

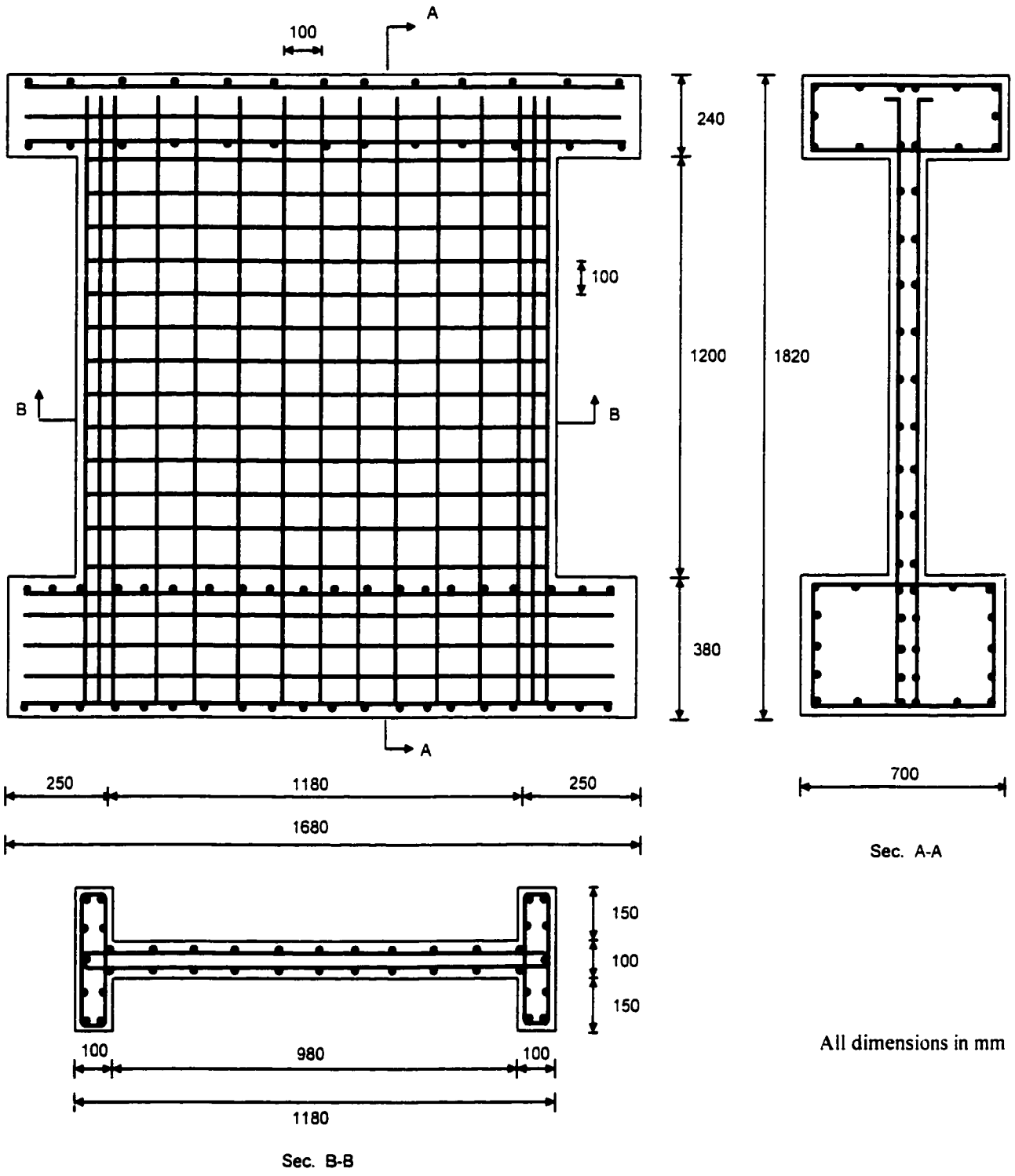

Fig. 4.10 Geometry and reinforcement details of shear walls S2, S3, and S6 tested by Maier [25]

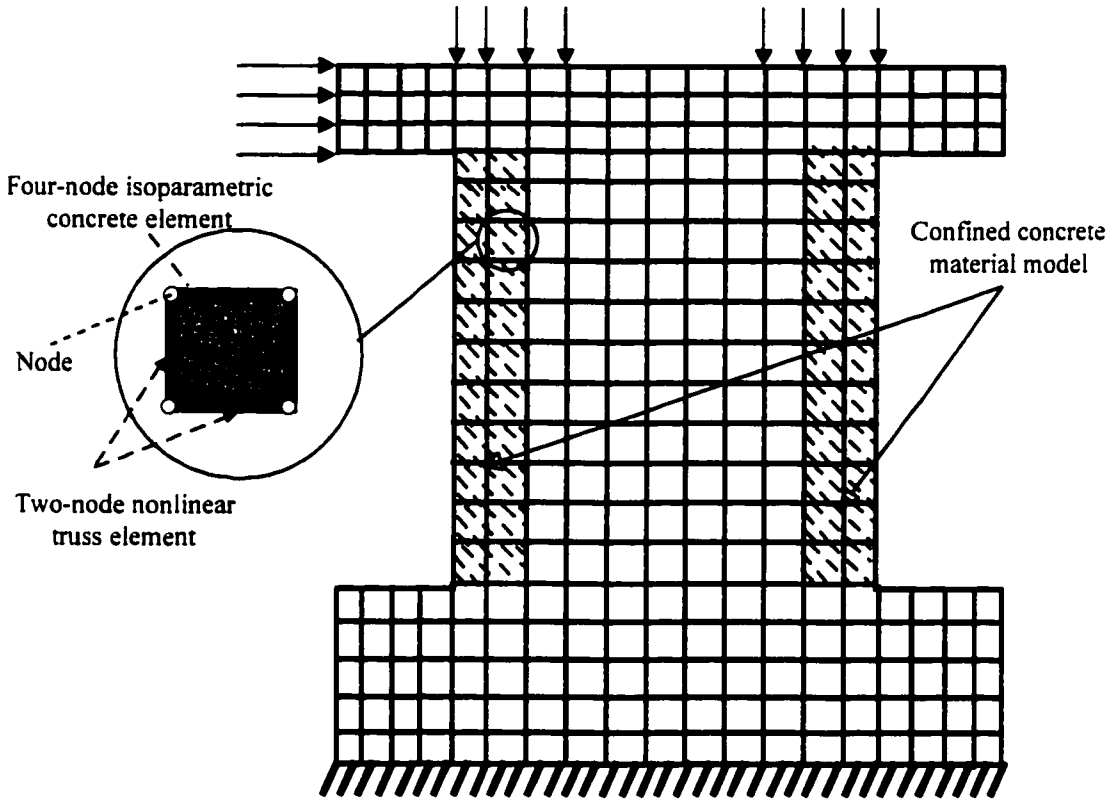

Fig. 4.11 Description of the finite element model in this research

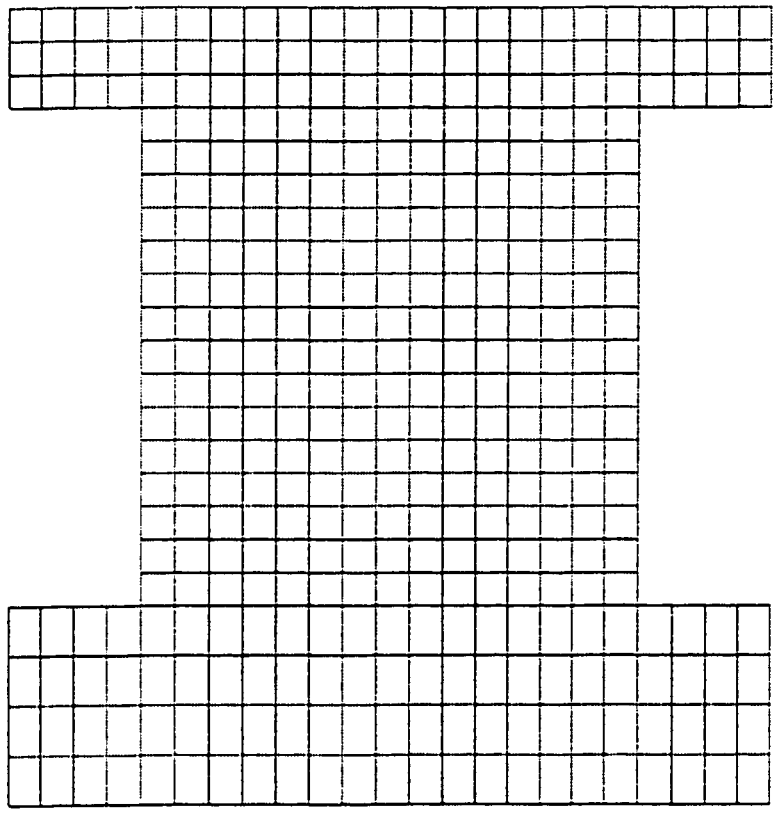

Fig. 4.12 Element scheme in finite element model
for shear walls SW14, SW15 and SW16

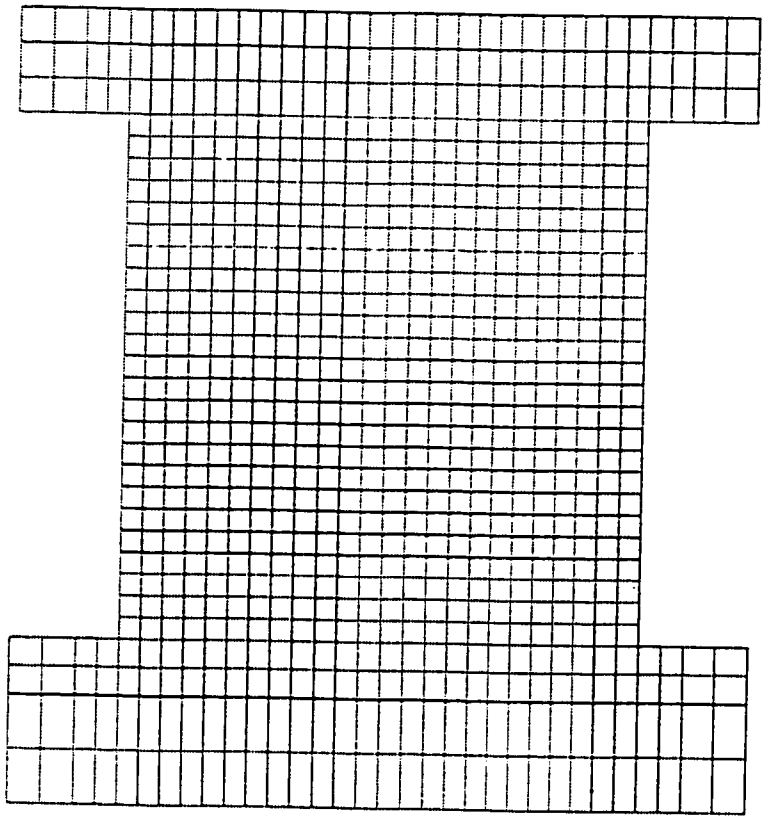

Fig. 4.13 Element scheme in finite element model for shear walls S2, S3 and S6

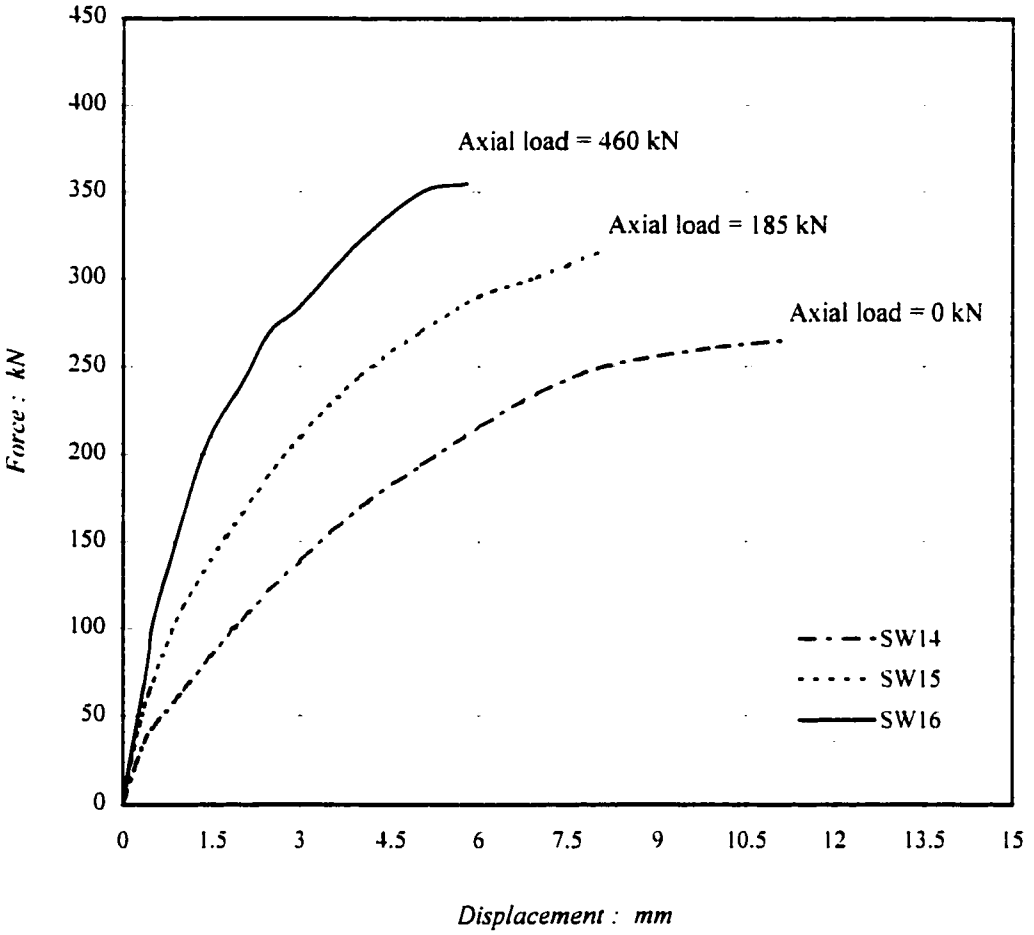

Fig. 4.14 Experimental force-displacement response of shear walls SW14, SW15 and SW16 tested by Lefas et al [23]

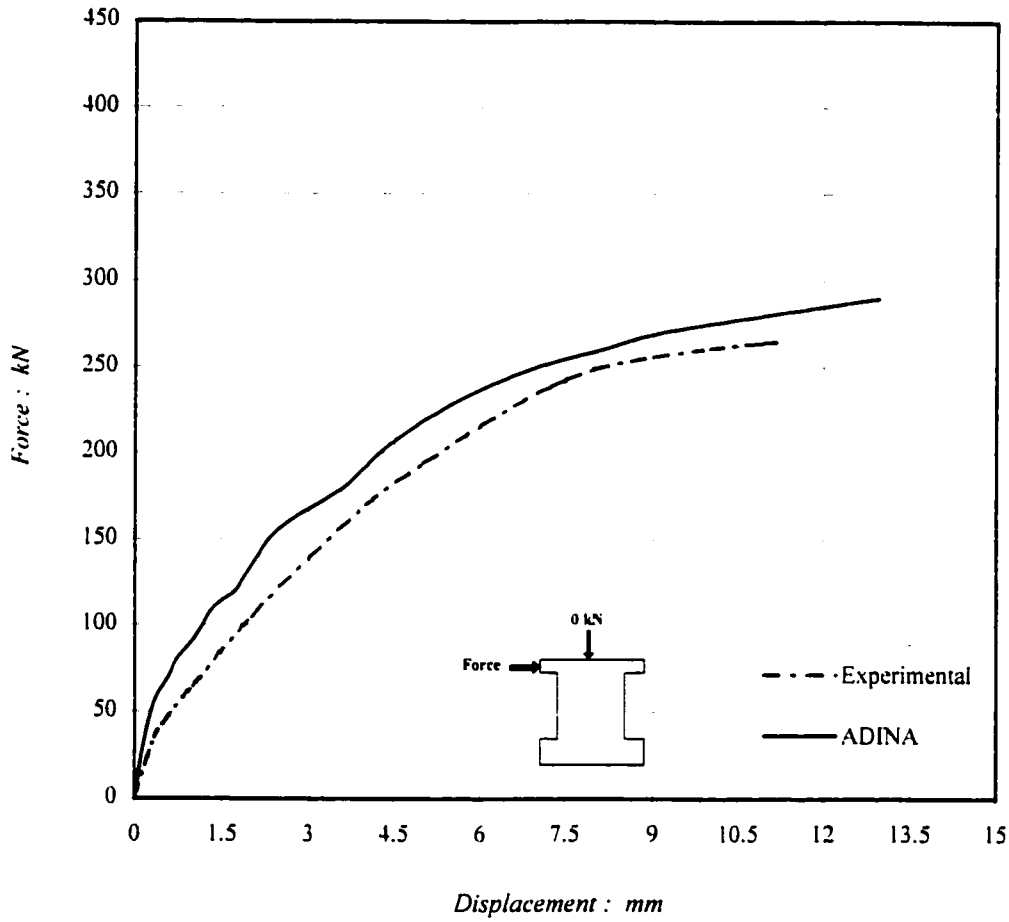

Fig. 4.15 Comparision of experimental and ADINA results for shear wall SW14

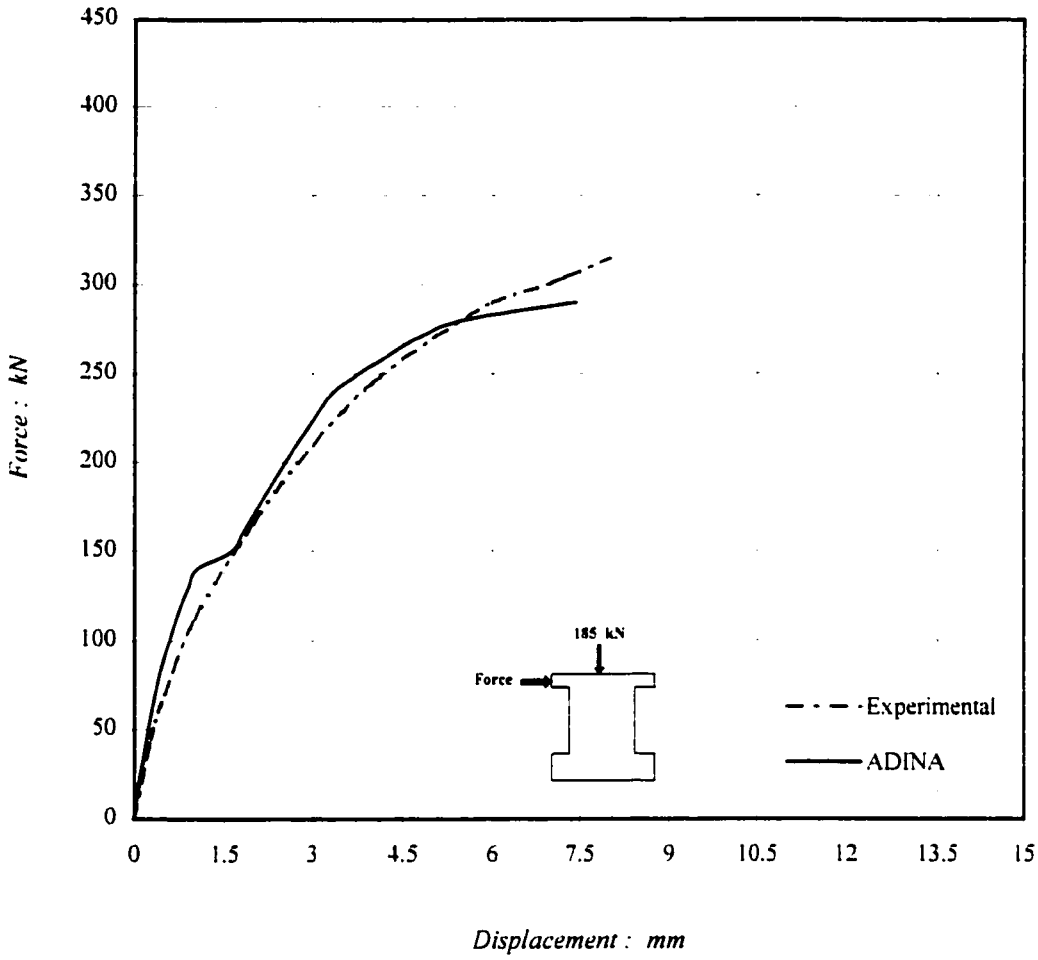

Fig. 4.16 Comparison of experimental and ADINA results for shear wall SW15

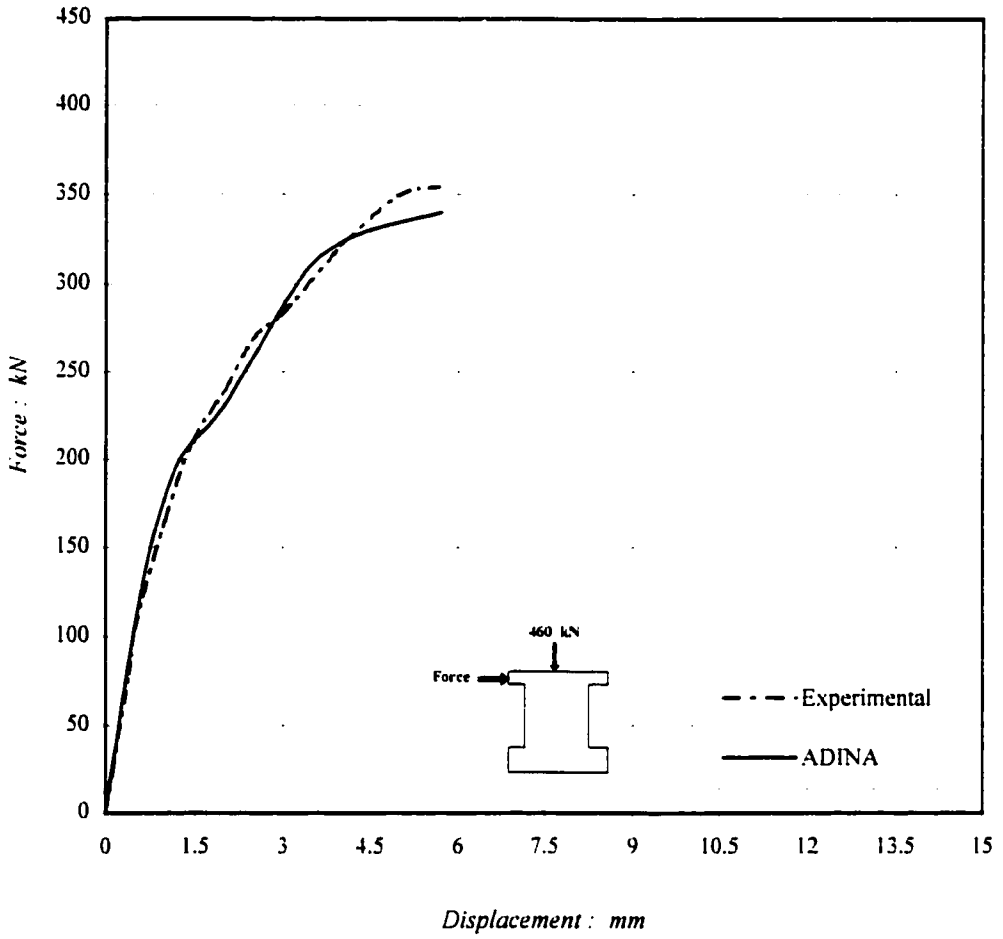

Fig. 4.17 Comparison of experimental and ADINA results for shear wall SW16

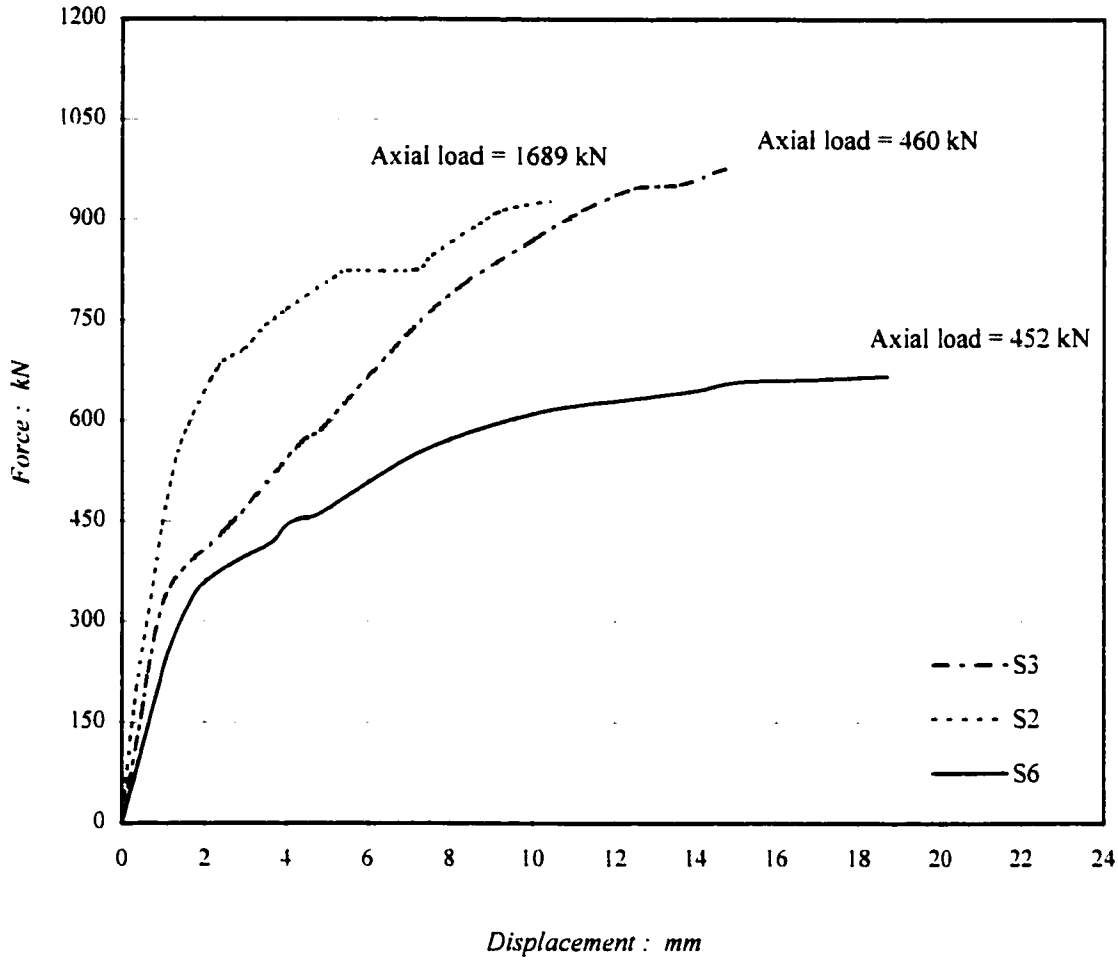

Fig. 4.18 Experimental force-displacement response of shear walls S2, S3 and S6 tested by Maier [25]

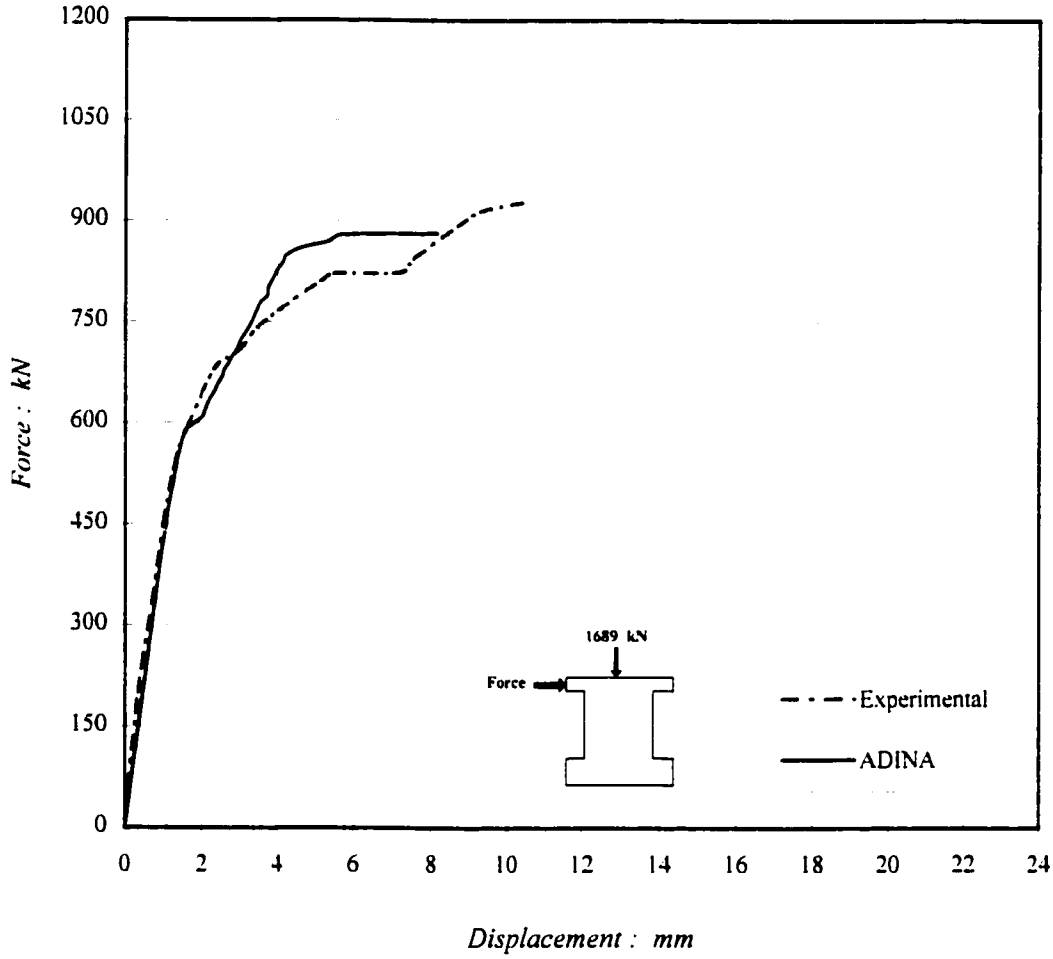

Fig. 4.19 Comparison of experimental and ADINA results for shear wall S2

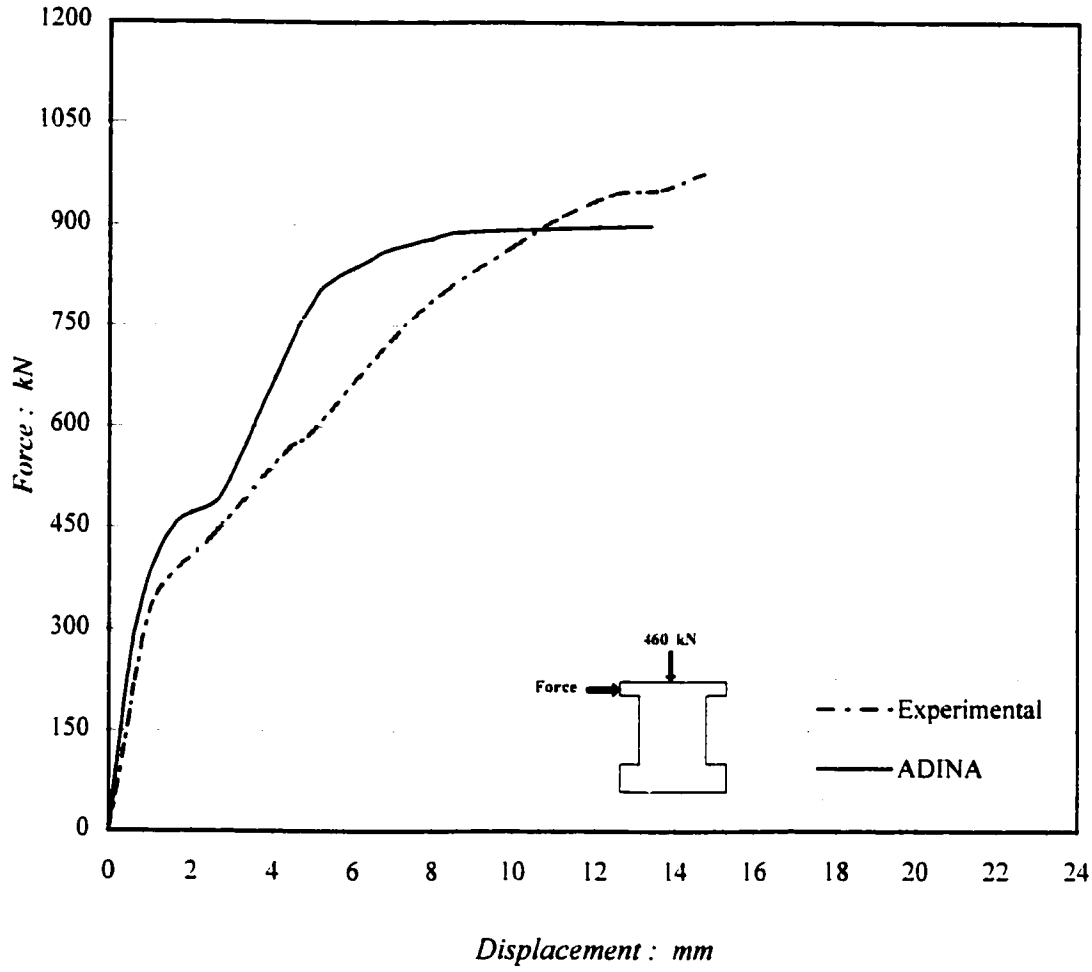

Fig. 4.20 Comparison of experimental and ADINA results for shear wall S3

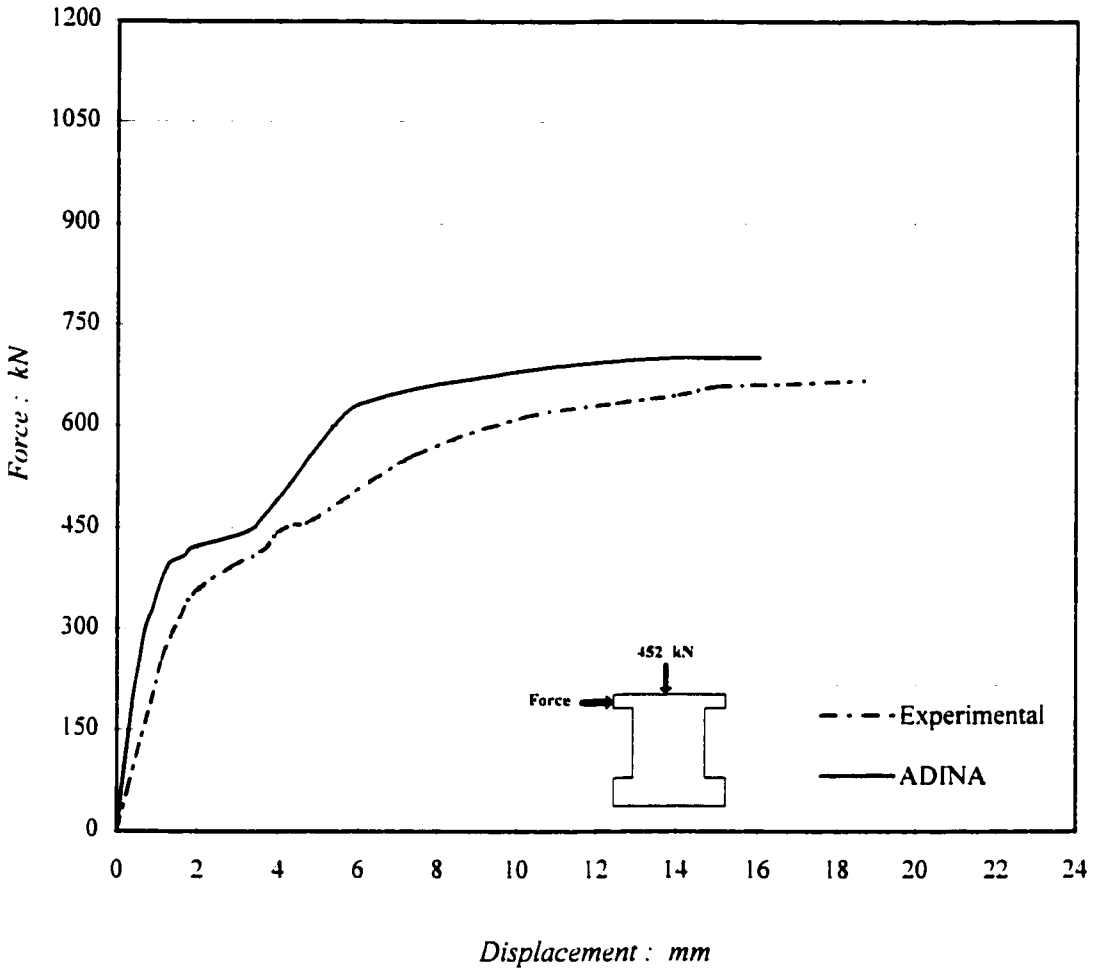

Fig. 4.21 Comparison of experimental and ADINA results for shear wall S6

Chapter 5

Parametric study of shear walls using finite element analysis

5.1 General

Structural applications generally require the consideration of various alternatives before an effective design could be obtained with required nominal dimensions. Therefore, it is important to assess the sensitivity of design parameters on overall behavior of structural components. A parametric investigation was conducted in this research program for low-rise shear walls to establish the significance of design parameters. The finite element program ADINA was used for this purpose. This program allows for nonlinear analysis of shear walls, which is essential for seismic investigation. The applicability of the program to reinforced concrete shear walls was demonstrated in the previous chapter.

The parametric study was carried out using 18 different shear walls, labeled as shear walls N1 through N18. The parameters included the influence of boundary elements,

hoop spacing in boundary elements, reinforcement ratio in boundary elements and in web, concrete strength, steel yield strength, wall aspect ratio, and concrete confinement. The results are presented in this chapter. The discussion of results and comparisons of walls with different design parameters are presented in Chapter 6.

A reference wall was first designed and labeled as shear wall N2. This was done on the basis of CSA standard A23.3-94 [47], using the provisions for ductile shear walls. This wall was used for the purpose of comparison with others. Shear wall N2 had a rectangular cross-section with boundary elements at both ends. This wall was 1200 mm high and 1200 mm wide with an aspect ratio of 1.0. The wall thickness was 150 mm. Fig. 5.1 shows the geometric properties of shear wall N2, including the reinforcement layout. A top beam was designed to transfer the shear force uniformly along the web. A foundation beam was designed to provide full fixity along the base.

The web reinforcement in vertical and horizontal directions, as well as the boundary elements consisted of 10 mm diameter (#10) mild steel. The hoop spacing in boundary elements was 65 mm. The yield strength of steel was 400 MPa and the modulus of elasticity was 200,00 MPa. Steel strain-hardening modulus was assumed to be 10,000 MPa. The reinforcement ratio for vertical and horizontal steel was 0.56%. The steel ratio for longitudinal reinforcement in the boundary elements was 2.2%. The compressive strength of concrete was 35 MPa, with modulus of elasticity of 29,943 MPa. The Poisson's ratio was taken to be 0.15. Stress-strain relationships for unconfined and confined concrete are shown in Fig. 5.2. The Saatcioglu and Razvi model [41] was used for the calculation of confined concrete properties. The loading consisted of a constant normal load of 10%(f'_c x A_g) or 630 kN. The normal load was applied first on the top beam, before the application of monotonically increasing horizontal shear force.

The finite element model consisted of 872 nodes. A total of 800 four-node isoparametric elements were used to model the concrete. Additional 1671 two-node nonlinear truss elements were employed to represent the reinforcing steel. Perfect bond was assumed between the reinforcing steel and surrounding concrete. Full-Newton iteration method

was employed with DTOL=0.5, DNORM=1.0, and ITEMAX=100. The load increment of 10 kN was considered for the application of monotonically increasing lateral load in all cases.

The configurations and specifications of all other walls considered in the parametric investigation were the same as those for shear wall N2, unless otherwise indicated in the following sections. Table 5.1 provides a summary of wall data for the 18 shear walls considered.

5.2 Effect of boundary elements

Shear wall N1 was representative of a rectangular wall without any boundary elements. Fig. 5.3 depicts the details of wall geometry and reinforcement. The dimensions were identical to the reference shear wall N2. Furthermore, the reinforcement ratio in horizontal and vertical directions was the same as that of wall N2 ($\rho_{wx} = \rho_{wy} = 0.56\%$). The only difference between shear walls N1 and N2 was the presence of boundary elements. Force-displacement characteristics of these two walls are compared in Fig. 5.4.

Shear wall N1 failed when the applied shear force reached 440 kN at 7.88 mm top deflection. Shear wall N2, with boundary elements, showed a higher load carrying capacity of 660 kN at a top displacement of 16.9 mm. Figures 5.5 to 5.10 illustrate the crushing and cracking patterns for these walls, as well as strain and stress distributions in horizontal and vertical directions.

5.3 Effect of hoop spacing

The effect of hoop spacing in boundary elements was investigated by analyzing shear walls N2, N3 and N4. The only difference between the walls was the hoop spacing. Shear wall N2 had 65 mm hoop spacing as compared to N3 with 130 mm spacing, and N4 with 195 mm hoop spacing. The variation in hoop spacing resulted in different levels of

concrete confinement in the boundary elements. Fig 5.11 shows stress-strain relationships of confined concrete for shear walls N3 and N4.

Figure 5.12 depicts load-displacement relationships for shear walls N2, N3, and N4. These results indicate that shear wall N3 resisted 630 kN shear force and deflected 14.9 mm before it failed. Shear wall N4 had a reduced ultimate capacity of 610 kN and deflection of 12.7 mm. Both of these walls showed lower strength and ductility as compared to the reference wall (N2). Figures 5.13 to 5.18 show the crack patterns, as well as strain and stress distributions for shear walls N3 and N4.

5.4 Effect of longitudinal reinforcement in boundary elements

The longitudinal reinforcement in boundary elements plays a crucial role on strength and ductility of shear walls. Shear wall N5 had a longitudinal reinforcement ratio of 1.1 %, whereas shear wall N6 had three times the steel, with 3.3% reinforcement. This was the only parameter that changed relative to the reference shear wall N2. The web reinforcement ratio remained at 0.56%, as in the case of shear wall N2. The hoop spacing also remained constant at 65 mm.

The force-displacement behaviors of these walls are compared in Fig. 5.19. The load capacity of shear wall N5 was 542.5 kN at 16.1 mm displacement. Shear wall N6 resisted 692.5 kN before failure at a top displacement of 13.64 mm. Figures 5.20 to 5.22 and 5.23 to 5.25 illustrate the cracking and crushing patterns, the strain and stress distributions during the final stage of loading, respectively.

5.5 Effect of horizontal web reinforcement

Shear walls N7 and N8 were analyzed to investigate the significance of horizontal reinforcement ratio on shear wall behavior. These walls were designed to have either one half or twice the horizontal steel used in wall N2. In other words, the horizontal reinforcement ratio for shear wall N7 and N8 were 0.28% and 1.1%, respectively. The vertical reinforcement ratio remained the same as that for shear wall N2.

Fig. 5.26 depicts the comparison of shear walls N2, N7, and N8. Accordingly, shear wall N7 resisted 600 kN lateral load at 11.54 mm top horizontal displacement. When the horizontal reinforcement ratio was 1.1% (N8), the ultimate load capacity was 700 kN with 14.93 mm horizontal displacement. Figures 5.27 to 5.32 show the crack configurations, as well as strain and stress distributions in shear walls N7 and N8.

5.6 Effect of vertical web reinforcement

Flexural reinforcement plays an important role on the capacity of low-rise shear walls. The effect of vertical reinforcement was studied by analyzing shear walls N9 and N10. The vertical reinforcement ratio assigned to N9 and N10 were 0.28% and 1.1%, respectively. The other parameters remained the same as those used for shear wall N2. As a result, the effect of vertical reinforcement was reflected in the overall behavior of shear walls N9 and N10.

Load-displacement characteristics of shear walls N2, N9, and N10 are shown in Fig. 5.33. Shear wall N9 had an ultimate load capacity of 647.5 kN at 18.49 mm top deflection when it was subjected to a normal force of 630 kN. When vertical reinforcement ratio was 1.1%, the shear wall (N10) showed 701.25 kN lateral load capacity at 15.34 mm displacement. Figs. 5.34 to 5.39 show the crushing and cracking patterns as well as the strain and stress distributions of these walls at the ultimate load step.

5.7 Effect of concrete strength

The effect of concrete strength was studied by analyzing shear wall N11. This wall had 50 MPa concrete, in comparison with N2 with 35 MPa. All other parameters remained the same as those for the reference shear wall N2. The stress-strain relationship of concrete for shear wall N11 is illustrated in Fig. 5.40.

The behavior of shear wall N11 is shown in Fig. 5.41. When the compressive strength of concrete was increased to 50 MPa, the ultimate load capacity of wall reached 750 kN at 20.48 mm top deflection. Figs. 5.42 to 5.44 illustrate the crack patterns for shear wall N11 during the ultimate stage of loading, as well as the internal strain and stress distributions.

5.8 Effect of steel yield strength

In this part of the study the influence of yield strength of reinforcing steel was investigated when the reinforcement configuration and ratio remained constant in both horizontal and vertical directions. The yield strength of all steel bars was 600 MPa in shear wall N12. This value was increased to 800 MPa in shear wall N13.

The behavior of walls N12 and N13 are compared in Fig. 5.45. Shear wall N12 failed at a top deflection of 14.25 mm. The ultimate lateral load capacity was 731.25 kN. Shear wall N13 resisted 770 kN force at 13.4 mm top deflection. Figs. 5.46 to 5.51 illustrate the crack configuration, stress and strain distributions for shear walls N12 and N13.

5.9 Effect of axial load

One of the important factors that affect the behavior of shear walls is the level of normal force. Two shear walls were analyzed and compared with shear wall N2 for this purpose.

Shear wall N14 was subjected only to lateral loading, with zero axial force. A companion shear wall (N15) was subjected to twice the reference shear wall (N2), or 1260 kN axial load. The axial load was applied on the top beam, and was kept constant while the lateral load was applied in increments. All other parameters remained the same as those of the reference shear wall N2.

The ultimate load capacity for shear walls N14 was 555 kN at 18.94 mm top deflection. This is illustrated in Fig. 5.52. Shear wall N15 failed when the applied shear force reached 690 kN, corresponding to 6.08 mm top deflection. The cracking and crushing patterns, as well as the strain and stress distributions for shear walls N14 and N15 are presented in Figs. 5.53 to 5.58.

5.10 Effect of wall aspect ratio

The aspect ratio of a shear wall is an important parameter that dictates the mode of behavior of the wall. Since the focus of this research was on low-rise shear walls, aspect ratios of less than or equal to one were investigated. The aspect ratio, which is defined as the ratio of wall height to wall width, was 0.75 for shear wall N16. The same ratio was 0.5 in shear wall N17. The reinforcement ratio and other parameters were kept constant at the same level as those for the reference shear wall N2.

Fig. 5.59 illustrates the overall behavior of shear walls N16 and N17. As shown in this graph, shear wall N16, with an aspect ratio of 0.75 resisted 740 kN force at a deflection of 6.47 mm before it failed. Shear wall N17, with an aspect ratio of 0.5 showed an increased lateral load capacity of 970 kN at 3.80 mm top displacement. Figs. 5.60 to 5.65 depict the stress and strain distributions, as well as crack patterns for shear walls N16 and N17.

5.11 Effect of concrete confinement

The last shear wall did not have any effect of concrete confinement in boundary elements. This was labeled as shear wall N18 with the same concrete properties assigned to the boundary elements as those used for the web. All other parameters remained the same as those for the reference shear wall N2.

Load-displacement results from shear wall N18 showed that when the effect of confinement was ignored the ultimate lateral load capacity of the shear wall was 565 kN at 10.88 mm top deflection. Figs. 5.67 to 5.69 depict the strain and stress distributions, as well as the cracking and crushing patterns for shear wall N18. Furthermore, the observed failure modes of shear walls N1 to N18 are presented in Table 5-2.

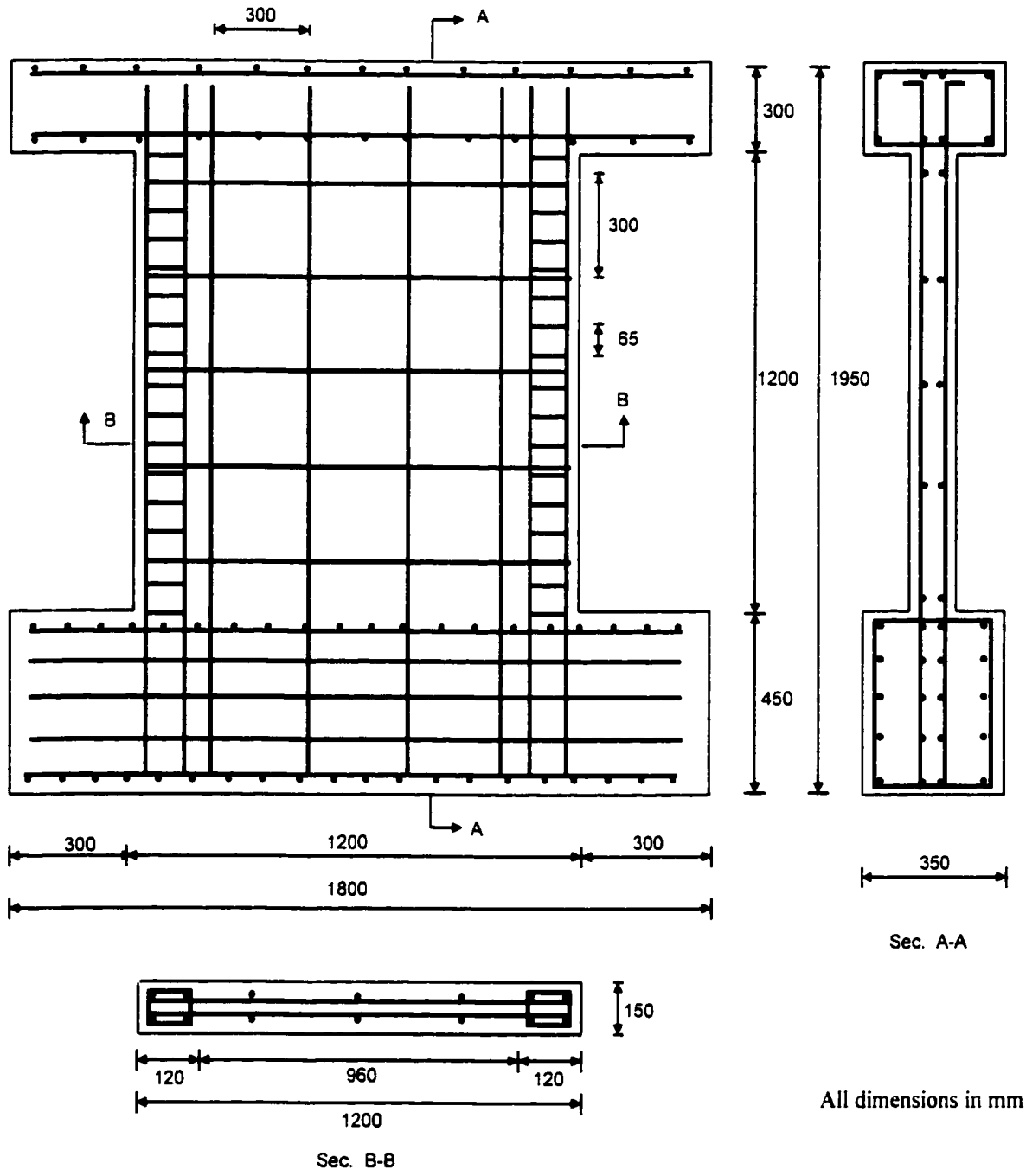

Fig. 5.1 Geometry and reinforcement details of shear wall N2

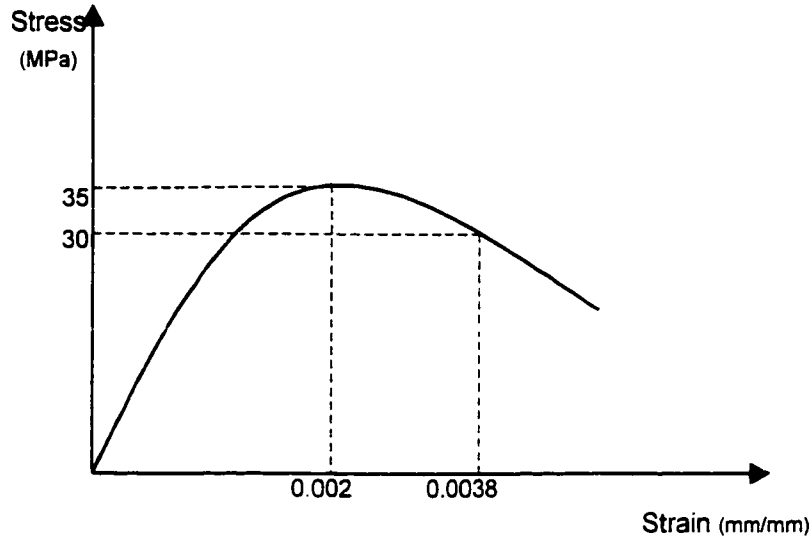

(a) Unconfined concrete

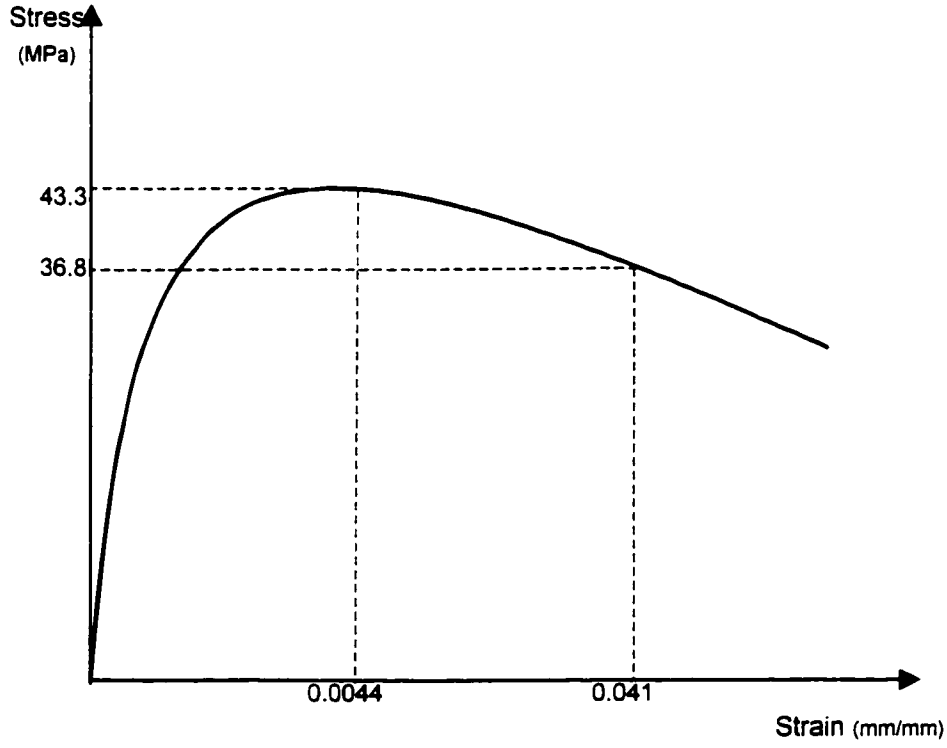

(b) Confined concrete

Fig. 5.2 Stress-strain relationship of concrete for shear wall N2

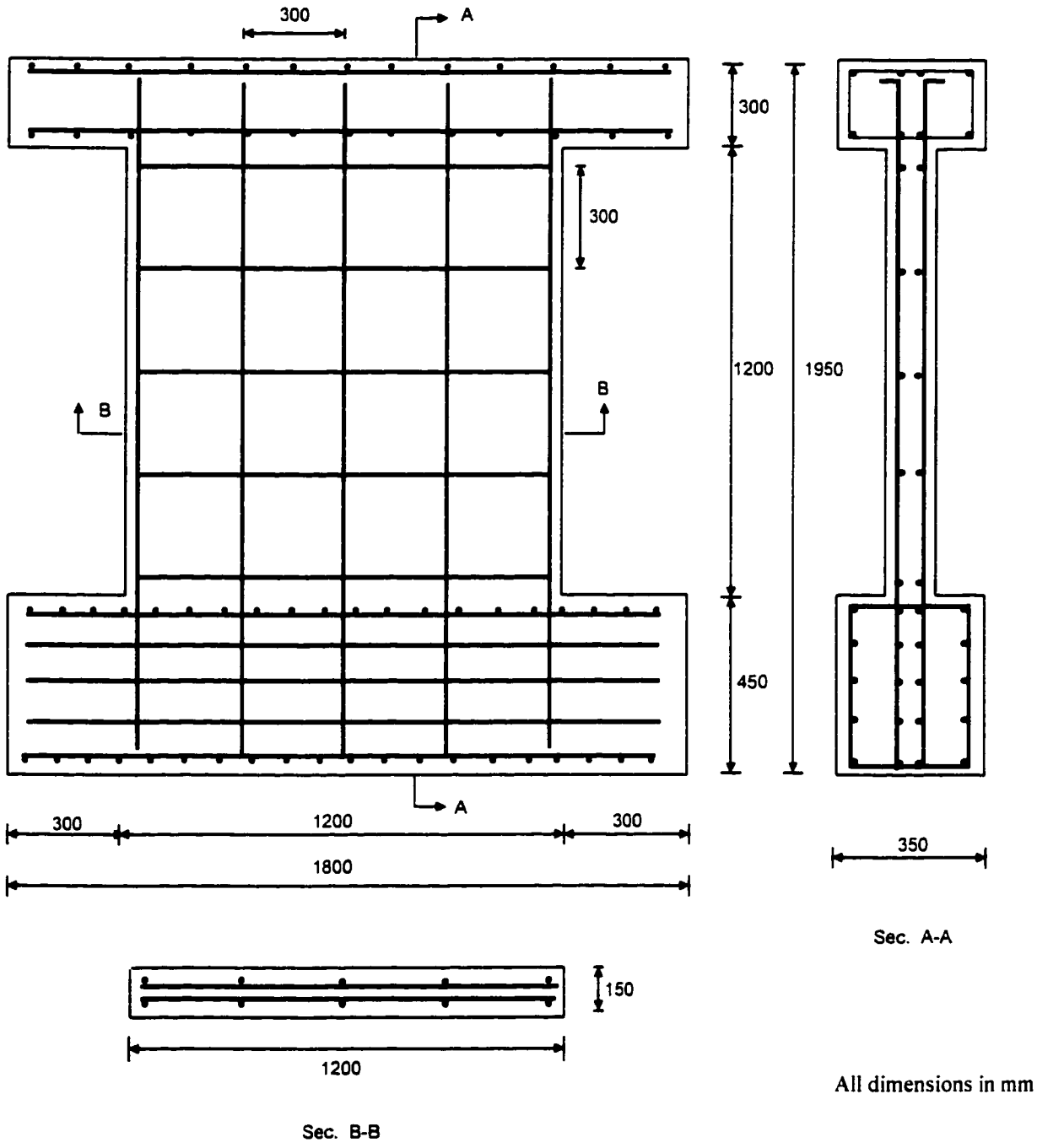

Fig. 5.3 Geometry and reinforcement details of shear wall N1

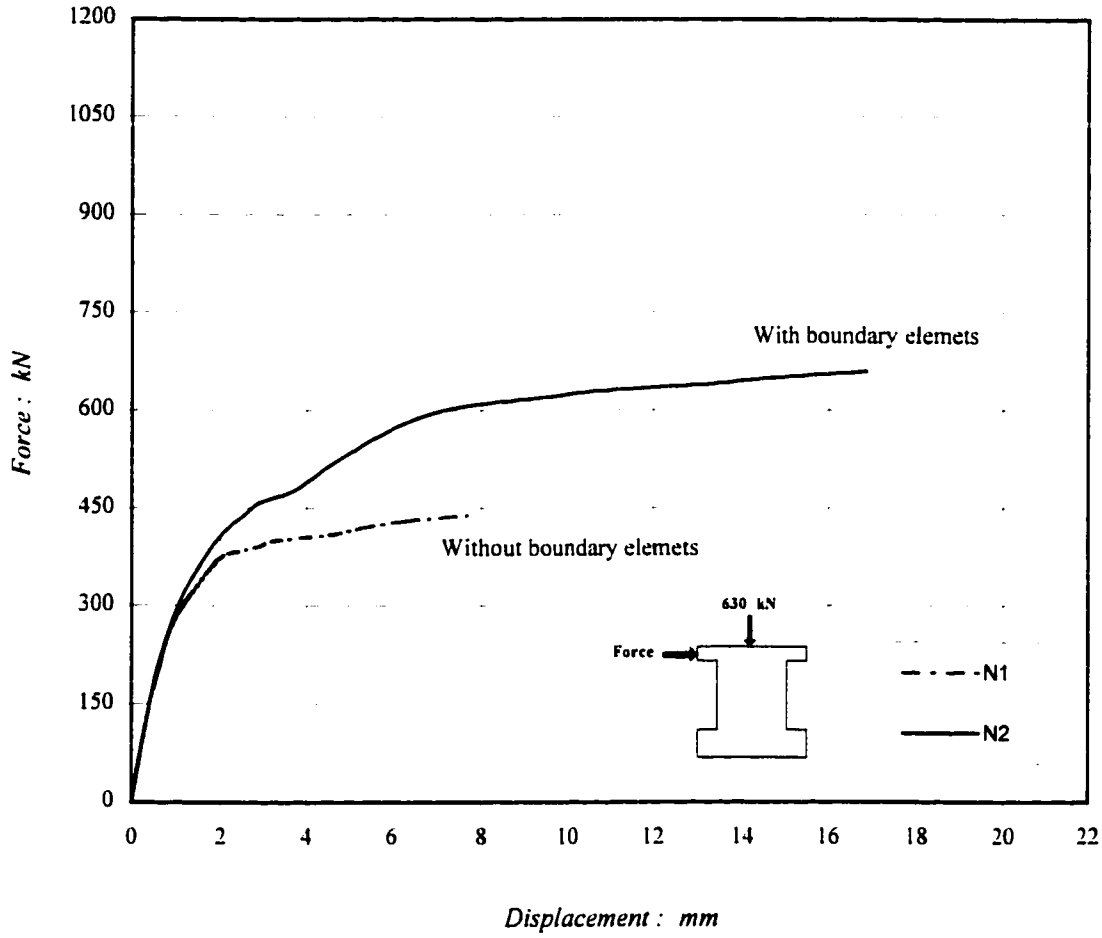

Fig. 5.4 Load-displacement response of shear walls N1 and N2

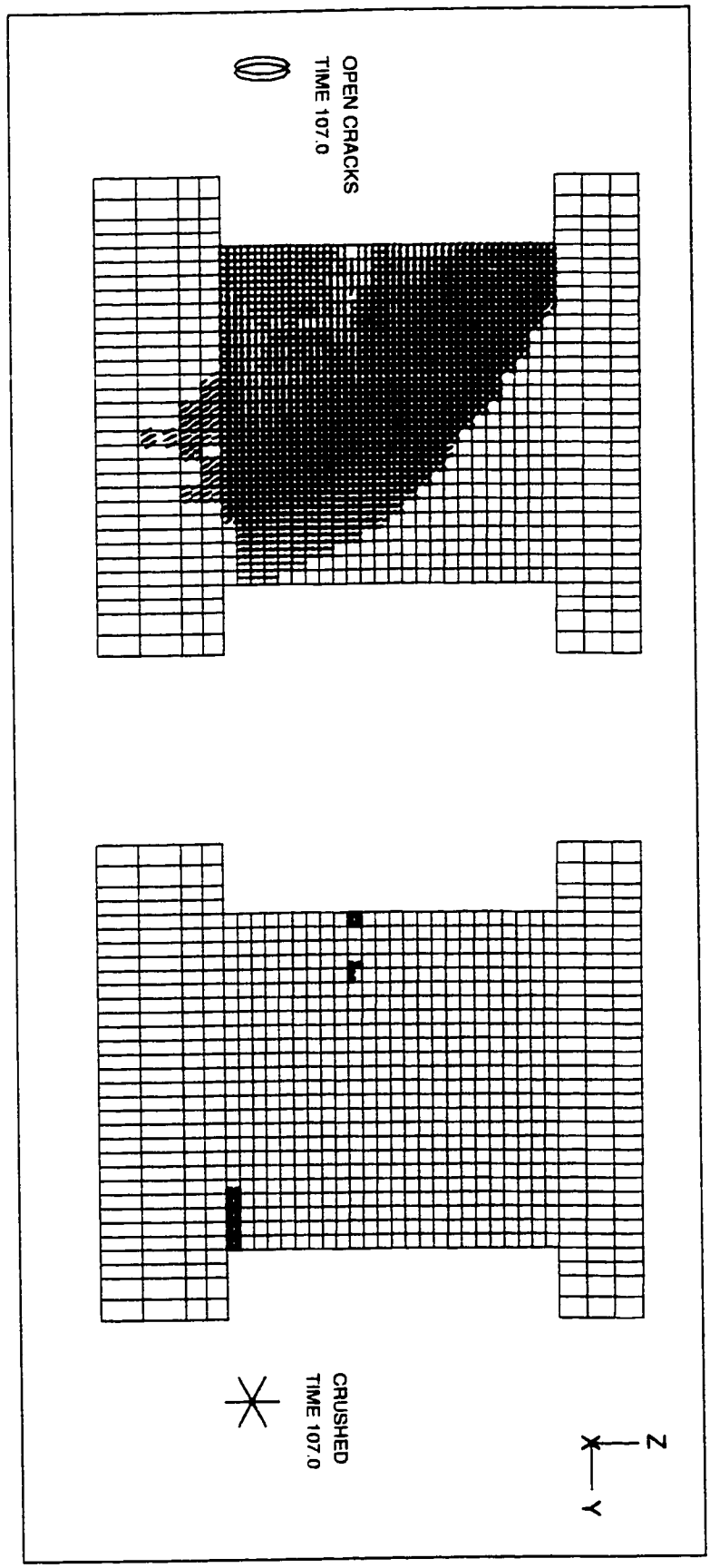

Fig. 5.5 Cracking and crushing pattern of shear wall N1

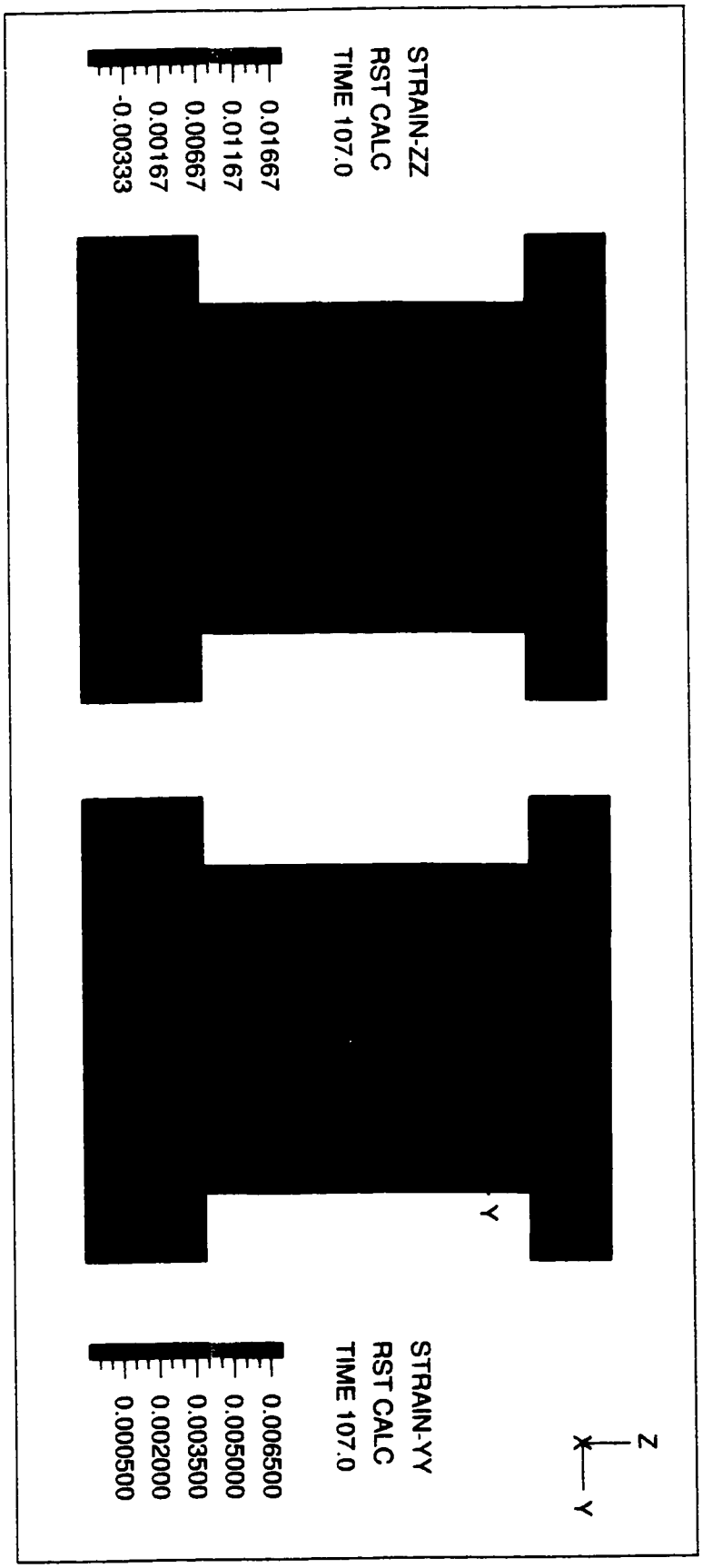

Fig. 5.6 Strain distribution of shear wall N1

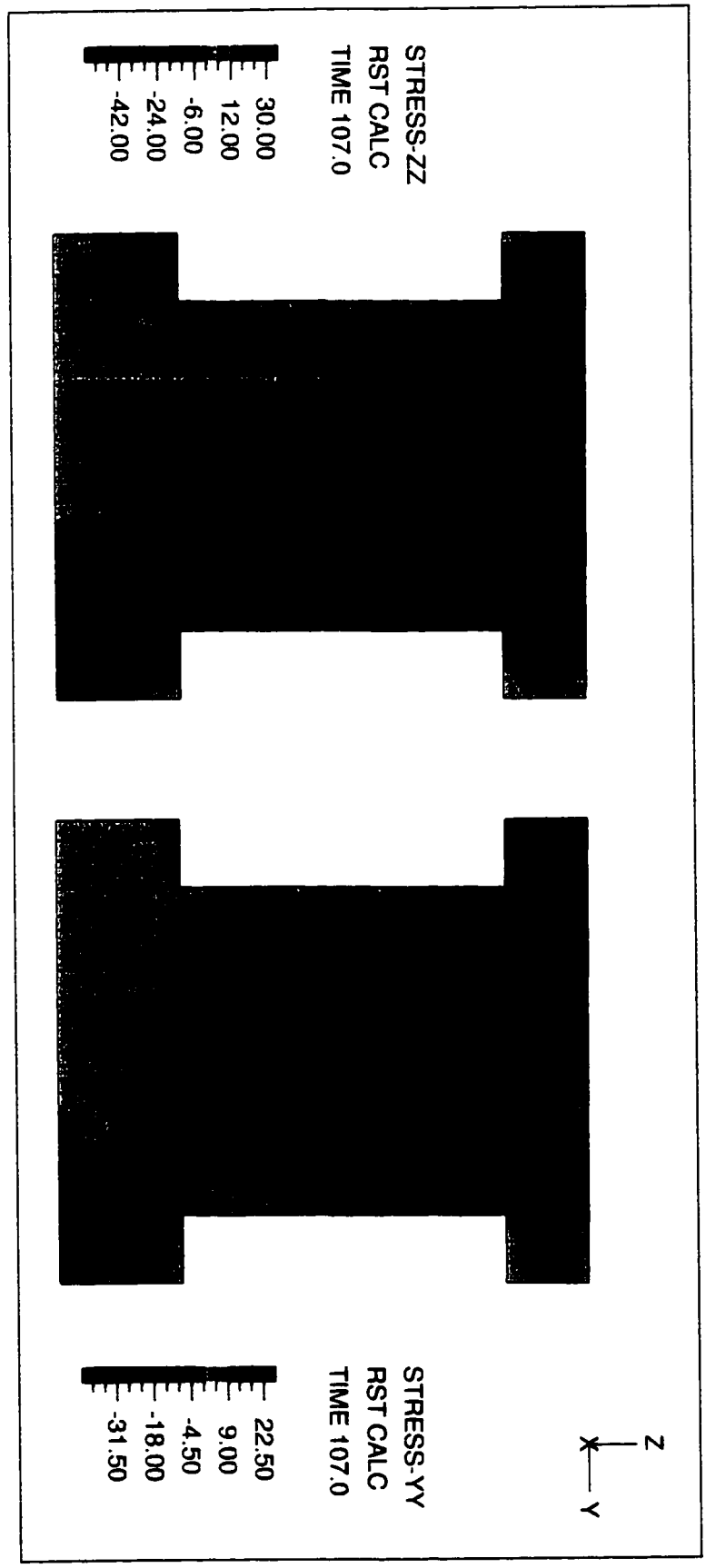

Fig. 5.7 Stress distribution of shear wall N1

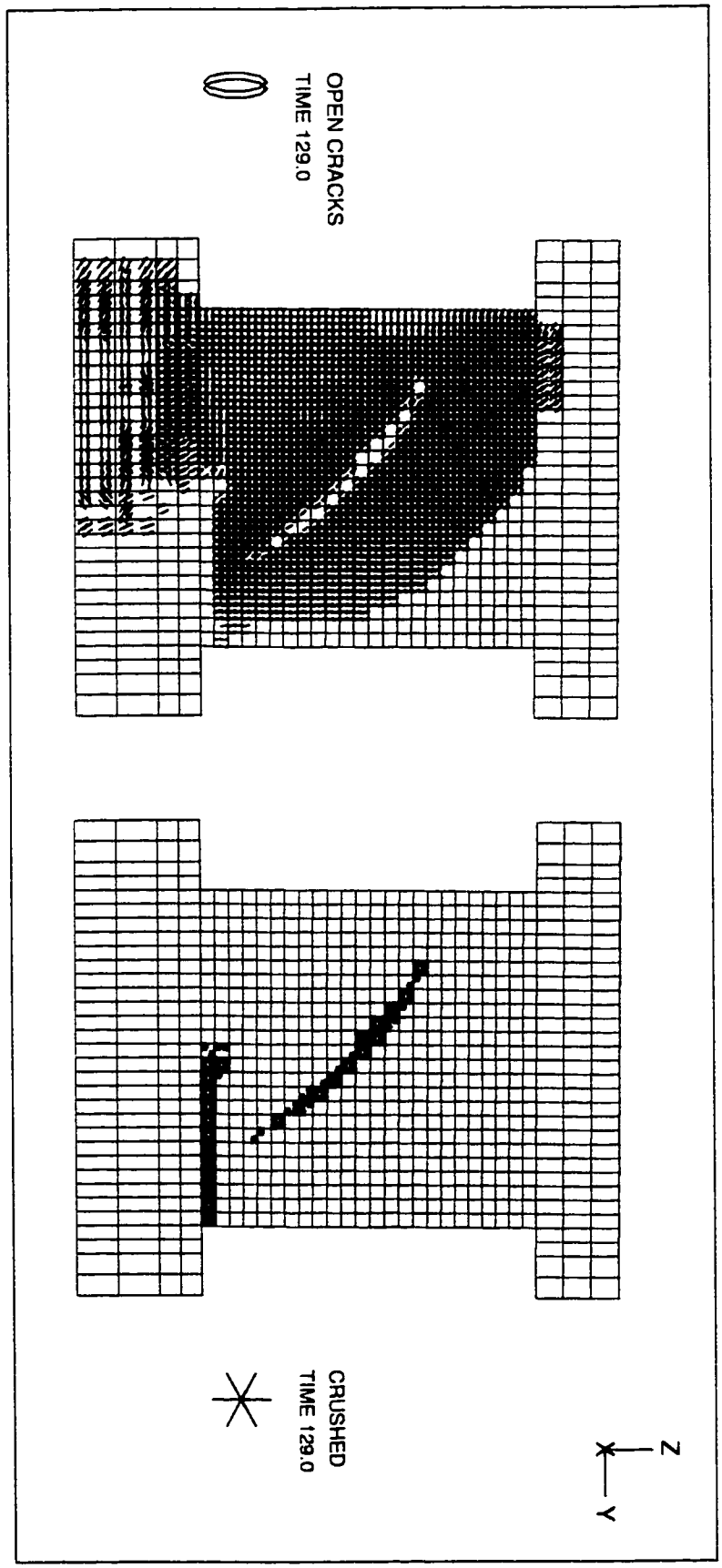

Fig. 5.8 Cracking and crushing pattern of shear wall N2

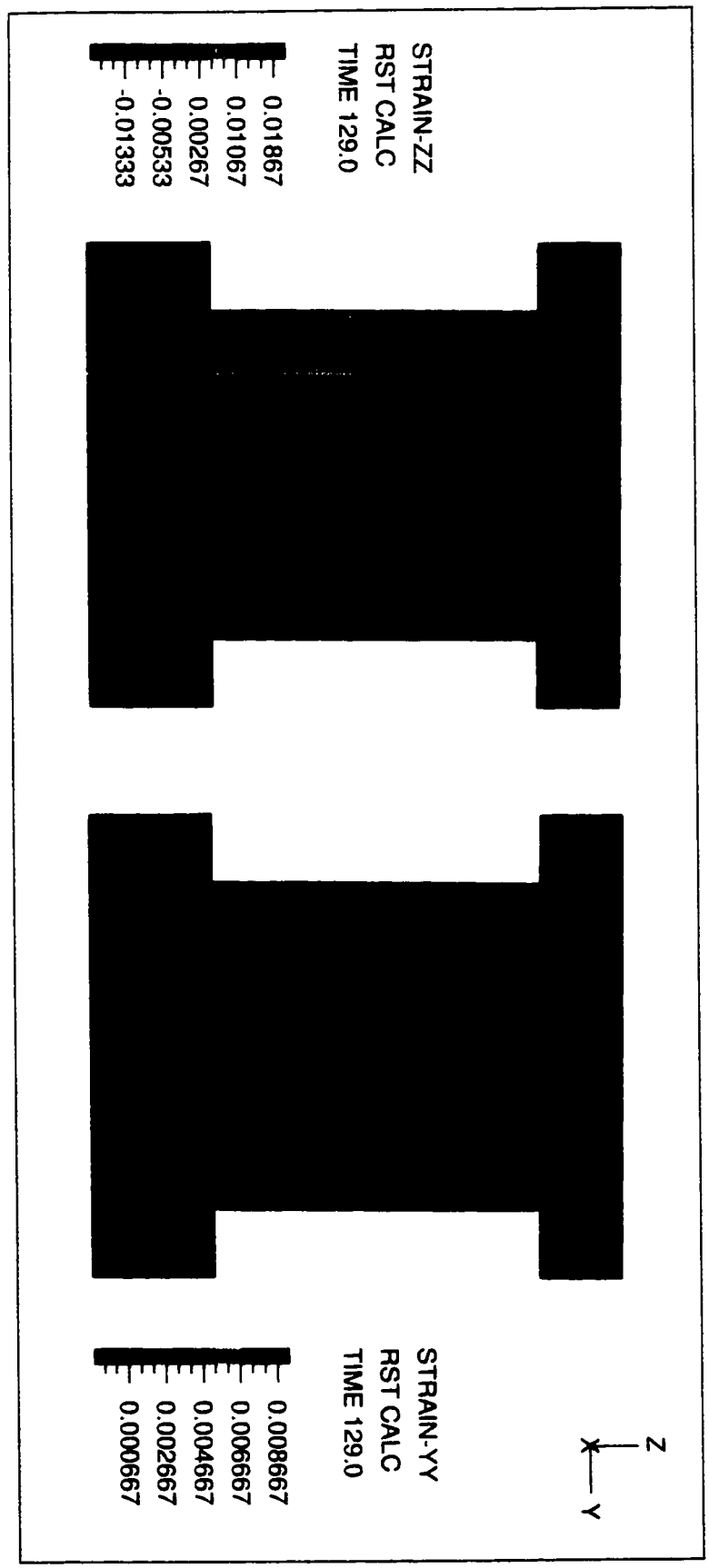

Fig. 5.9 Strain distribution of shear wall N2

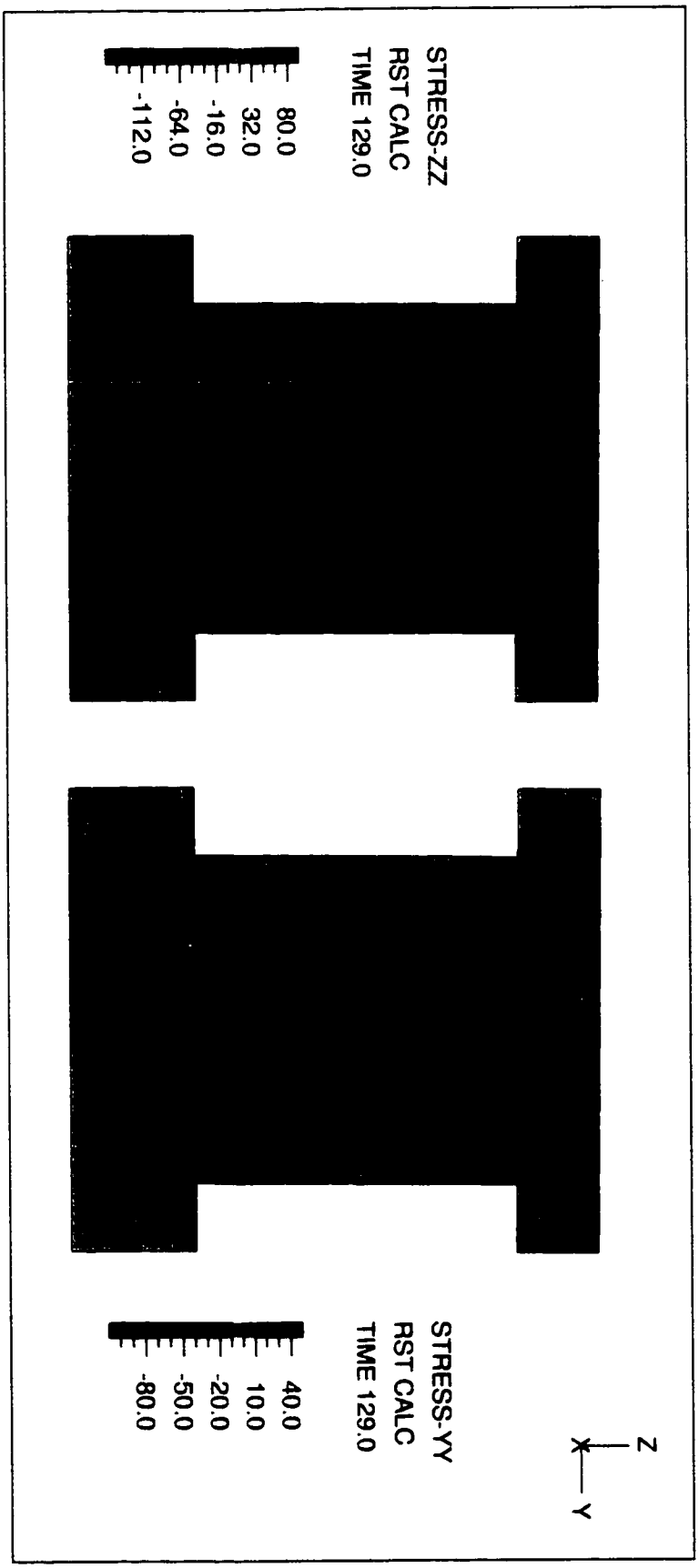

Fig. 5.10 Stress distribution of shear wall N2

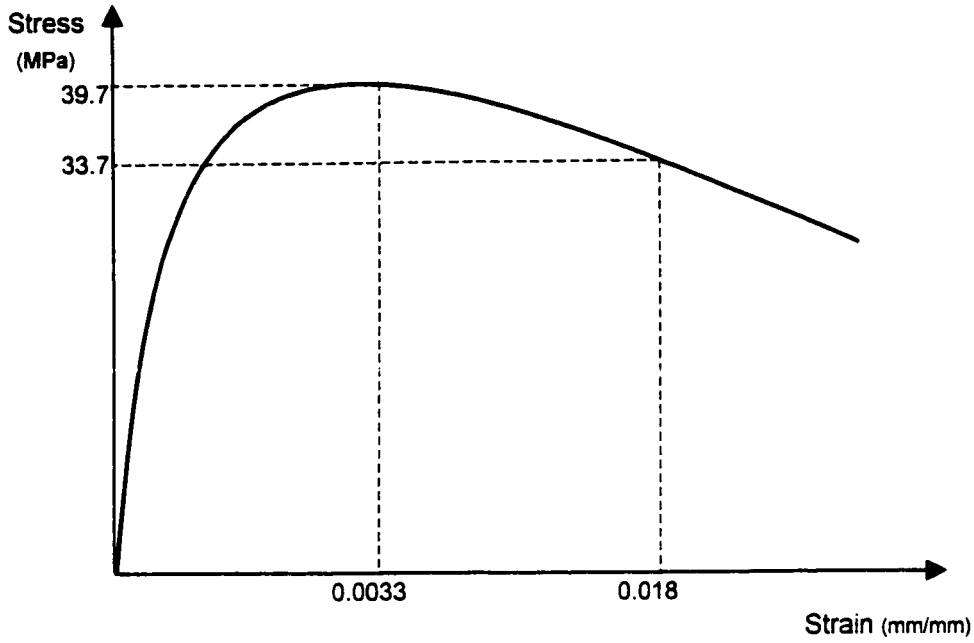

(a) Shear wall N3

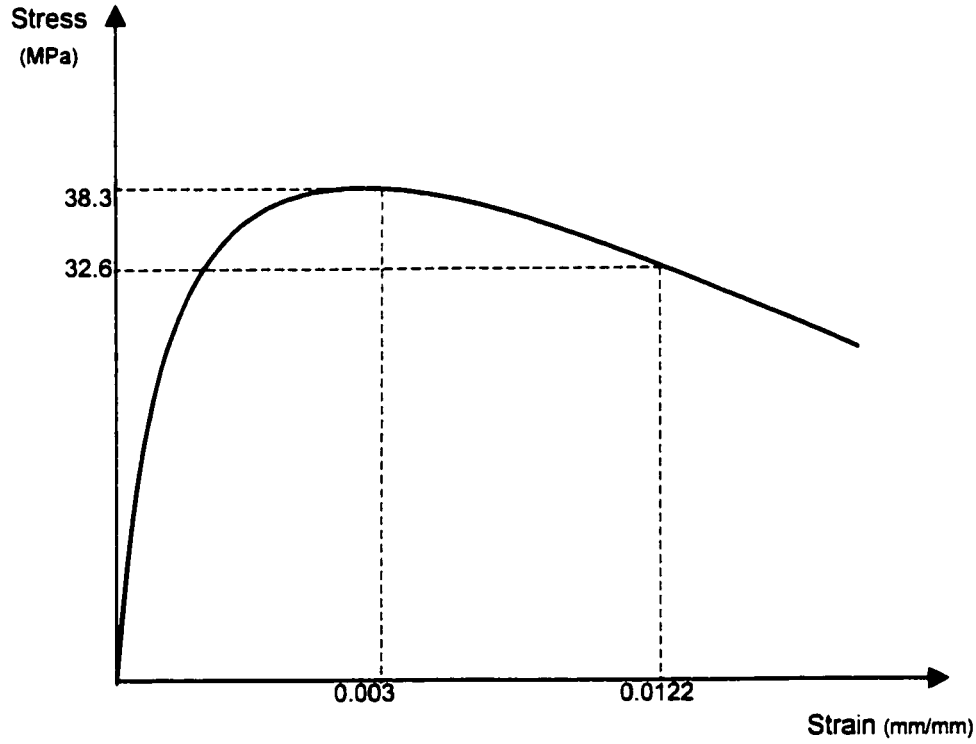

(b) Shear wall N4

Fig. 5.11 Stress-strain relationship of confined concrete for shear walls N3 and N4

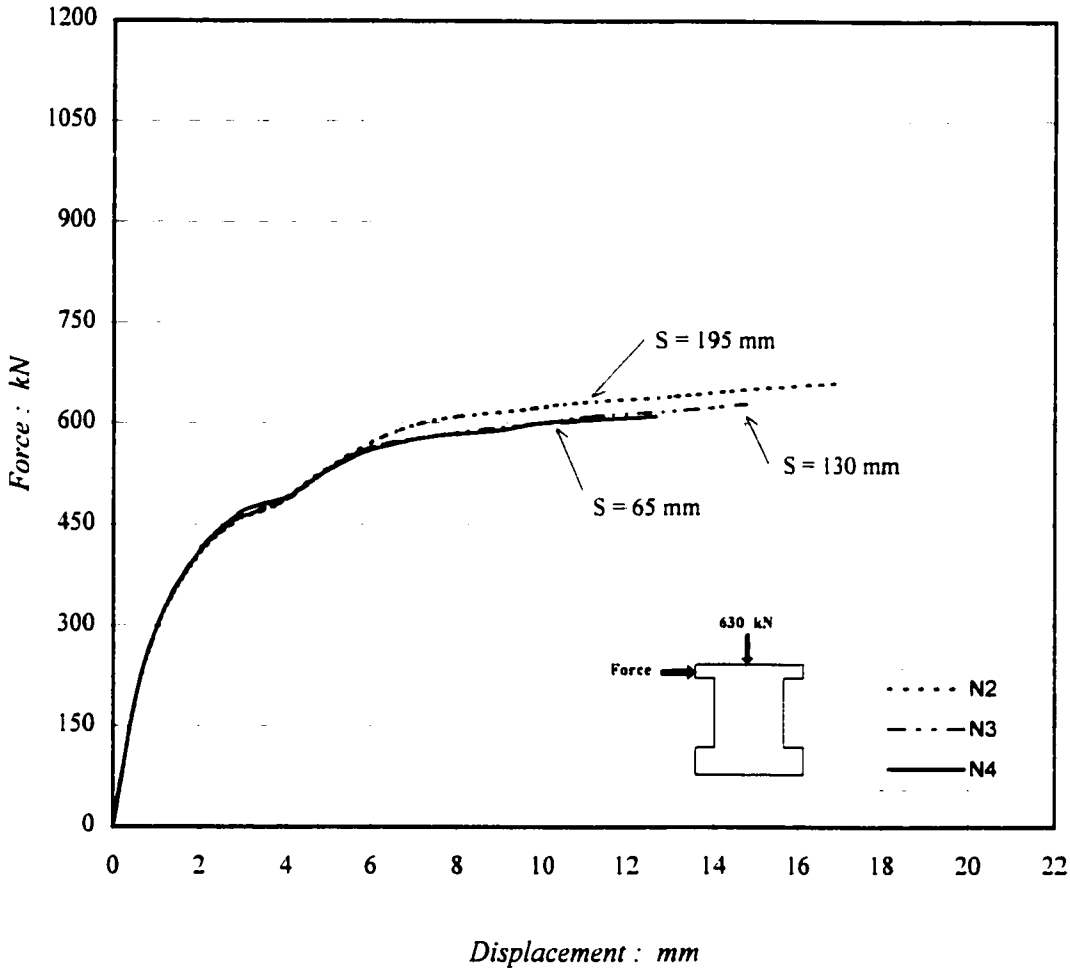

Fig. 5.12 Load-displacement response of shear walls N2, N3 and N4

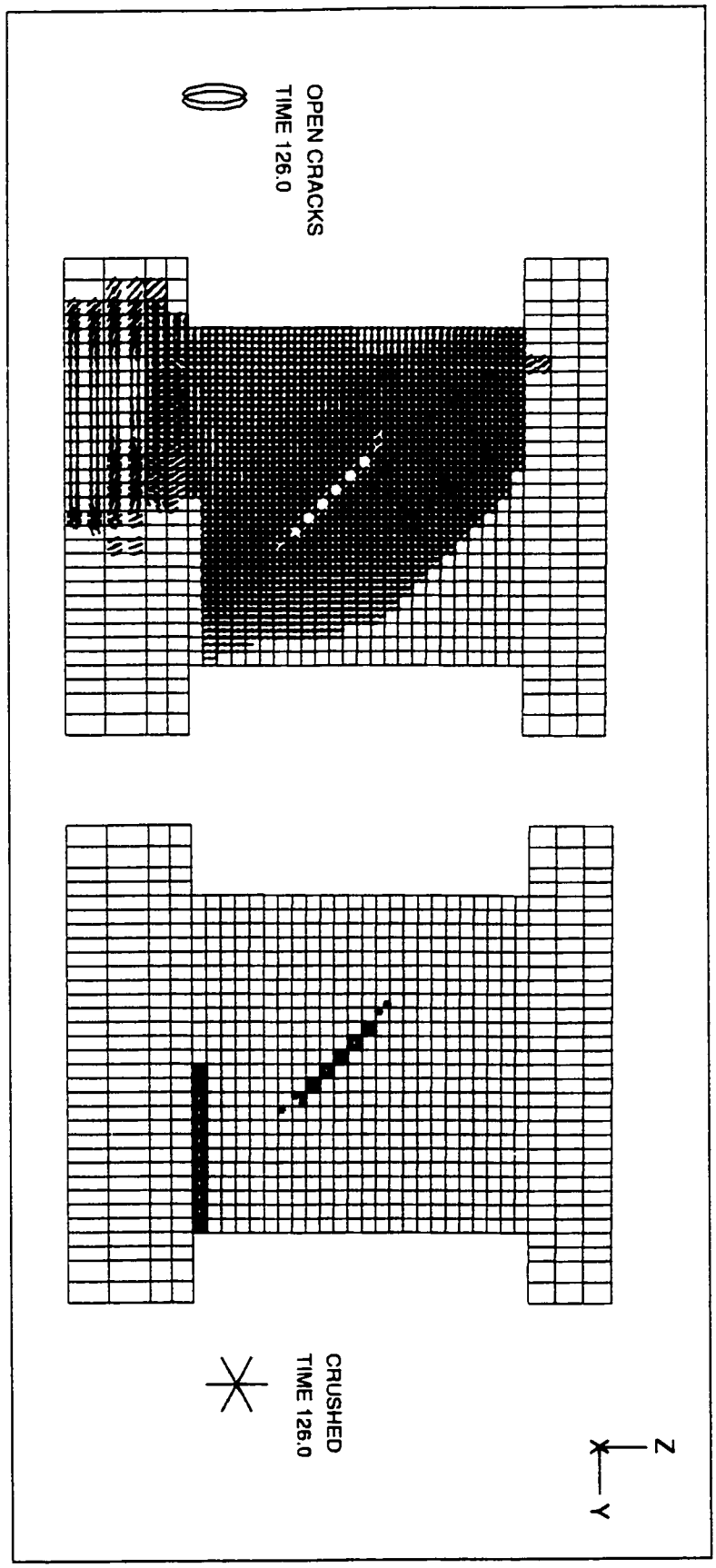

Fig. 5.13 Cracking and crushing pattern of shear wall N3

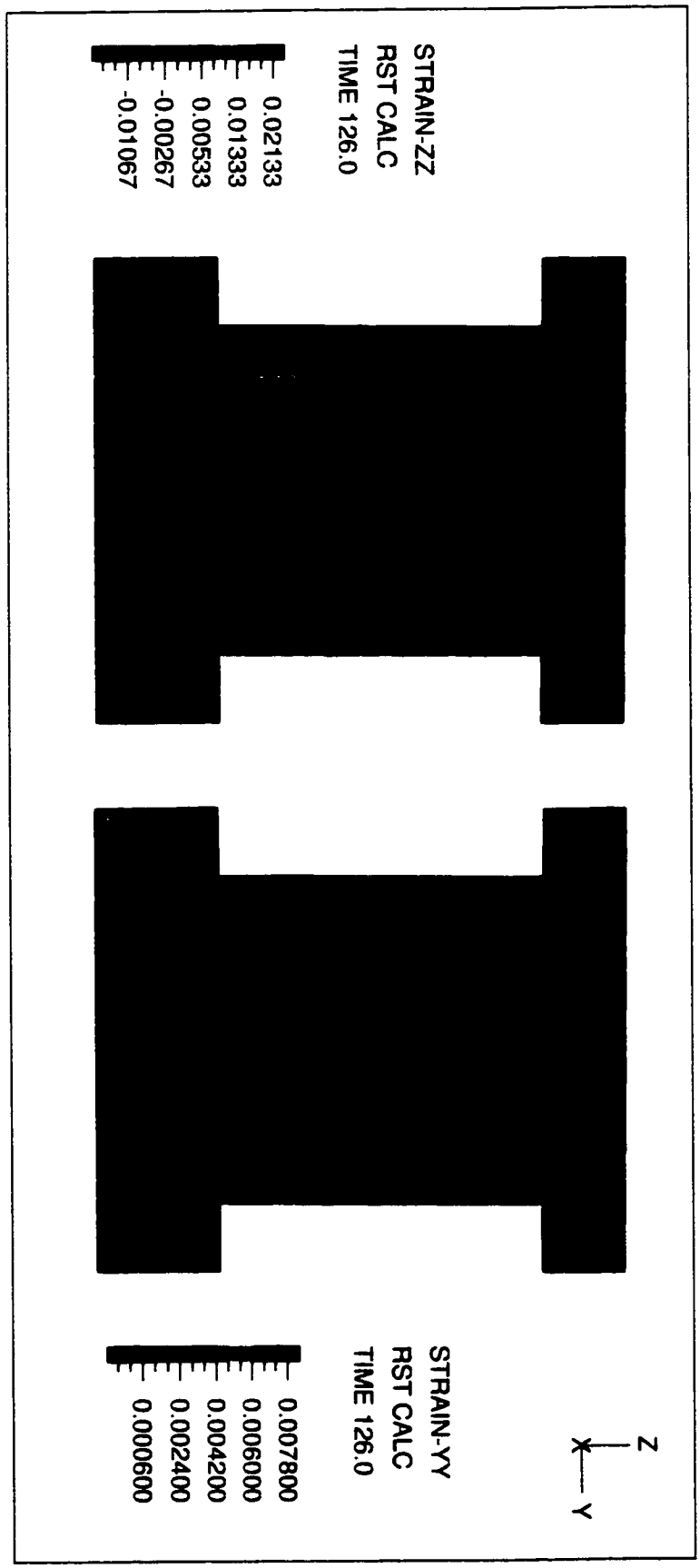

Fig. 5.14 Strain distribution of shear wall N3

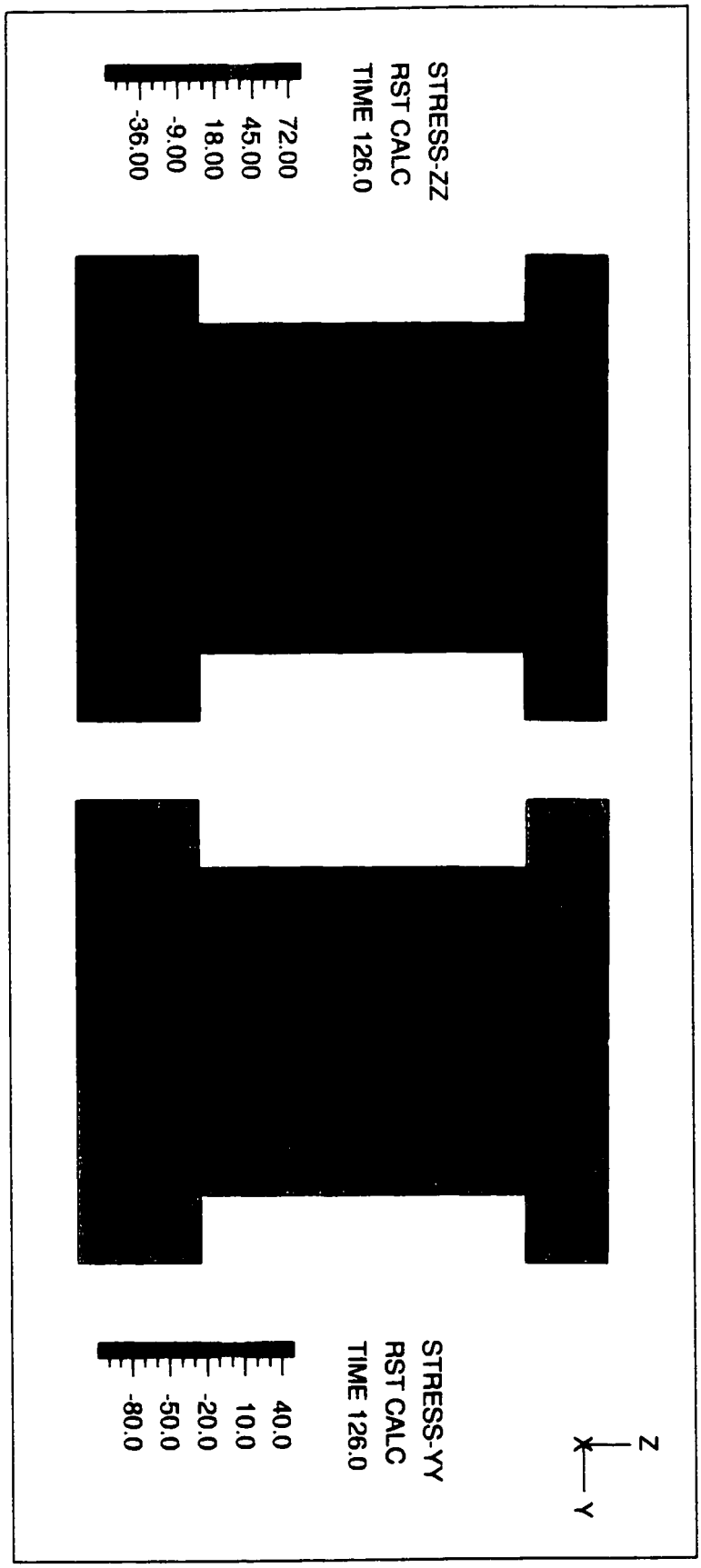

Fig. 5.15 Stress distribution of shear wall N3

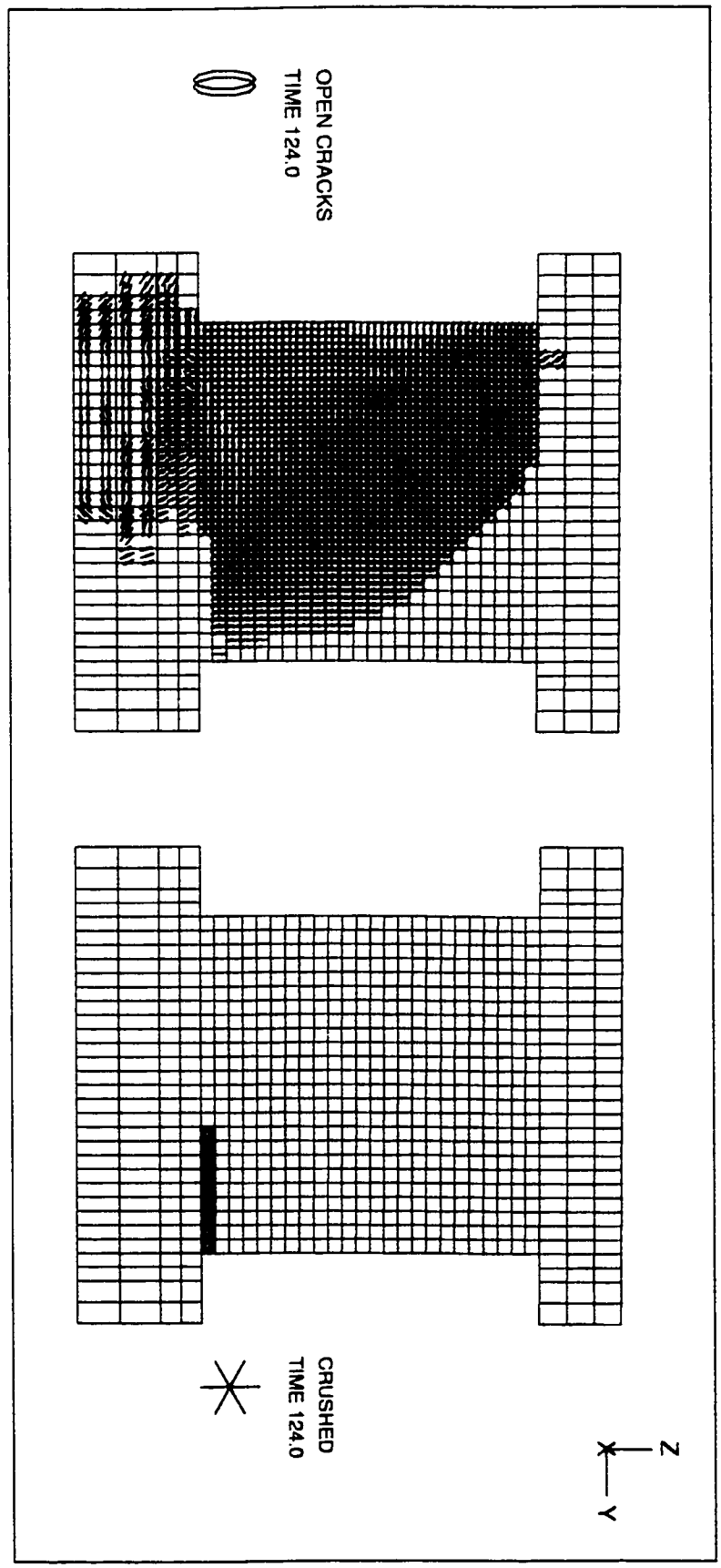

Fig. 5.16 Cracking and crushing pattern of shear wall N4

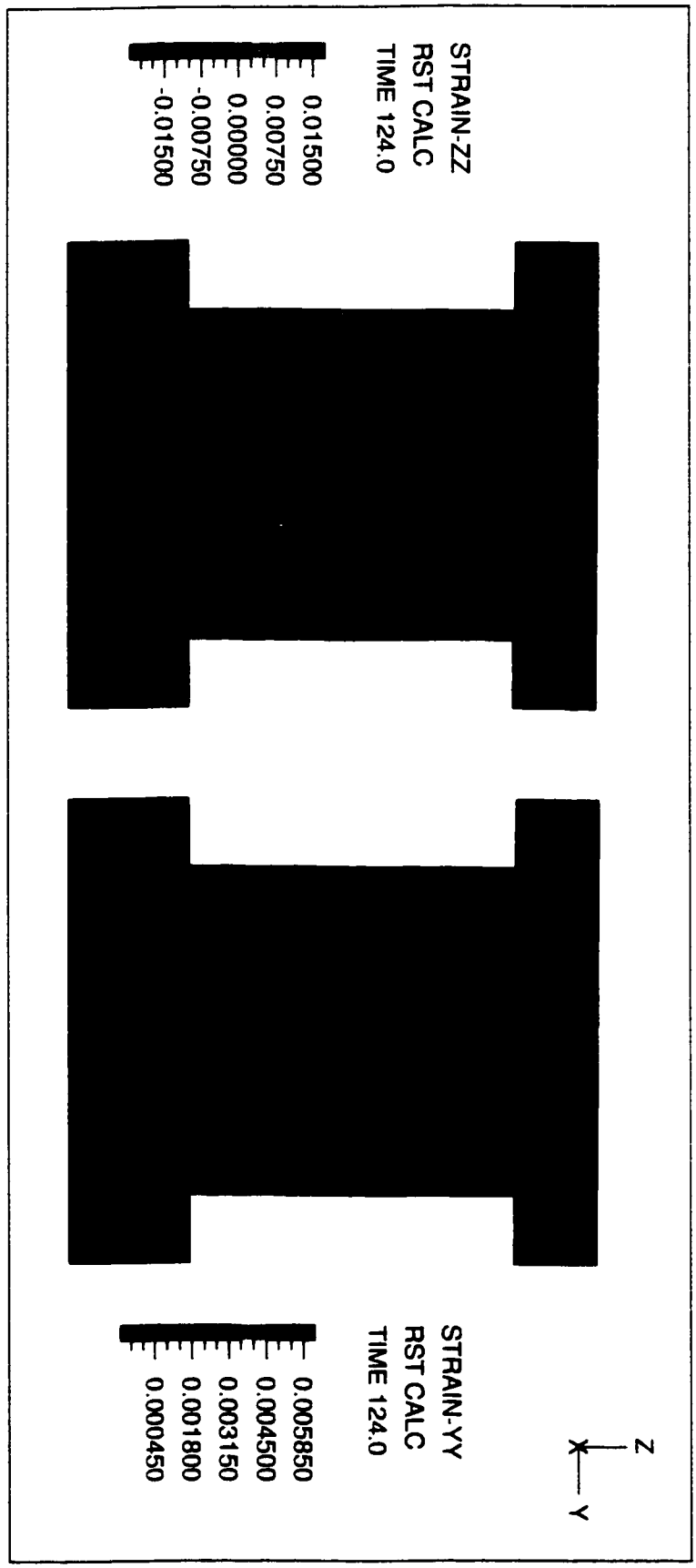

Fig. 5.17 Strain distribution of shear wall N4

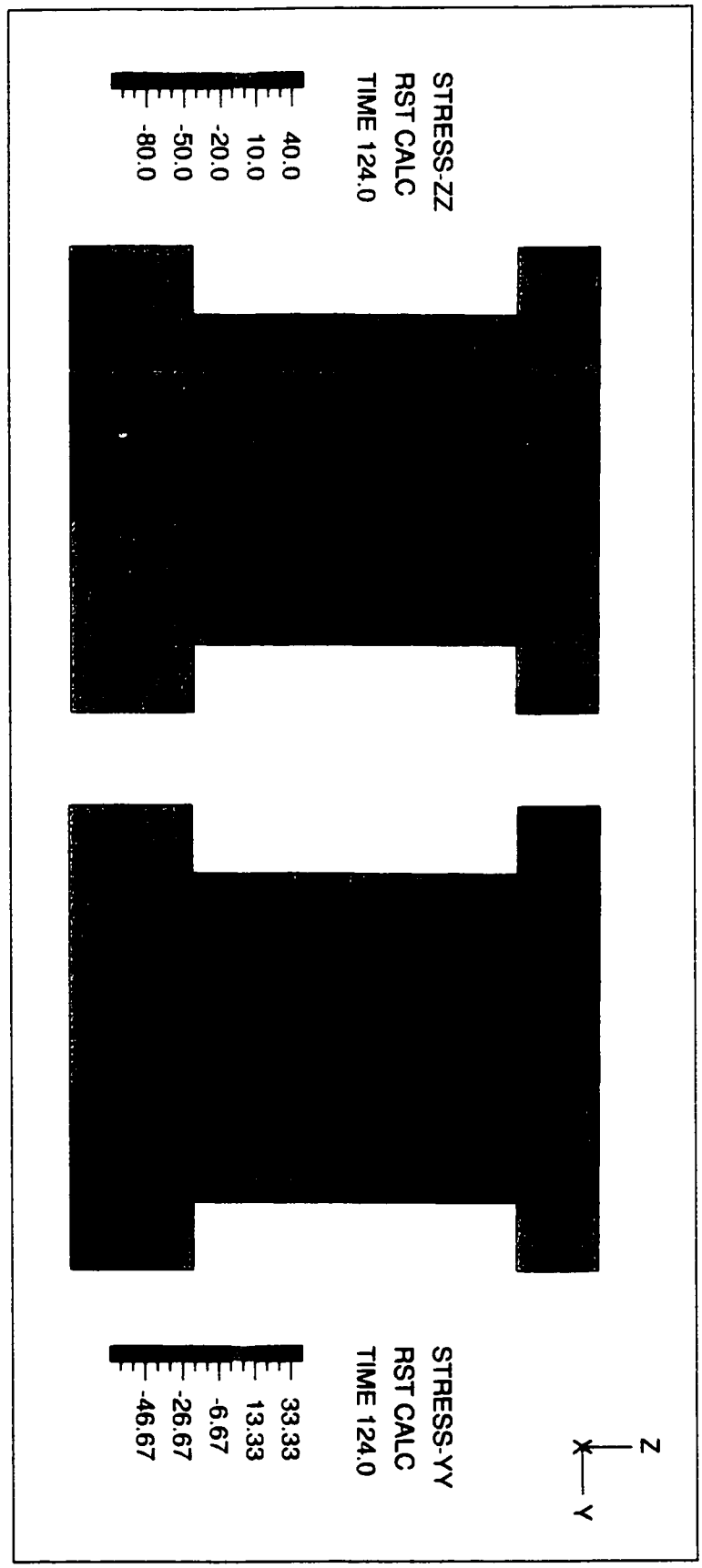

Fig. 5.18 Stress distribution of shear wall N4

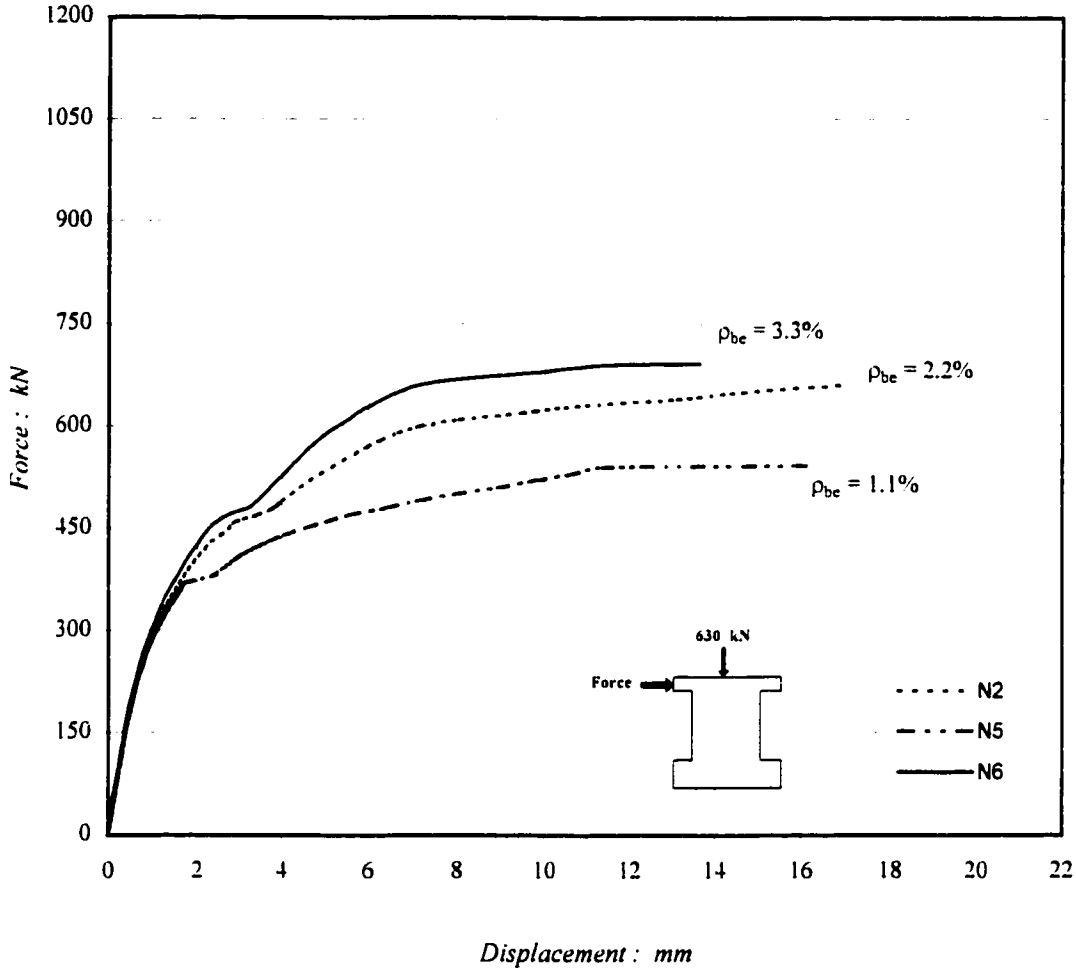

Fig. 5.19 Load-displacement response of shear walls N2, N5 and N6

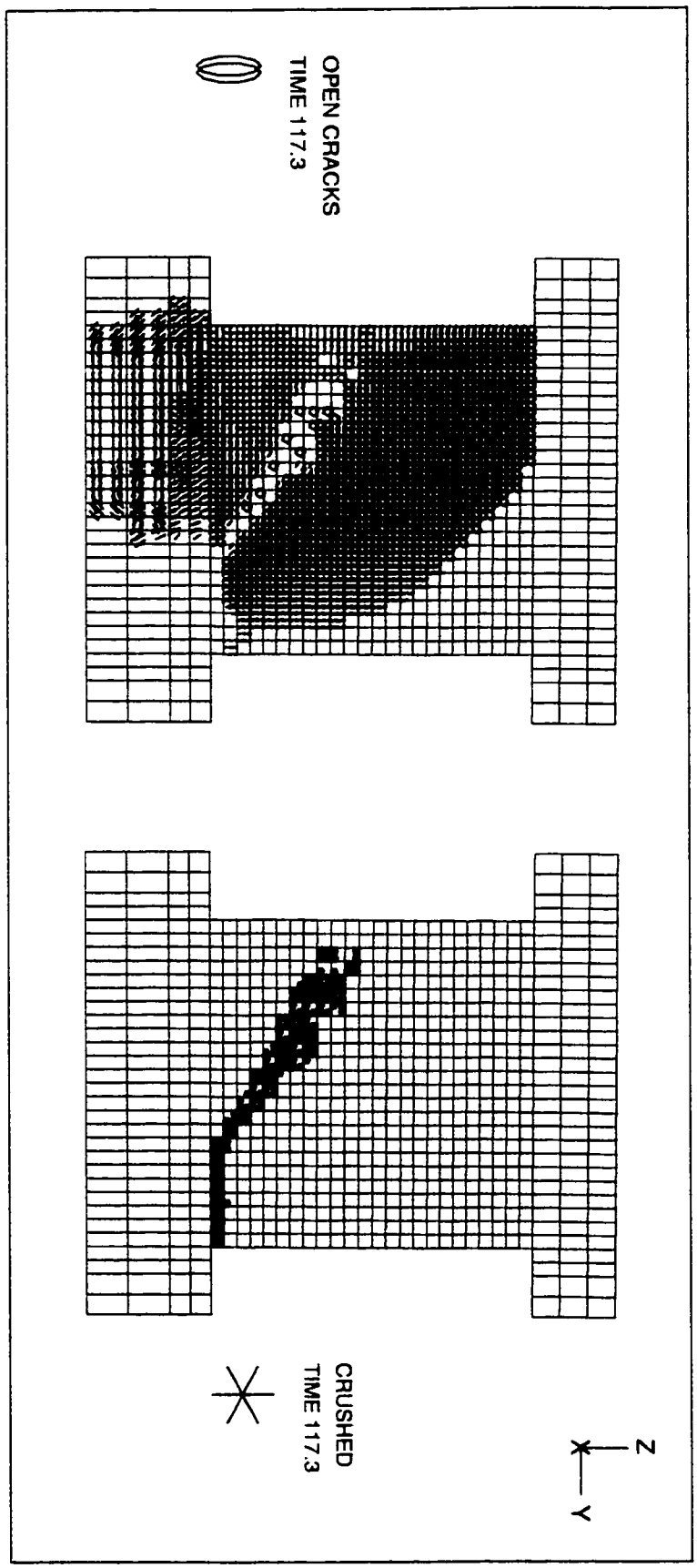

Fig. 5.20 Cracking and crushing pattern of shear wall N5

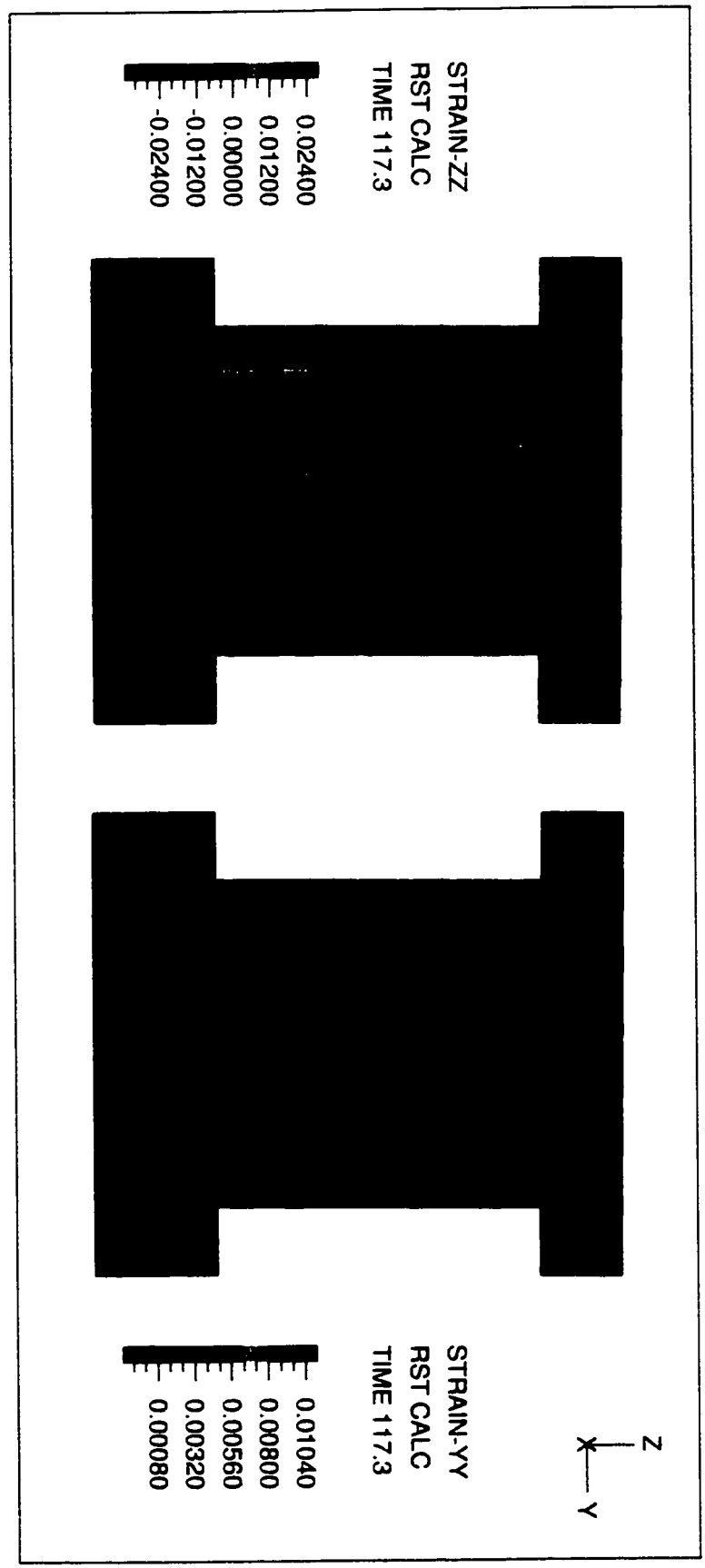

Fig. 5.21 Strain distribution of shear wall N5

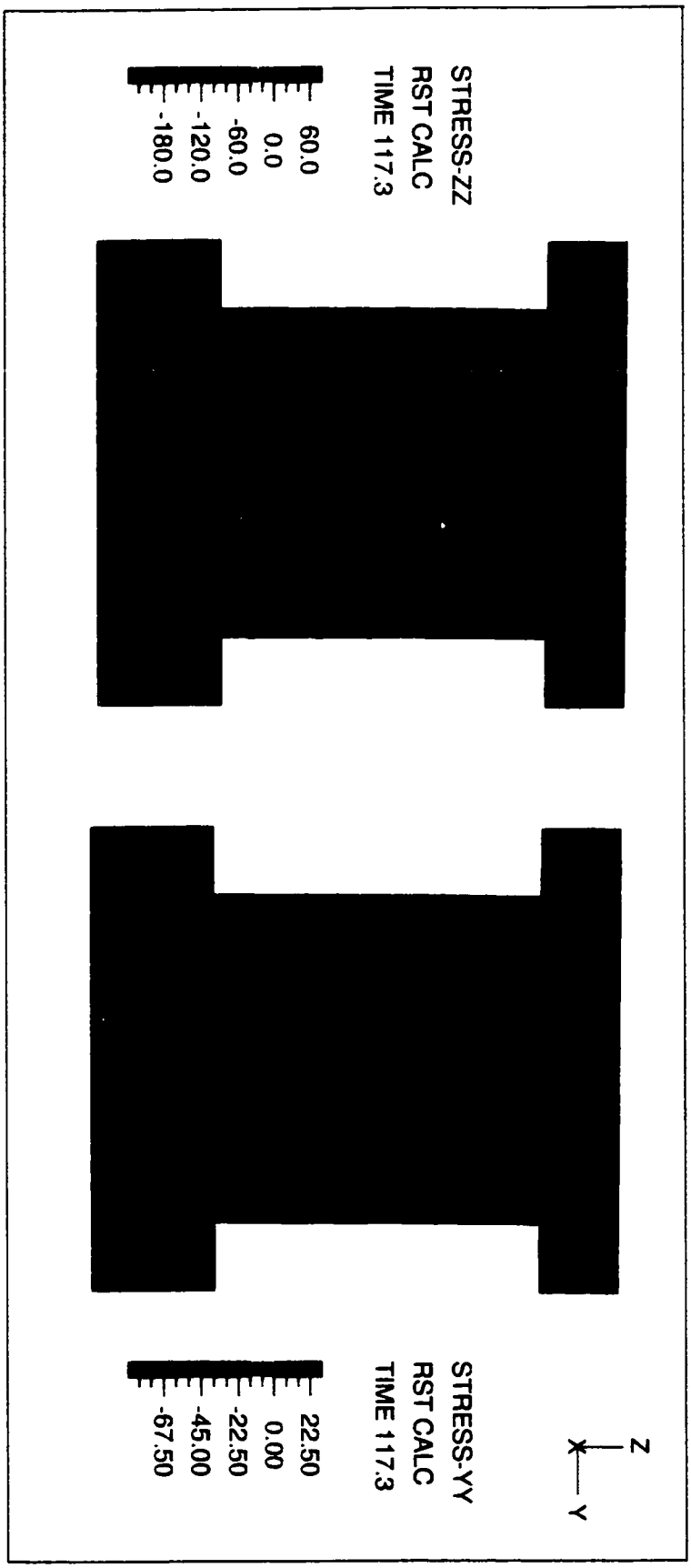

Fig. 5.22 Stress distribution of shear wall N5

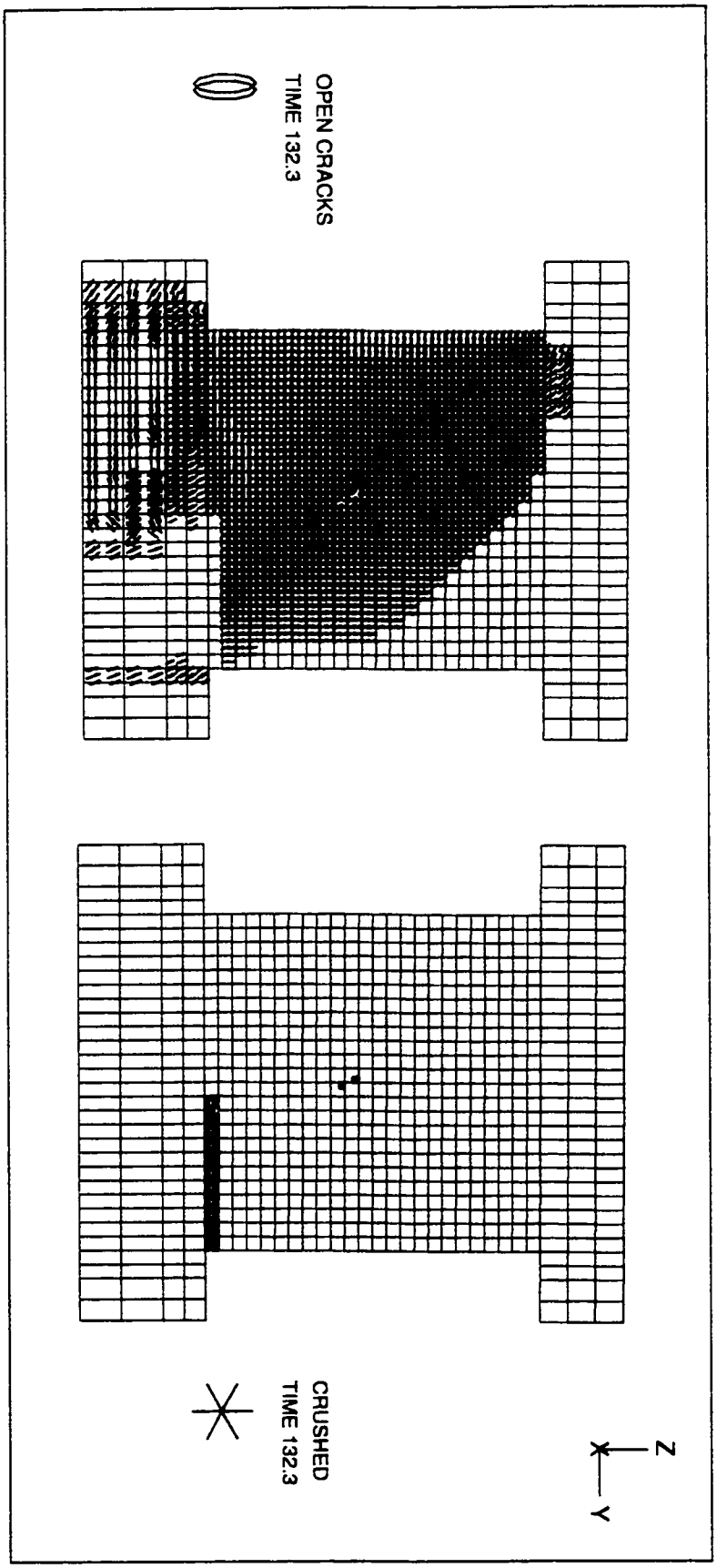

Fig. 5.23 Cracking and crushing pattern of shear wall N6

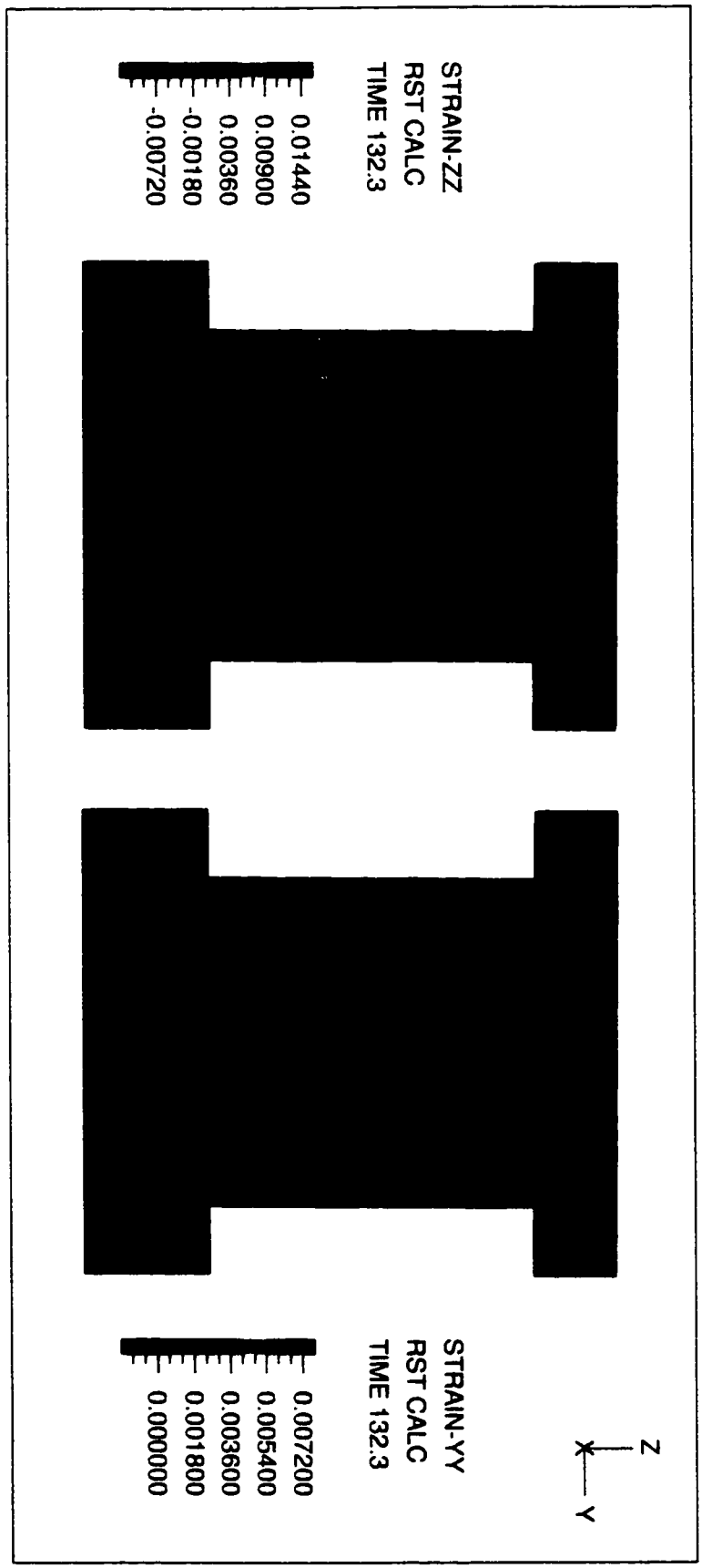

Fig. 5.24 Strain distribution of shear wall N6

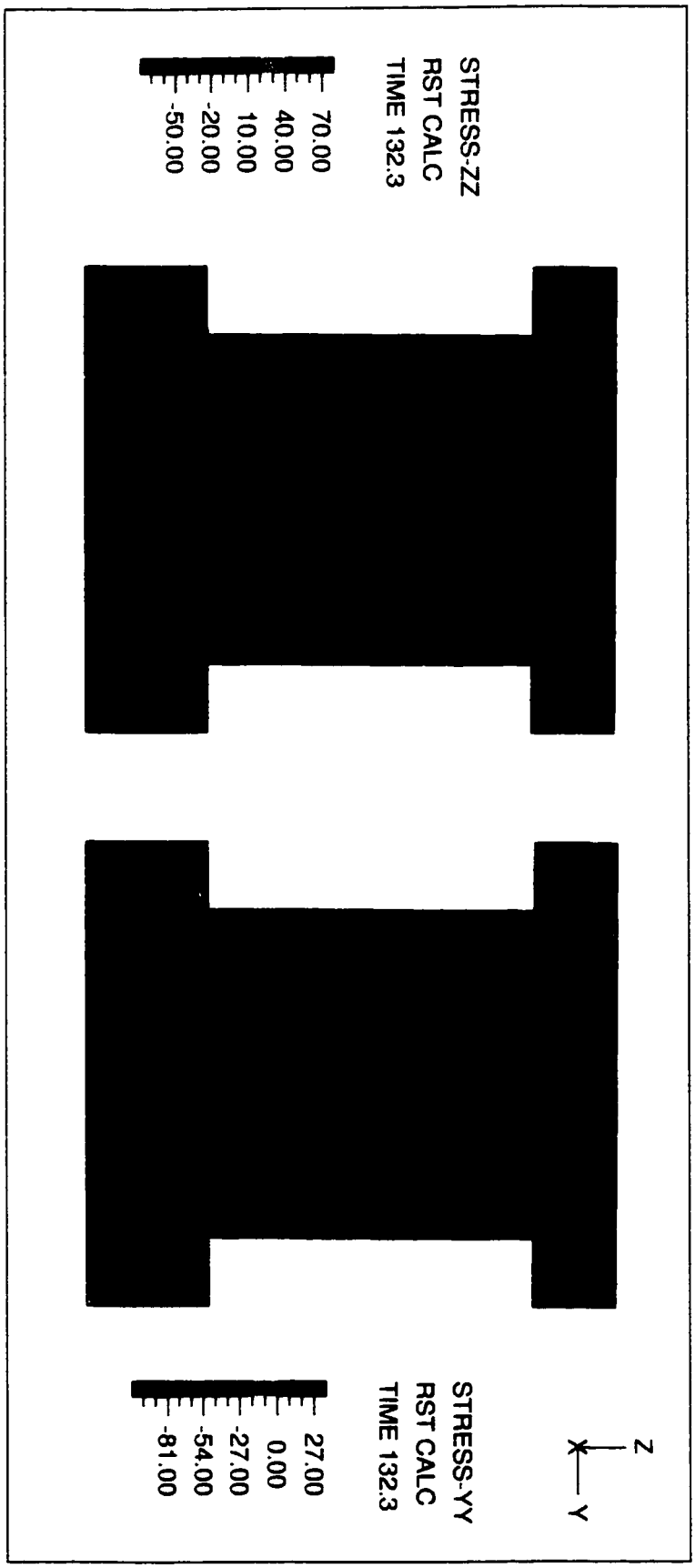

Fig. 5.25 Stress distribution of shear wall N6

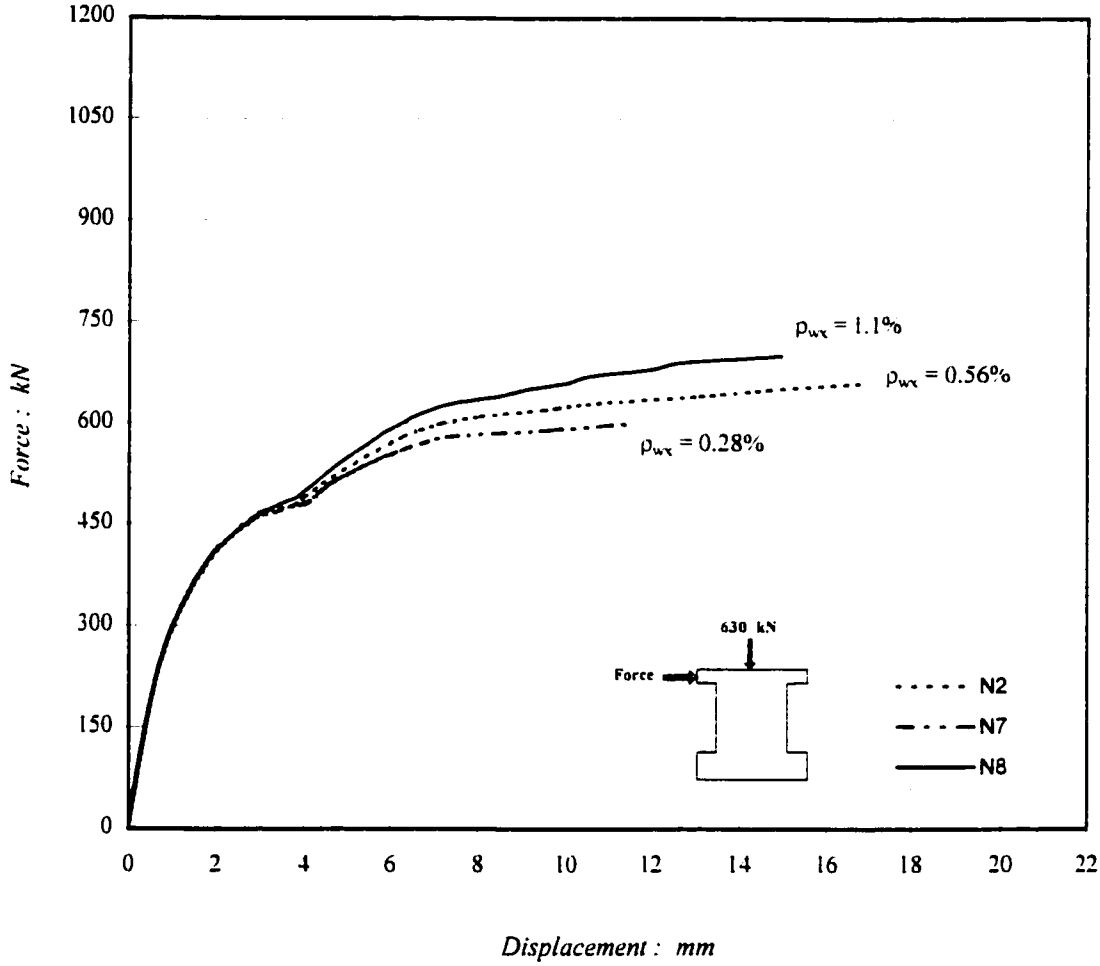

Fig. 5.26 Load-displacement response of shear walls N2, N7 and N8

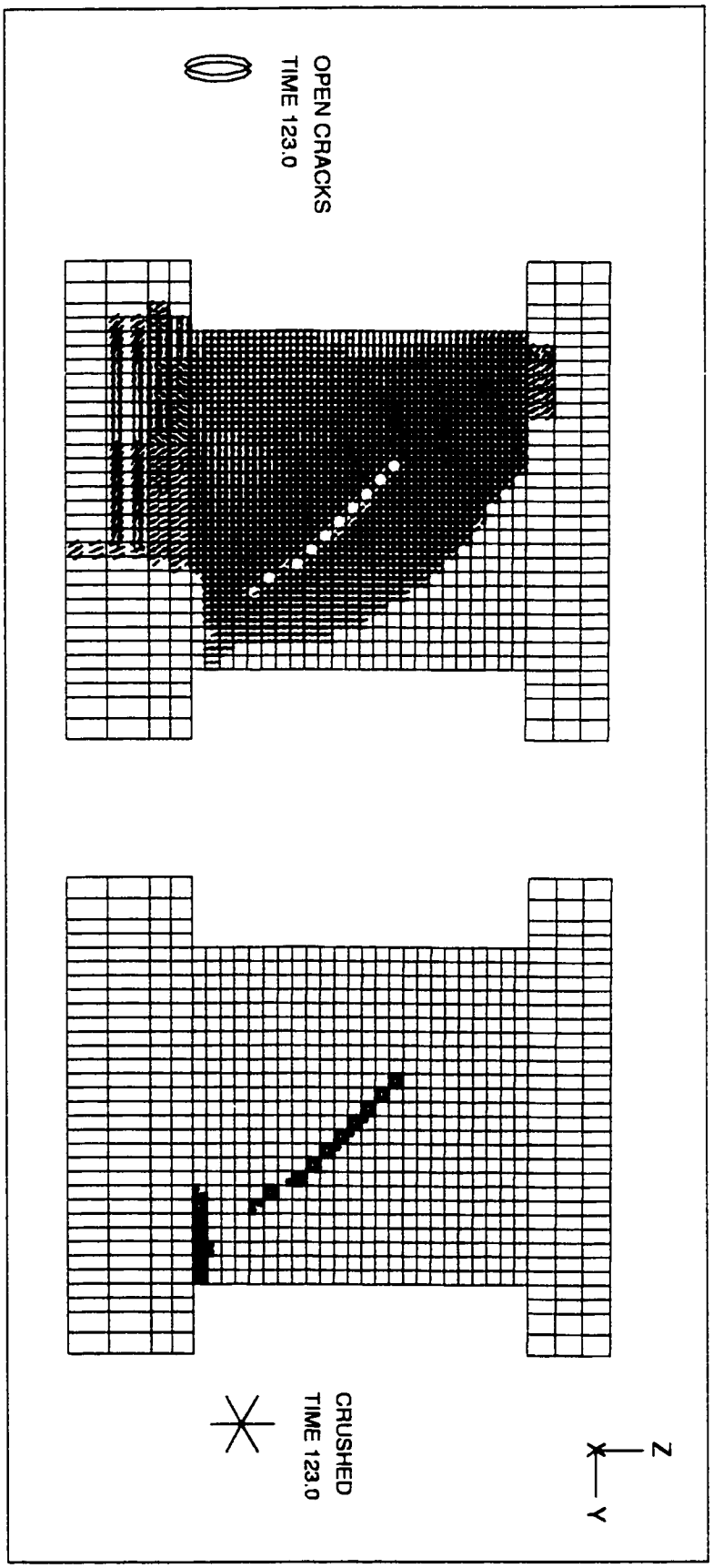

Fig. 5.27 Cracking and crushing pattern of shear wall N7

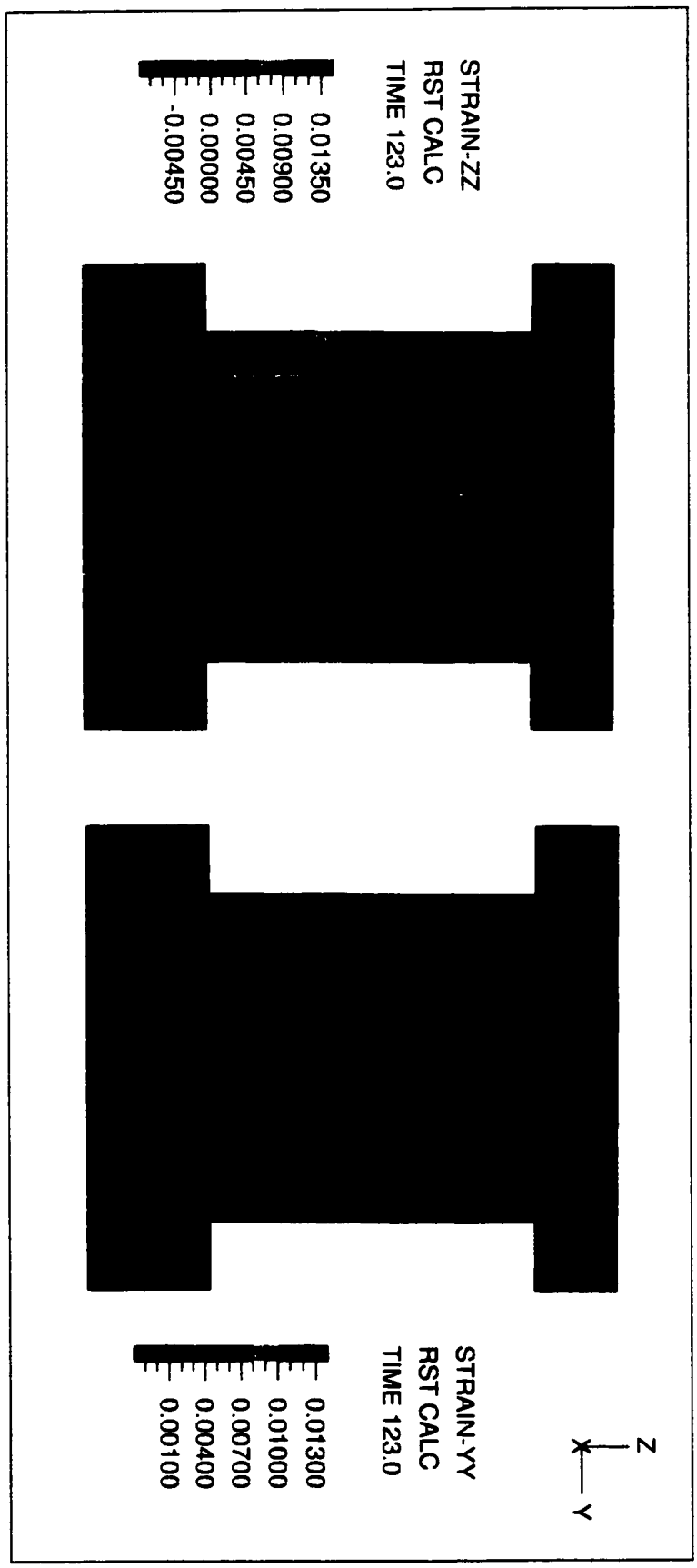

Fig. 5.28 Strain distribution of shear wall N7

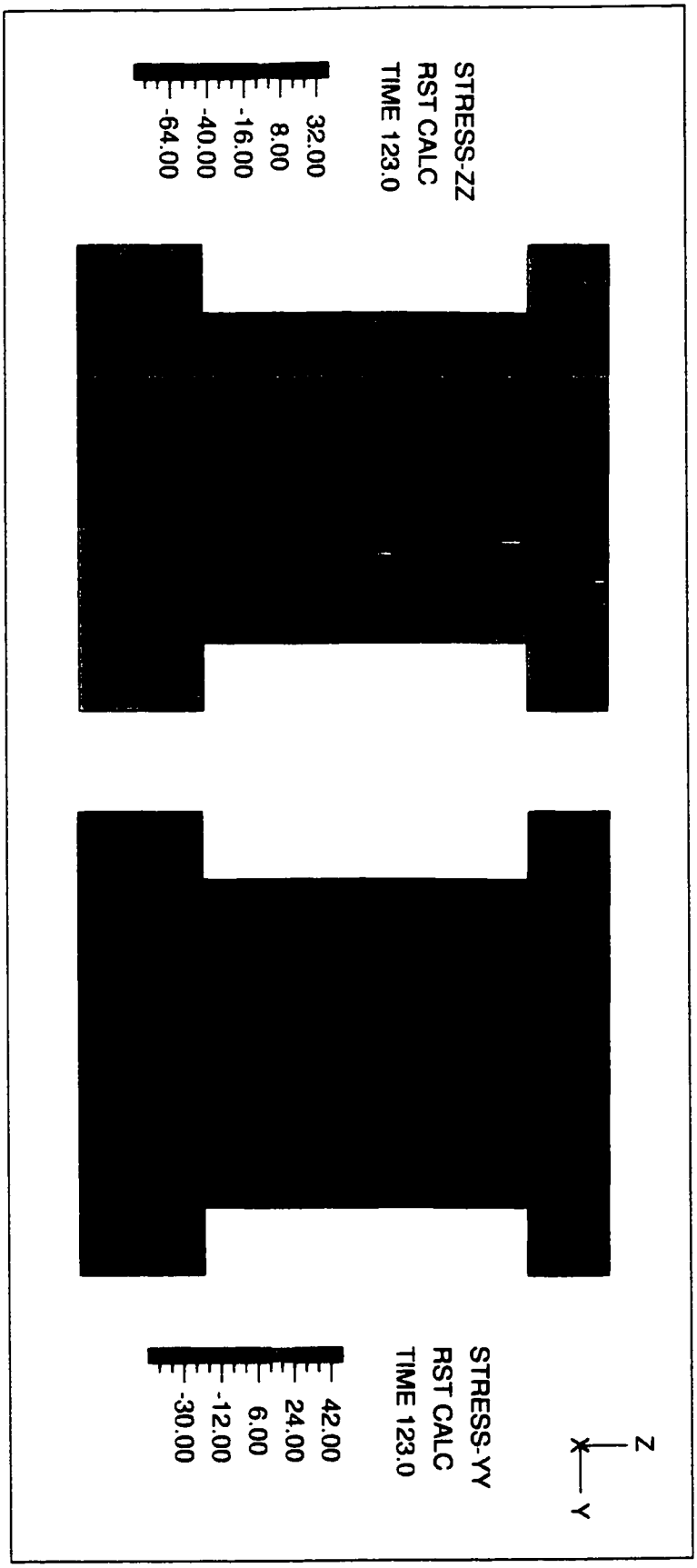

Fig. 5.29 Stress distribution of shear wall N7

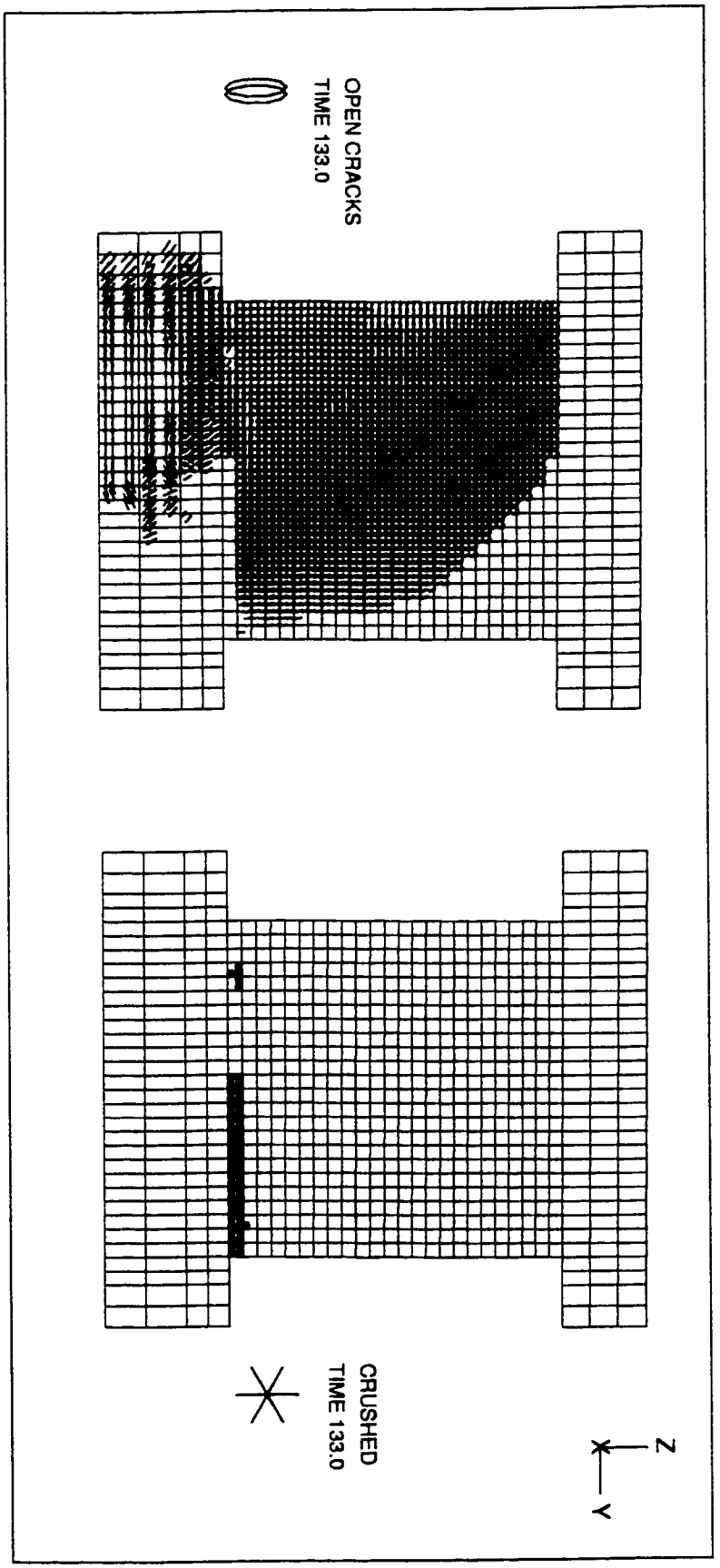

Fig. 5.30 Cracking and crushing pattern of shear wall N8

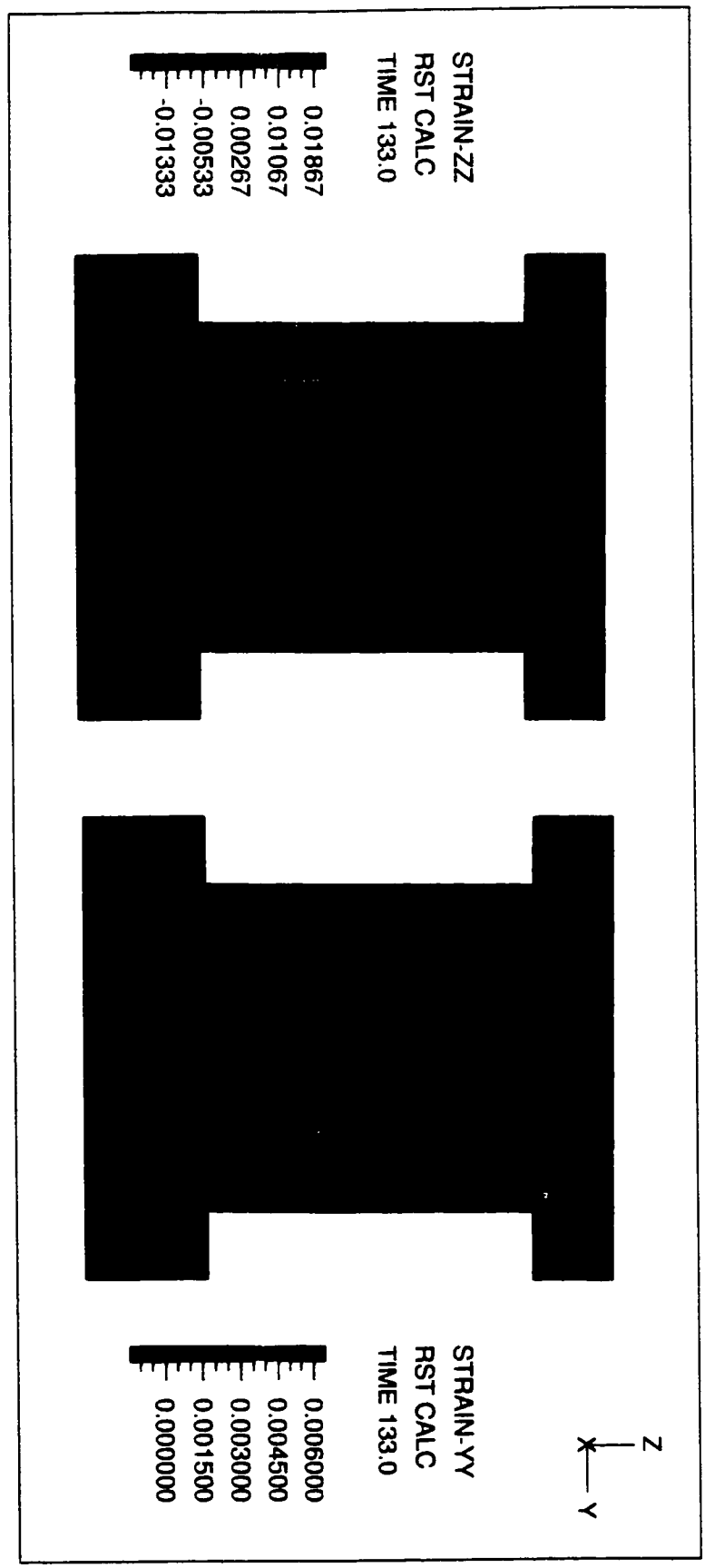

Fig. 5.31 Strain distribution of shear wall N8

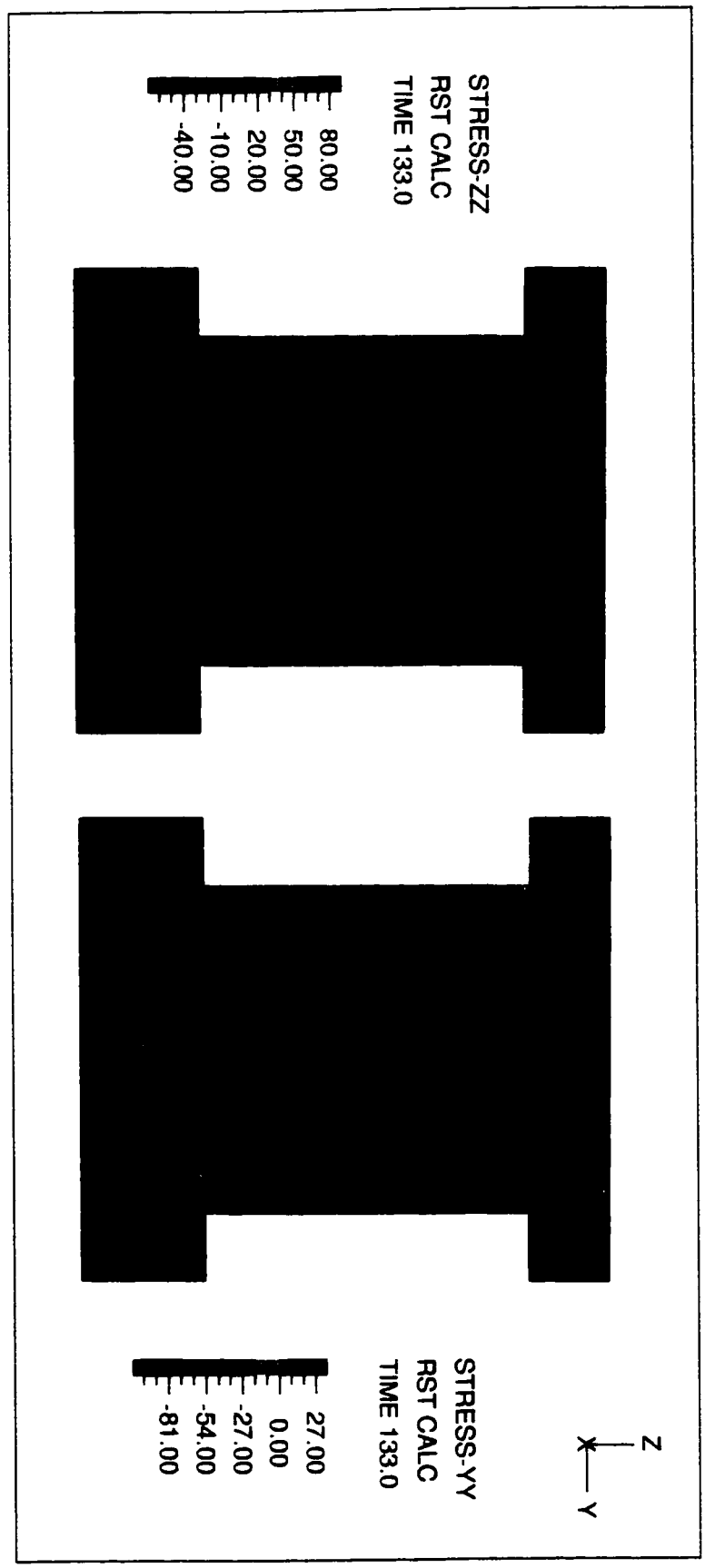

Fig. 5.32 Stress distribution of shear wall N8

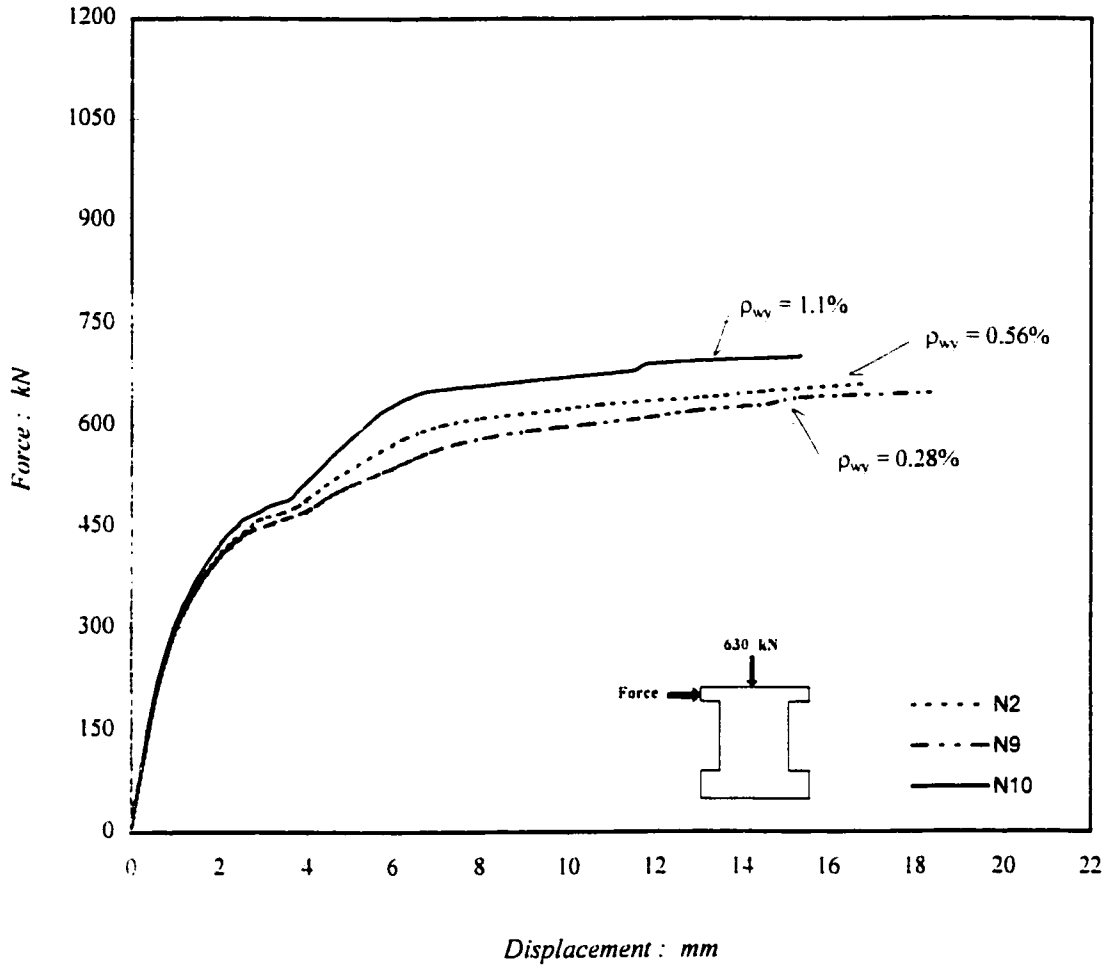

Fig. 5.33 Load-displacement response of shear walls N2, N9 and N10

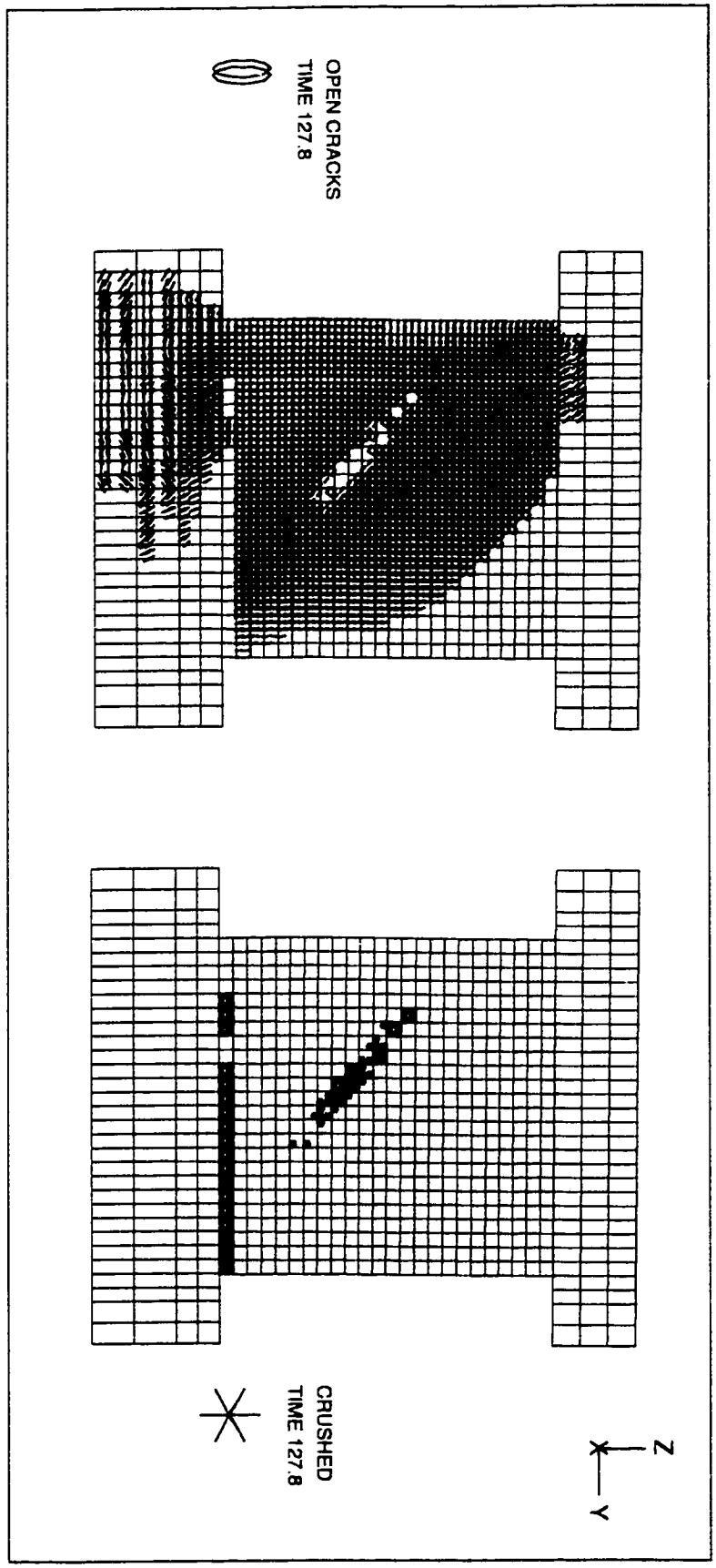

Fig. 5.34 Cracking and crushing pattern of shear wall N9

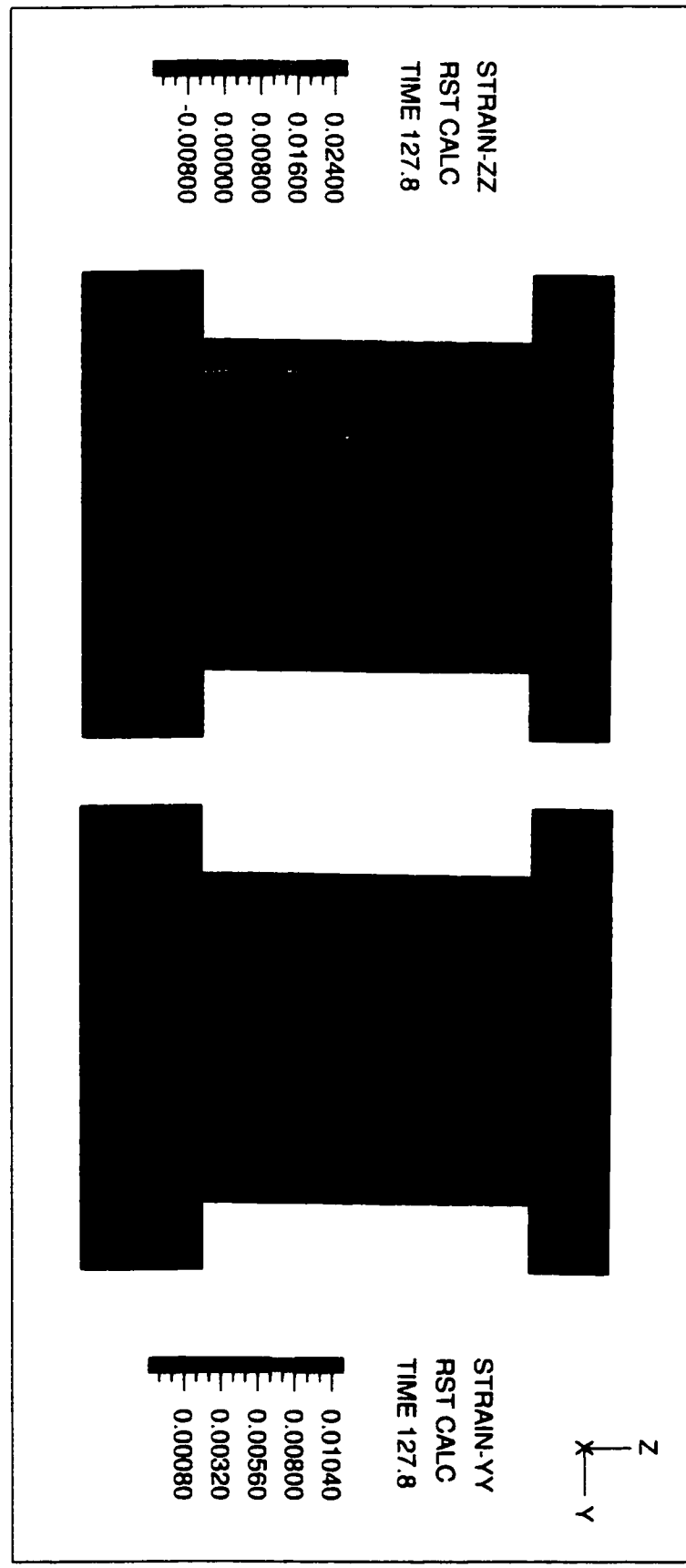

Fig. 5.35 Strain distribution of shear wall N9

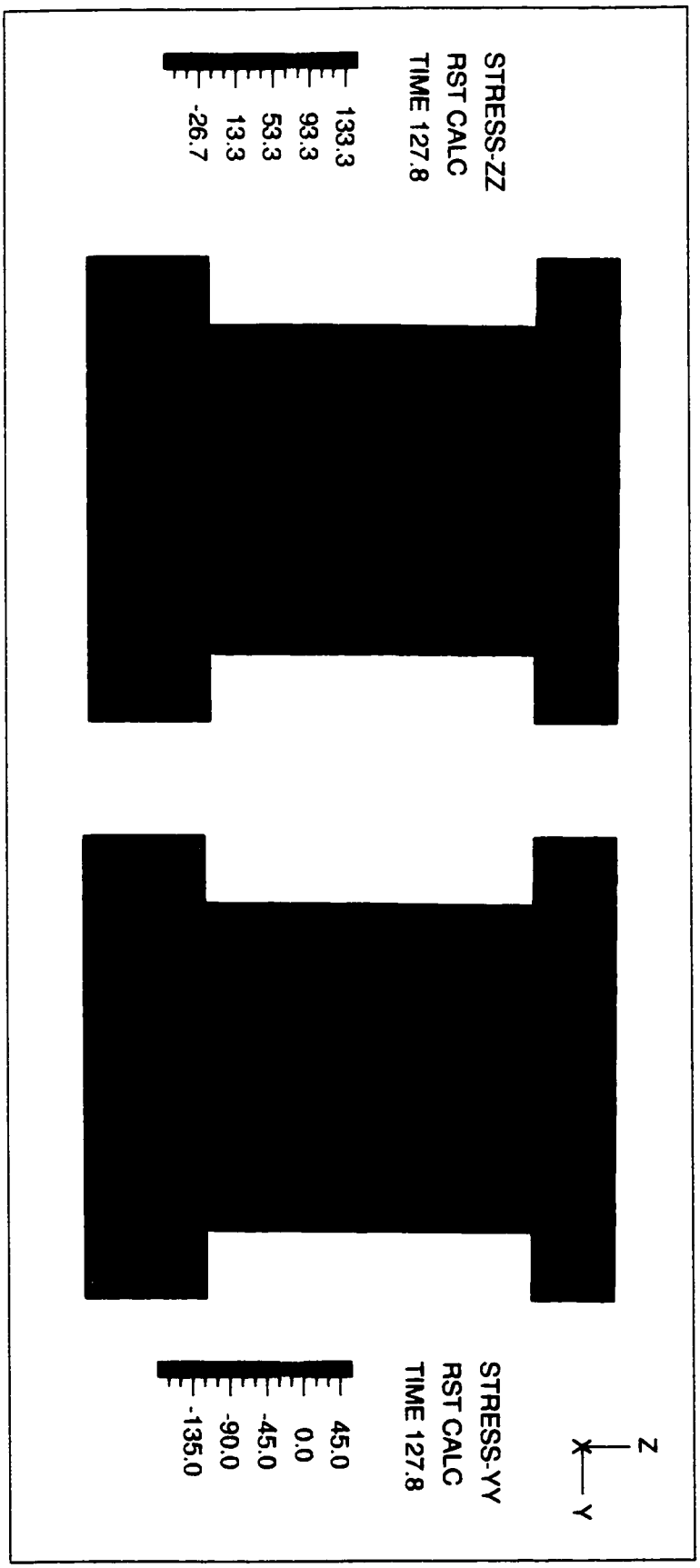

Fig. 5.36 Stress distribution of shear wall N9

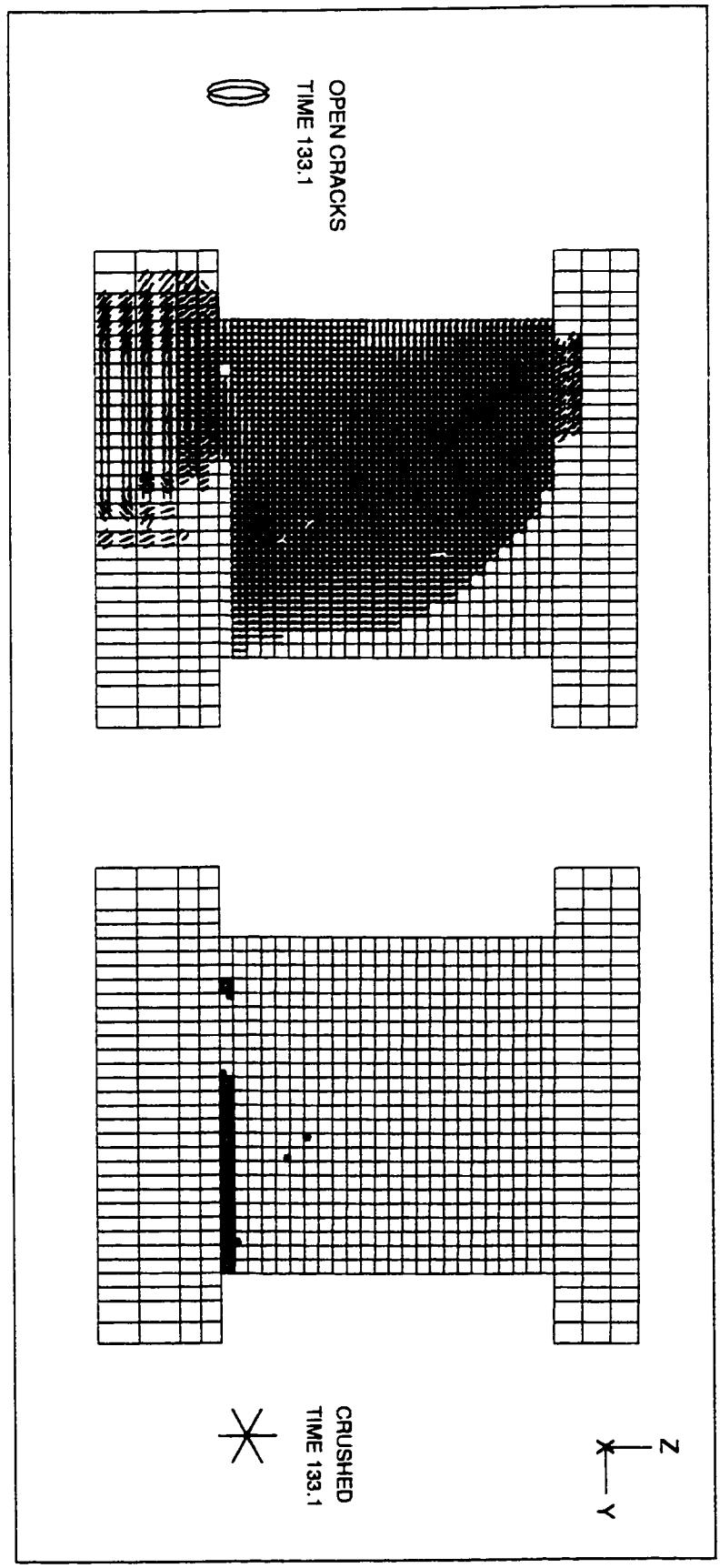

Fig. 5.37 Cracking and crushing pattern of snear wall N10

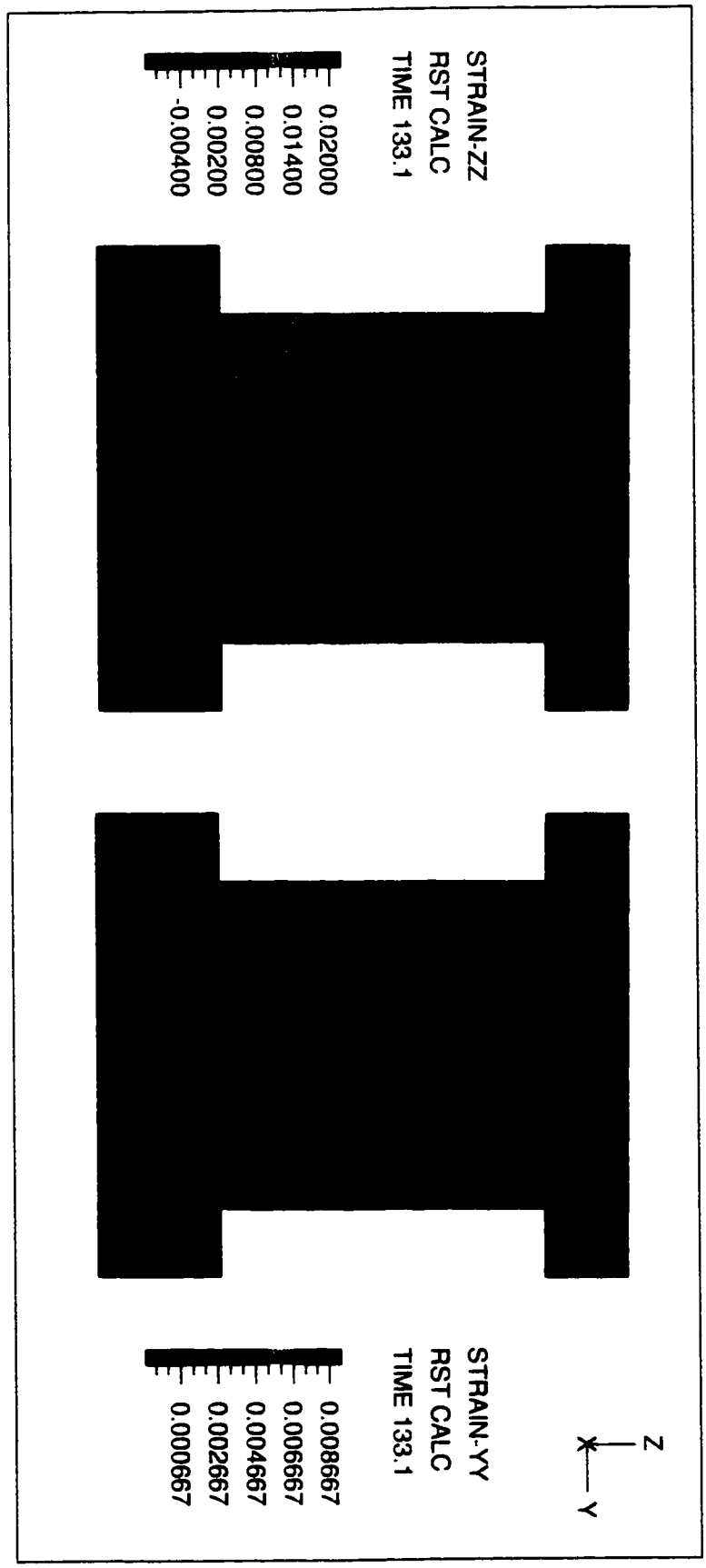

Fig. 5.38 Strain distribution of shear wall N10

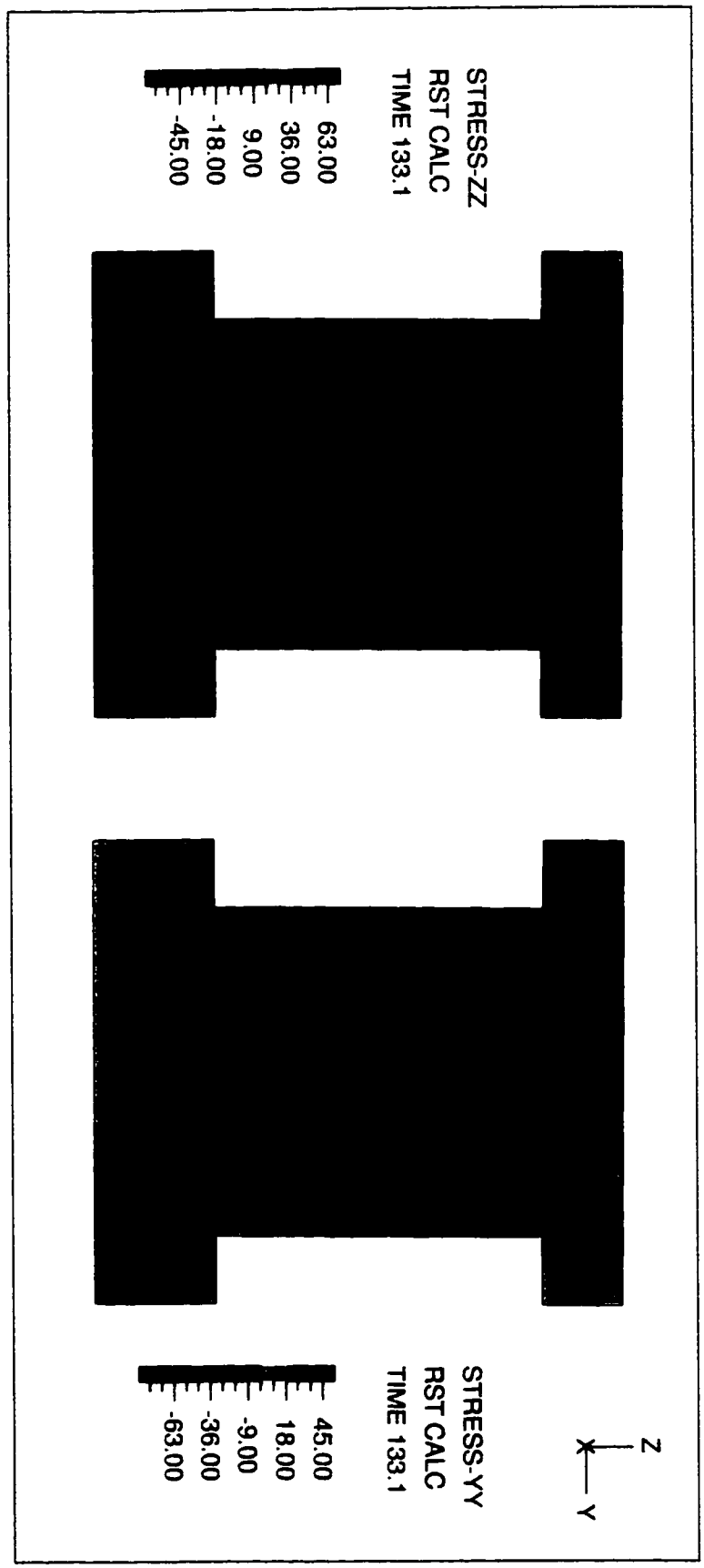

Fig. 5.39 Stress distribution of shear wall N10

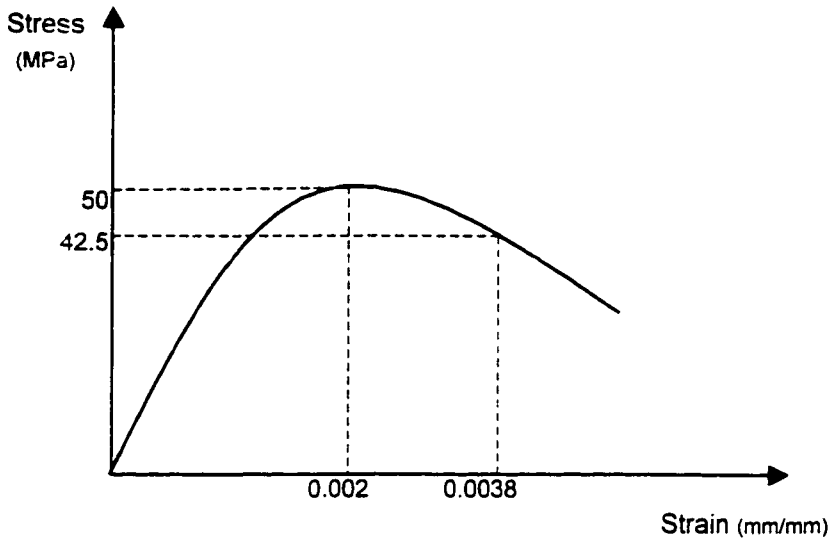

(a) Unconfined concrete

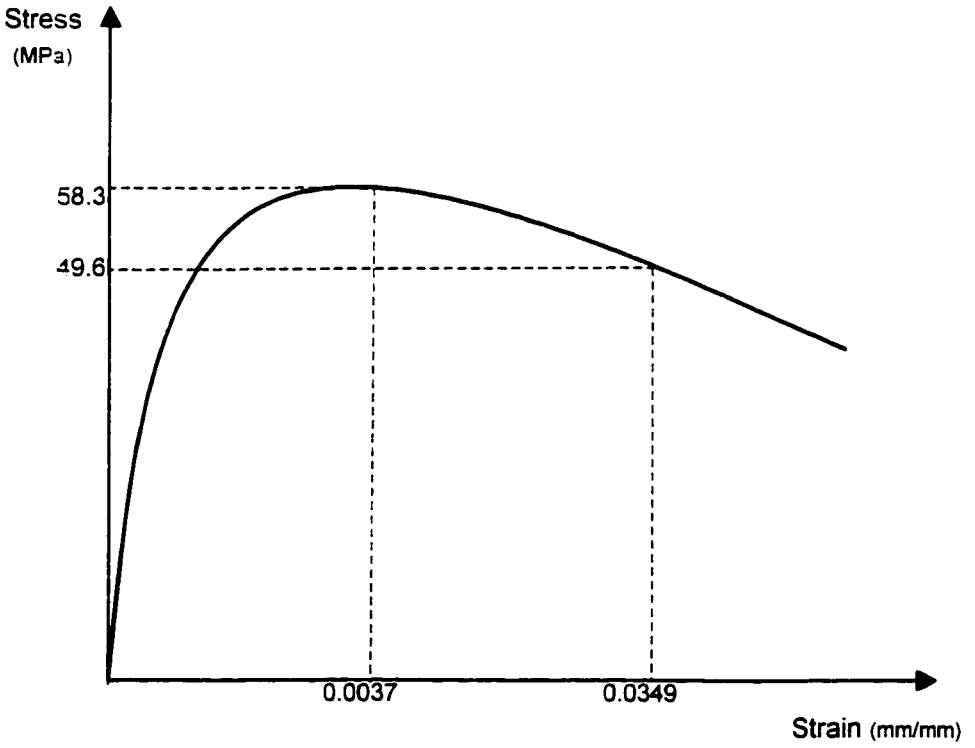

(b) Confined concrete

Fig. 5.40 Stress-strain relationship of concrete for shear wall N11

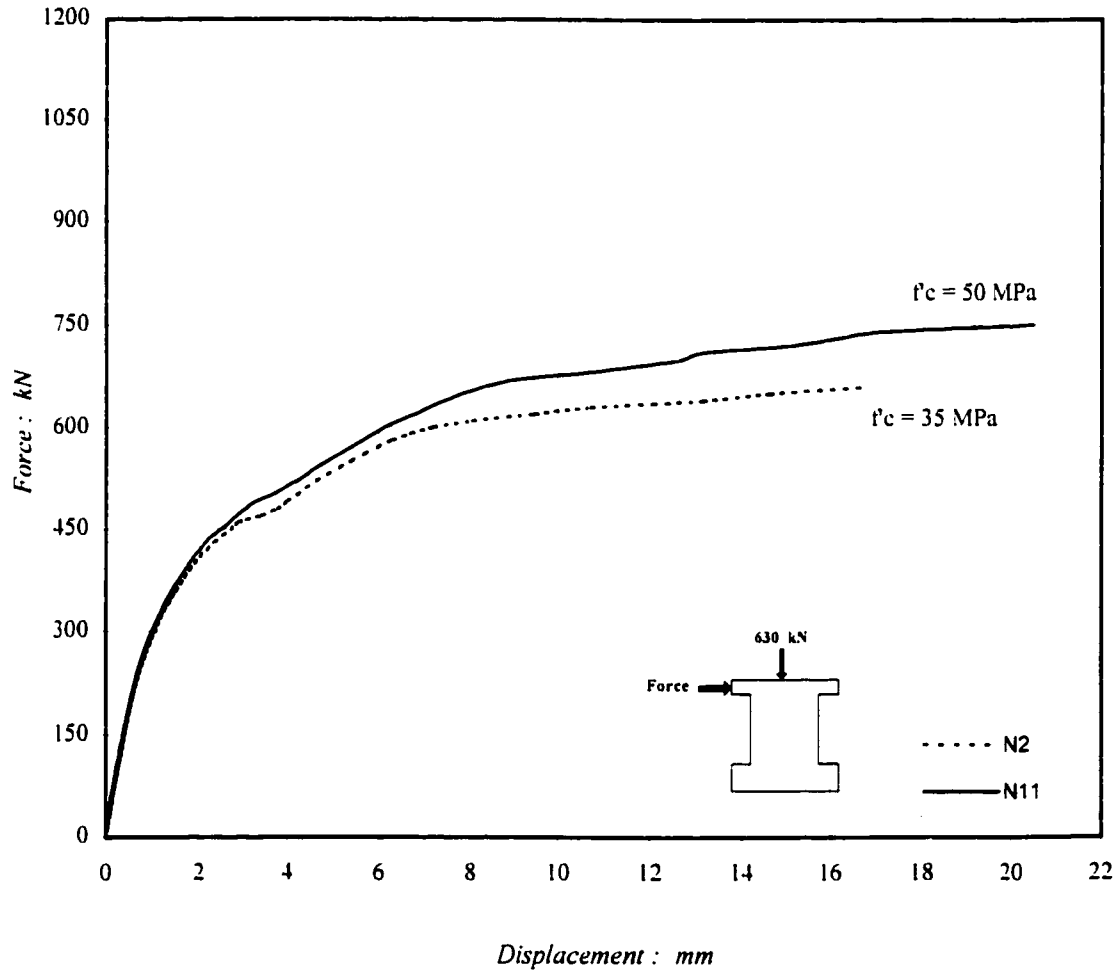

Fig. 5.41 Load-displacement response of shear walls N2 and N11

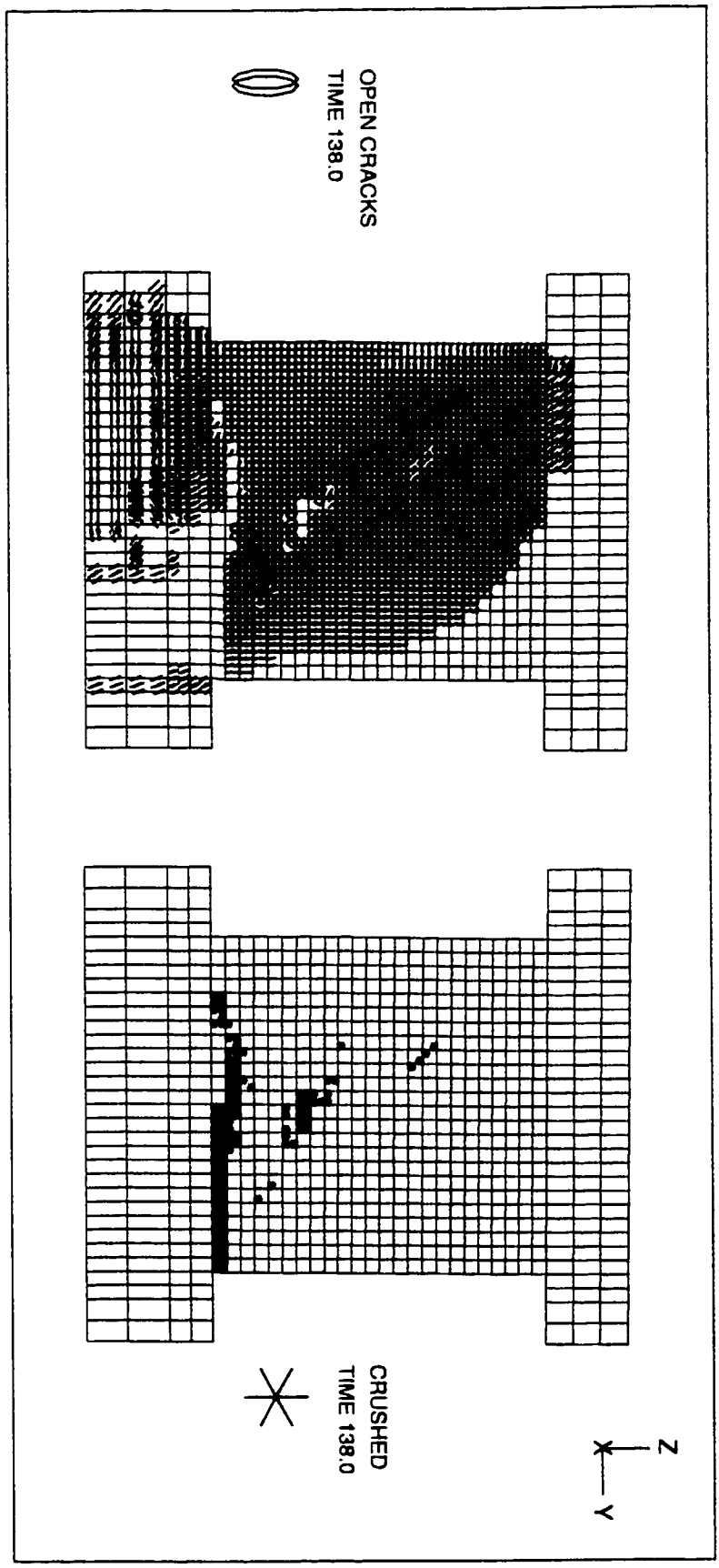

Fig. 5.42 Cracking and crushing pattern of shear wall N11

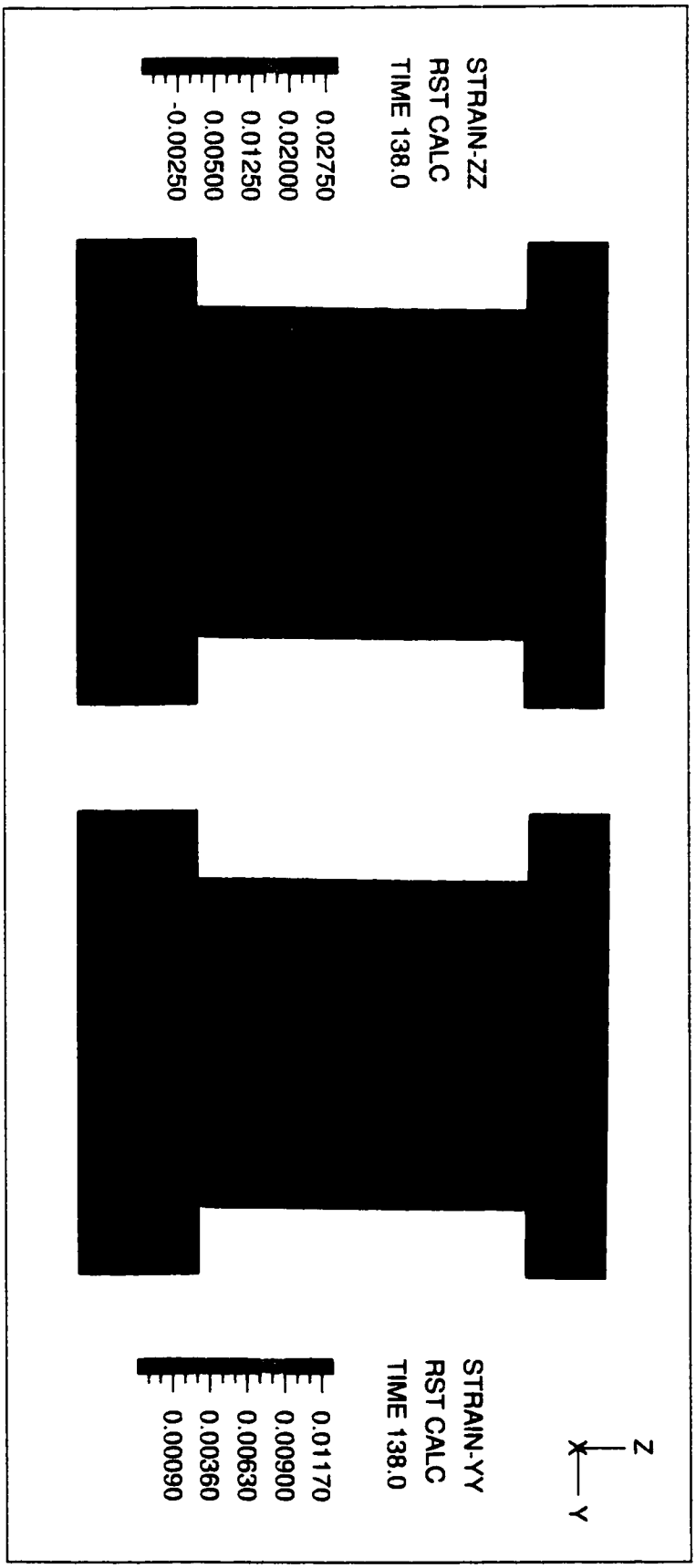

Fig. 5.43 Strain distribution of shear wall N11

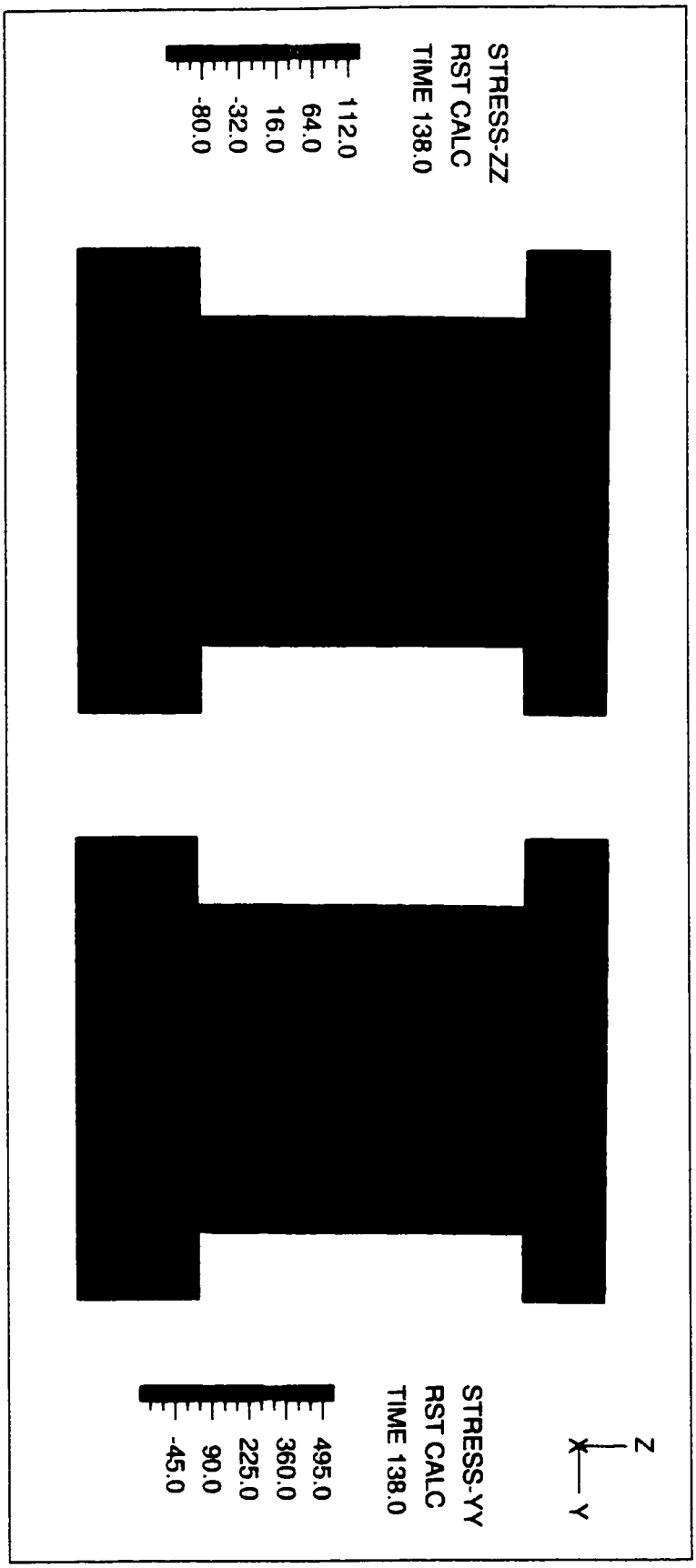

Fig. 5.44 Stress distribution of shear wall N11

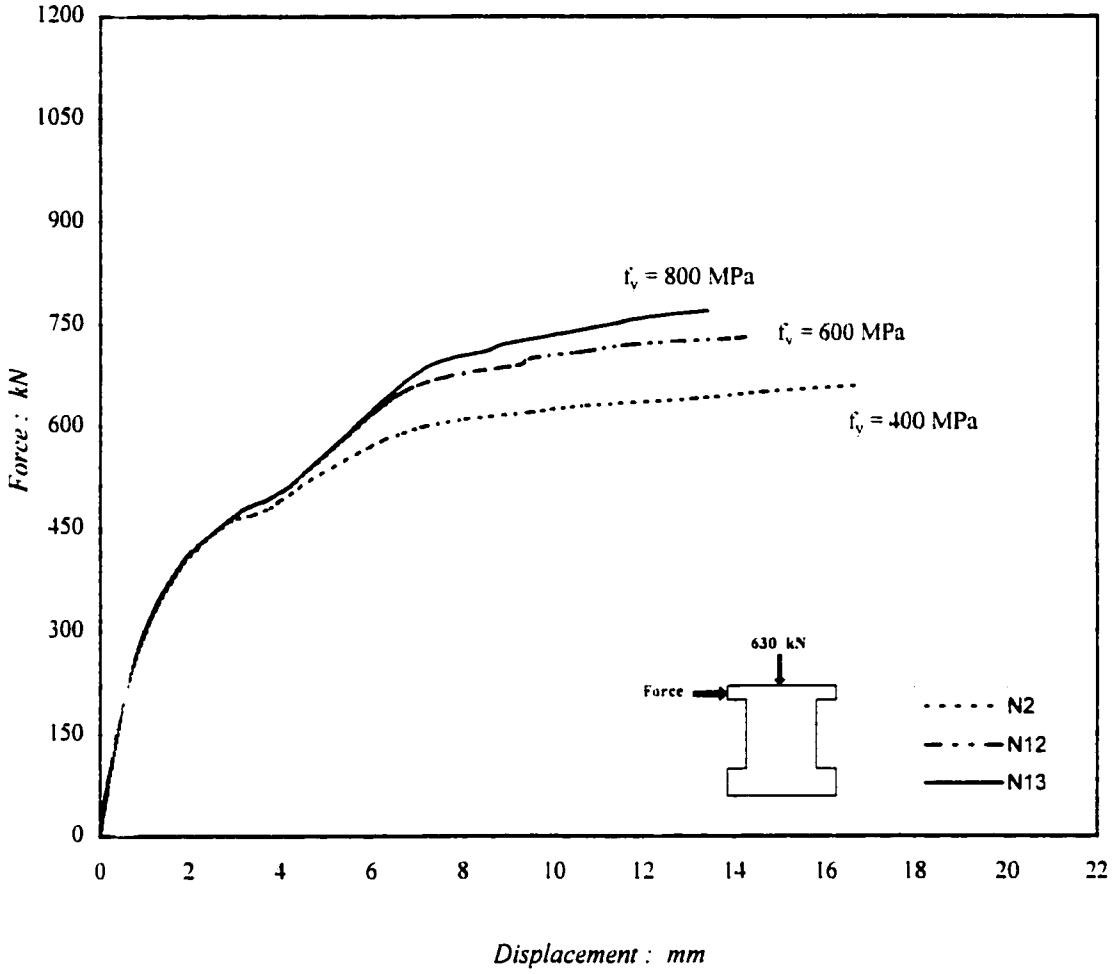

Fig. 5.45 Load-displacement response of shear walls N2, N12 and N13

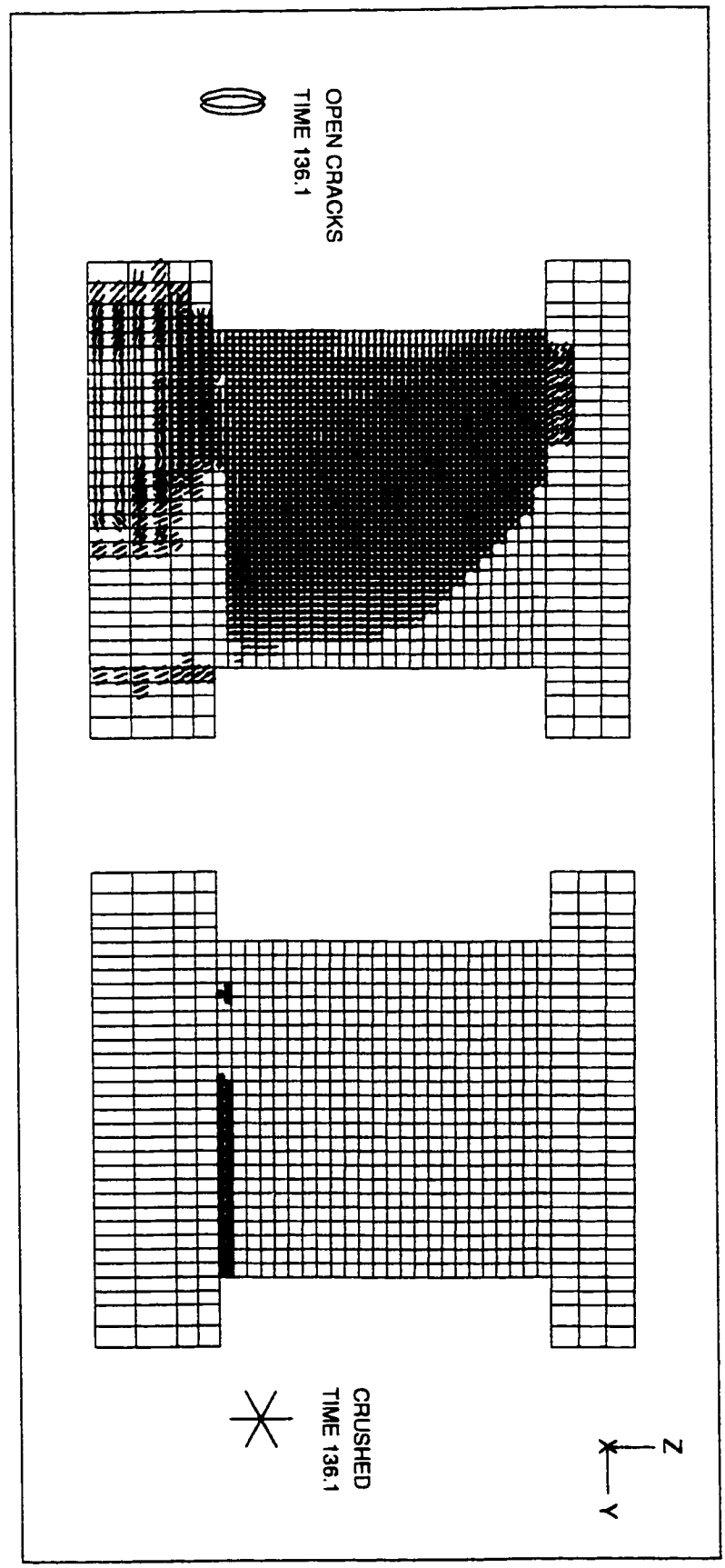

Fig. 5.46 Cracking and crushing pattern of shear wall N12

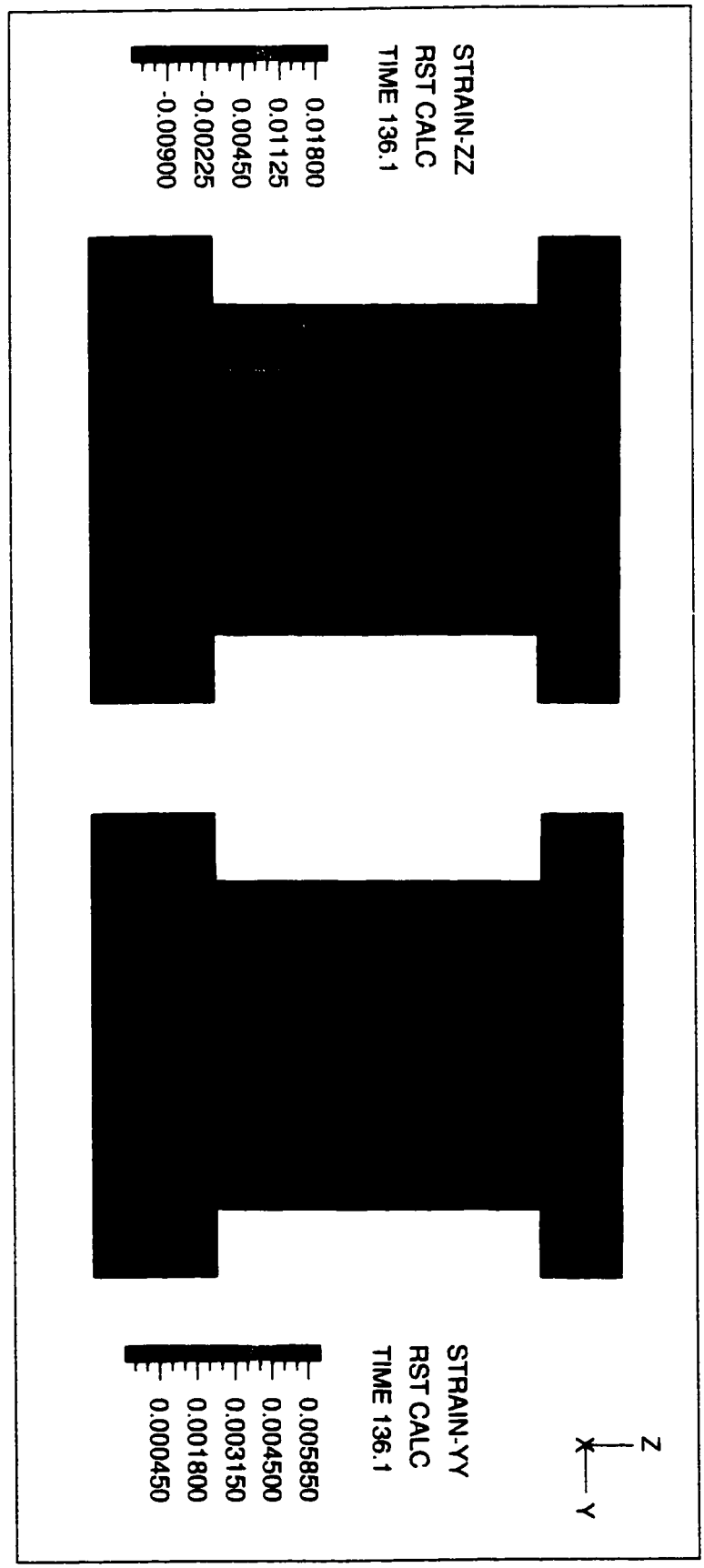

Fig. 5.47 Strain distribution of shear wall N12

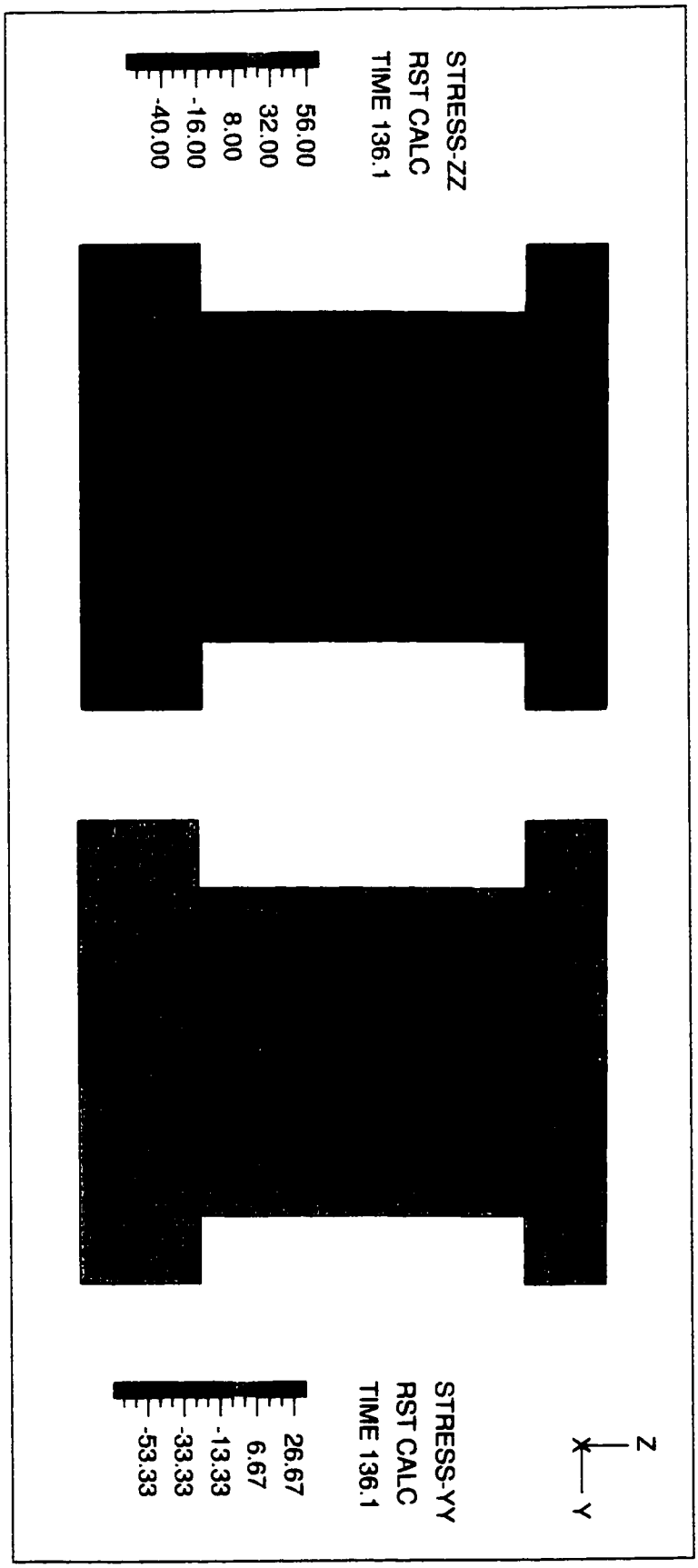

Fig. 5.48 Stress distribution of shear wall N12

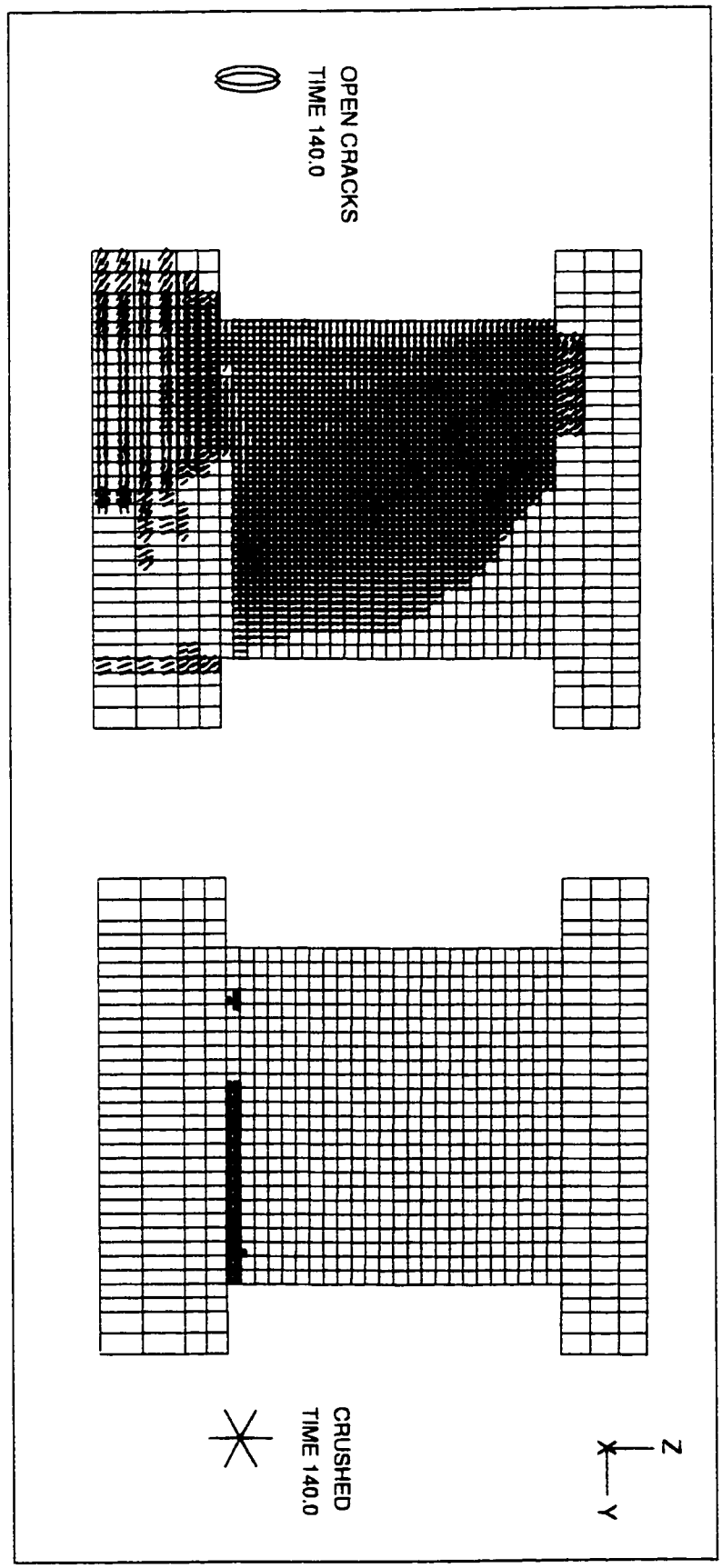

Fig. 5.49 Cracking and crushing pattern of shear wall N13

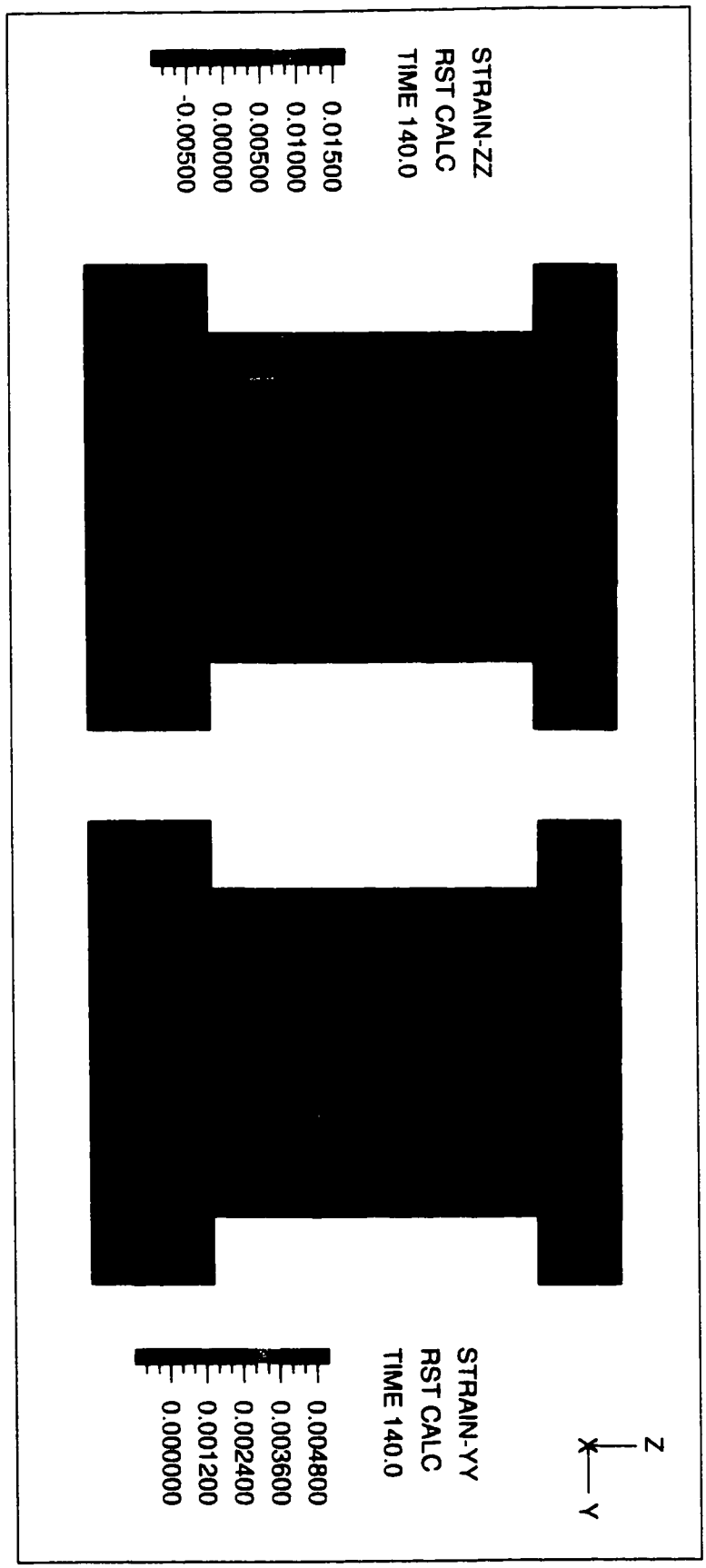

Fig. 5.50 Strain distribution of shear wall N13

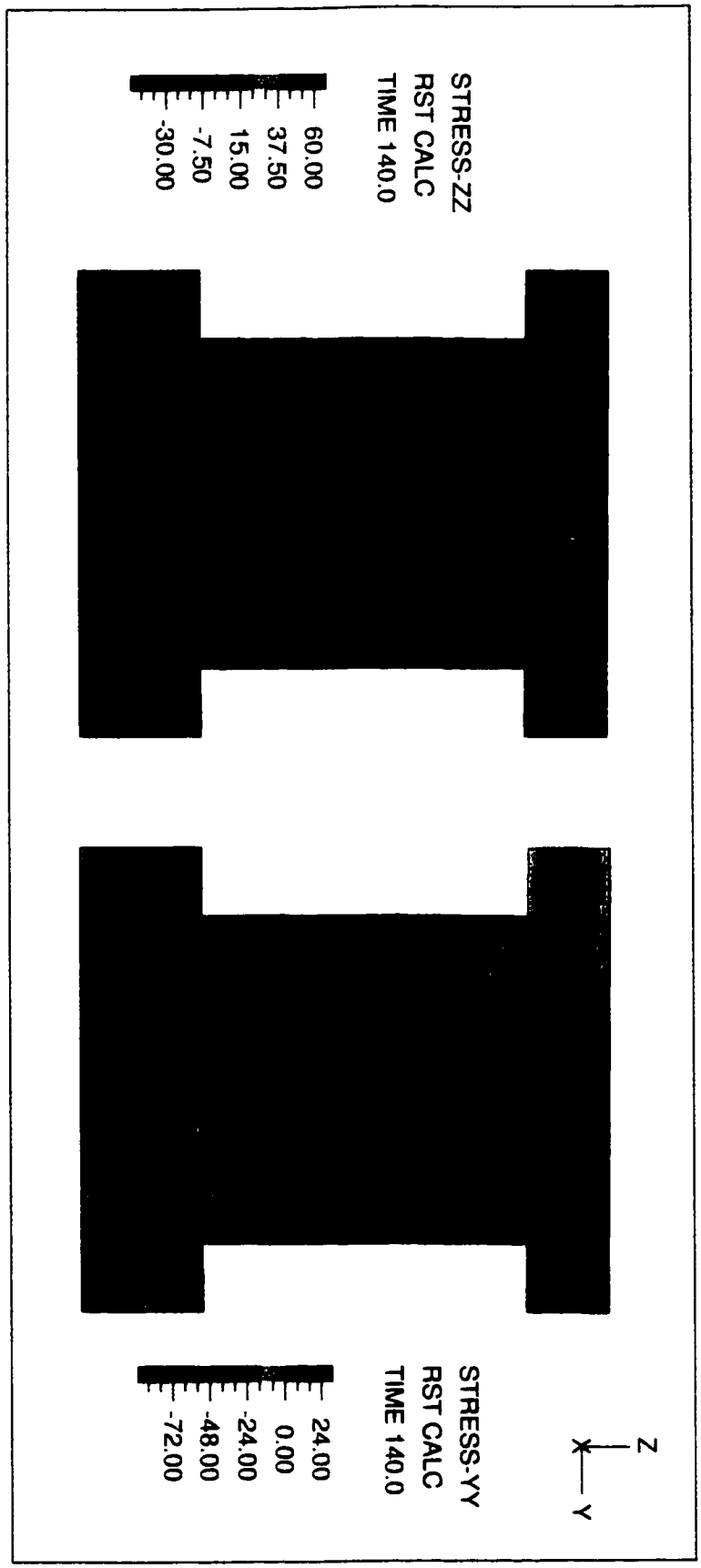

Fig. 5.51 Stress distribution of shear wall N13

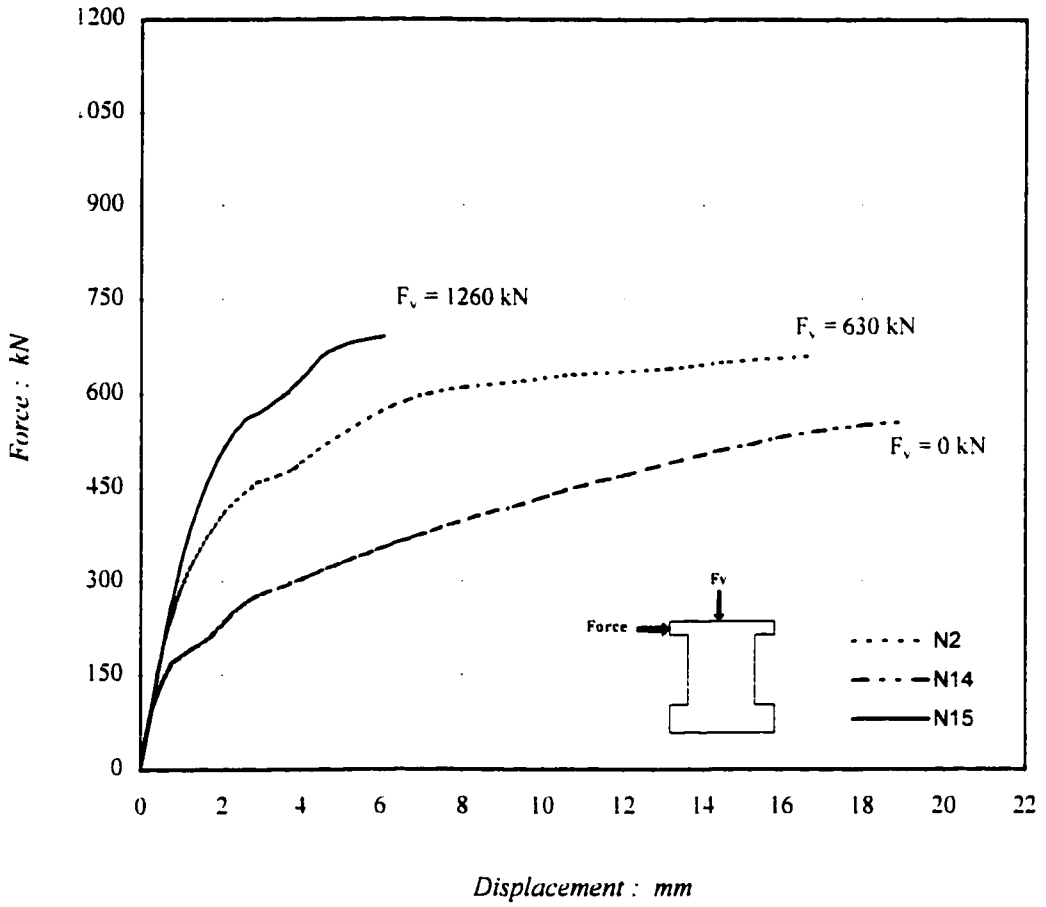

Fig. 5.52 Load-displacement response of shear walls N2, N14 and N15

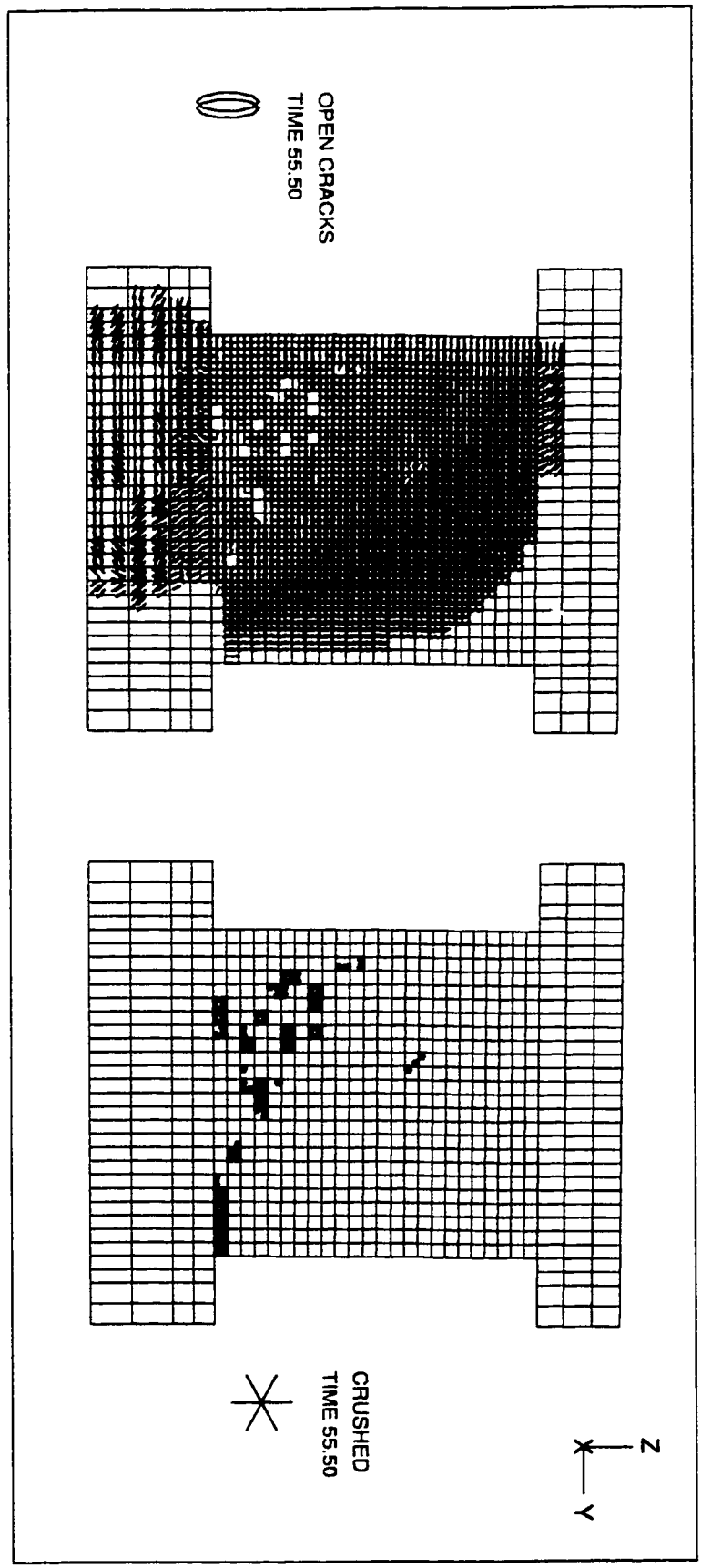

Fig. 5.53 Cracking and crushing pattern of shear wall N14

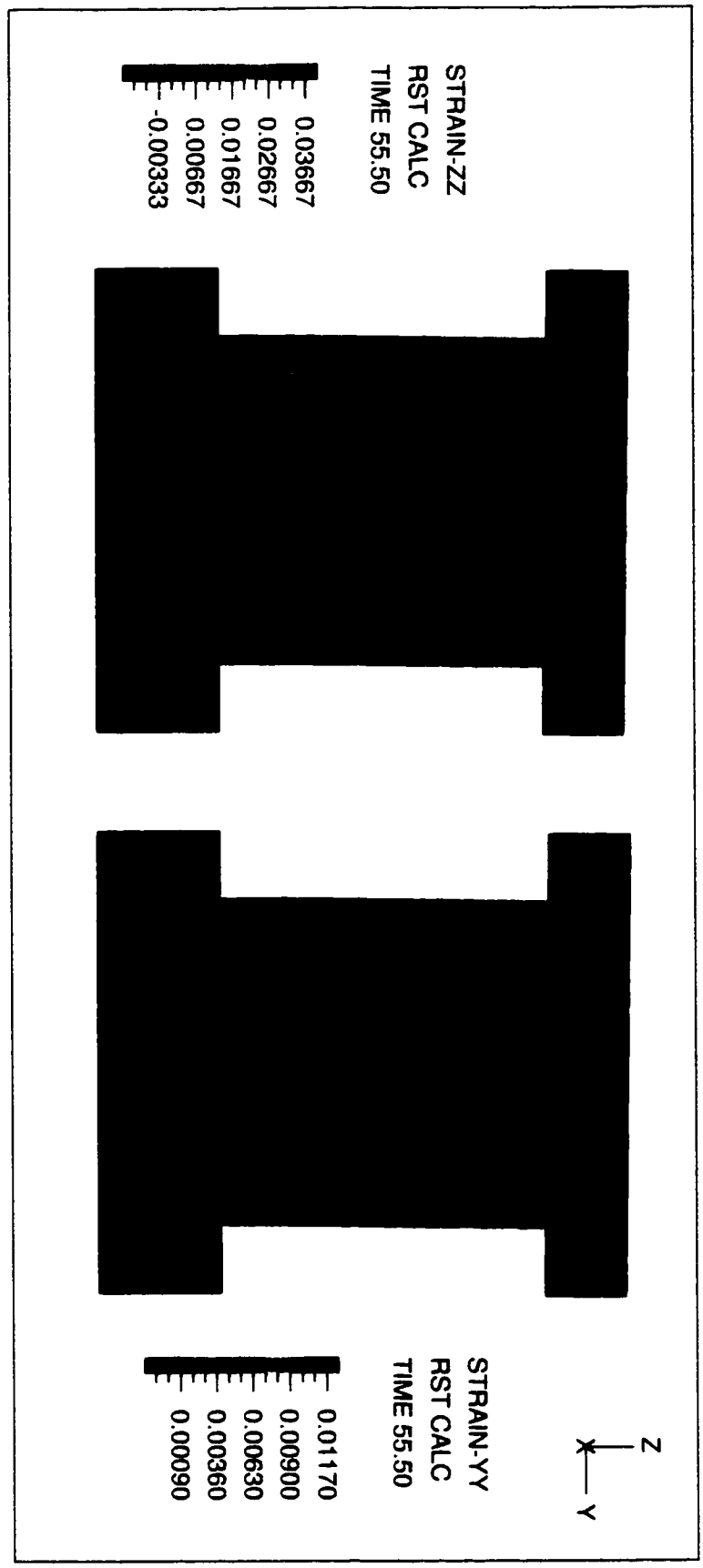

Fig. 5.54 Strain distribution of shear wall N14

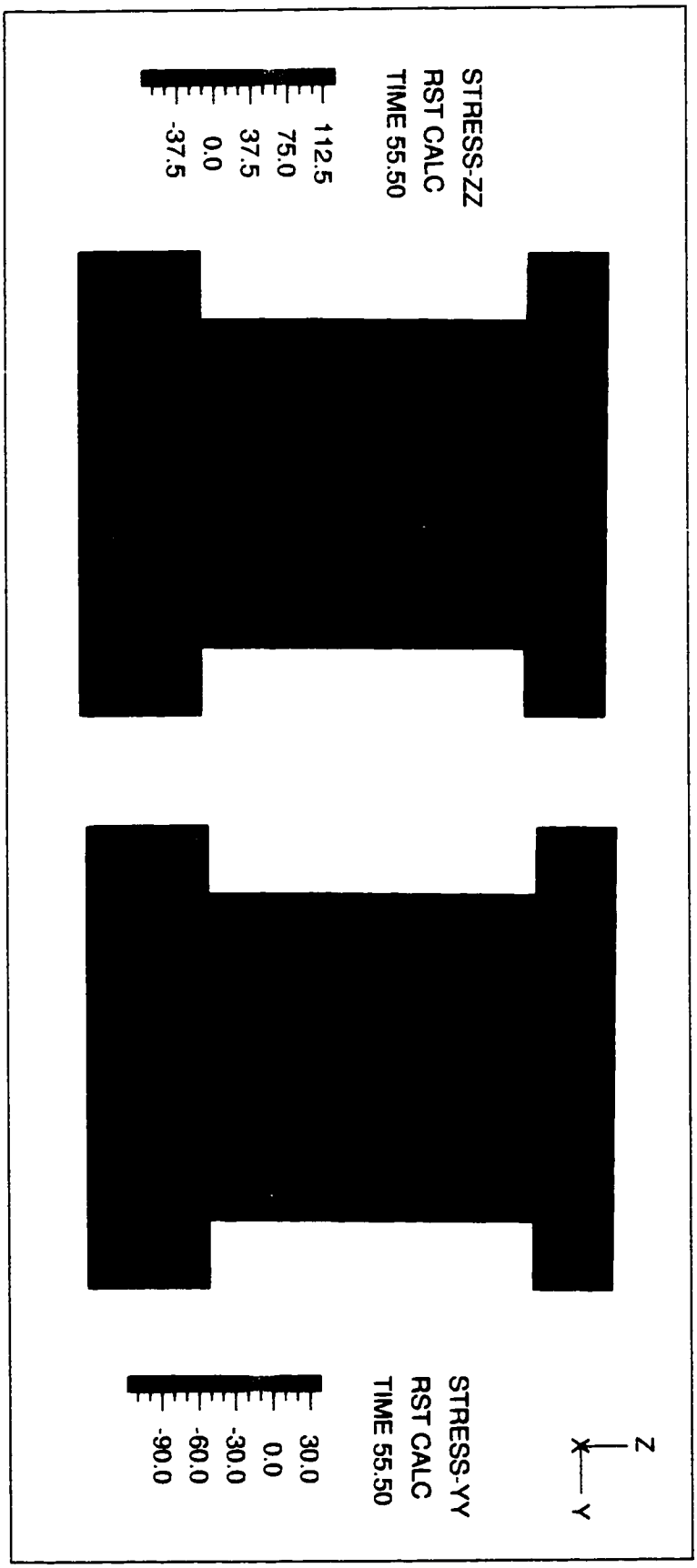

Fig. 5.55 Stress distribution of shear wall N14

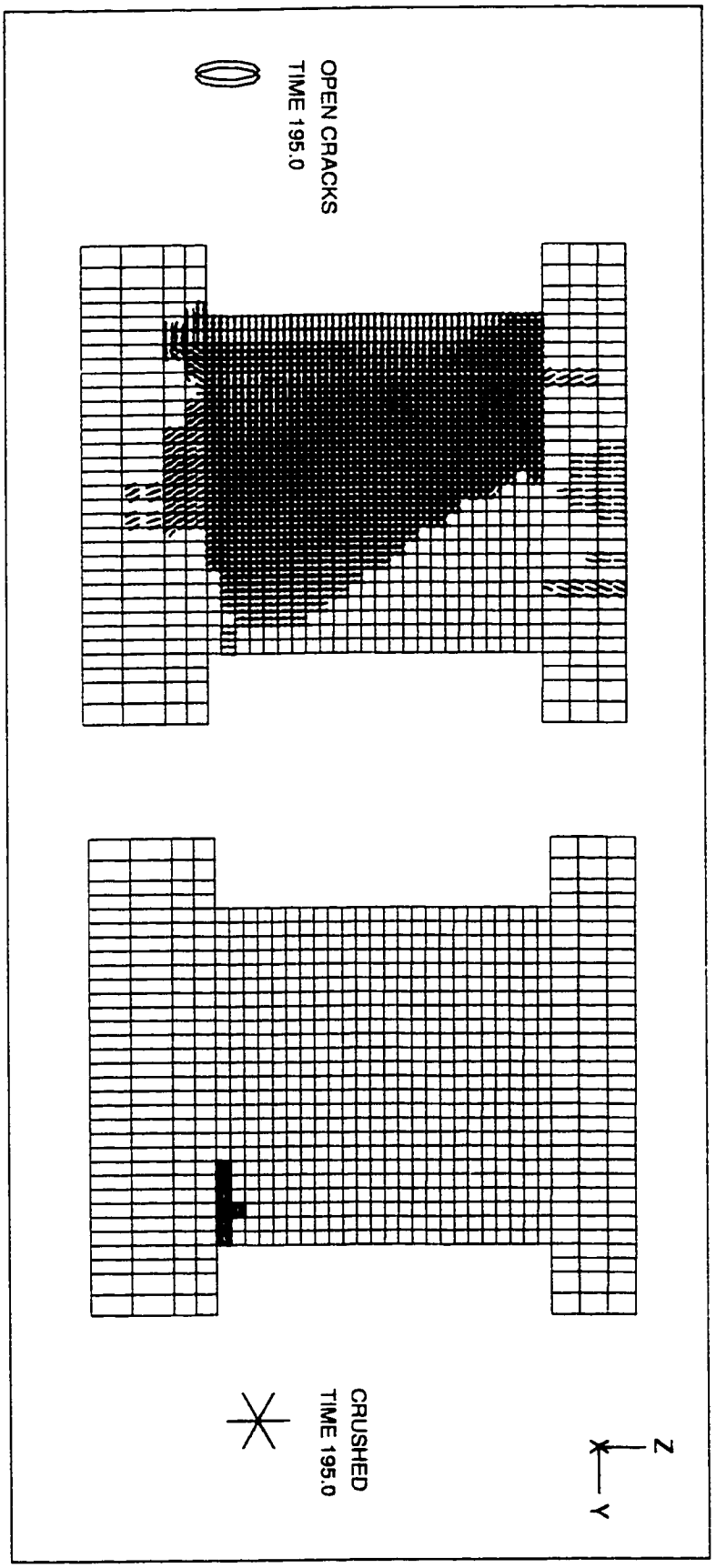

Fig. 5.56 Cracking and crushing pattern of shear wall N15

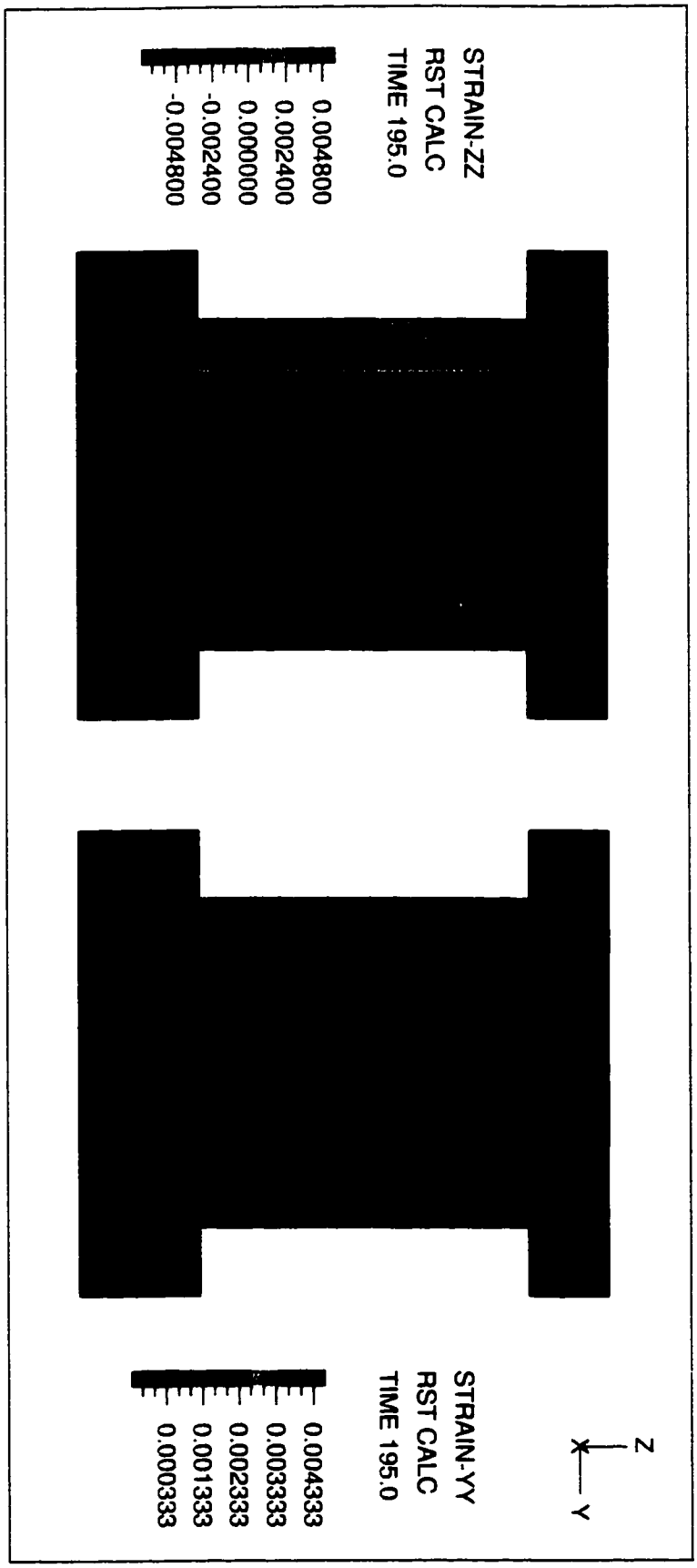

Fig. 5.57 Strain distribution of shear wall N15

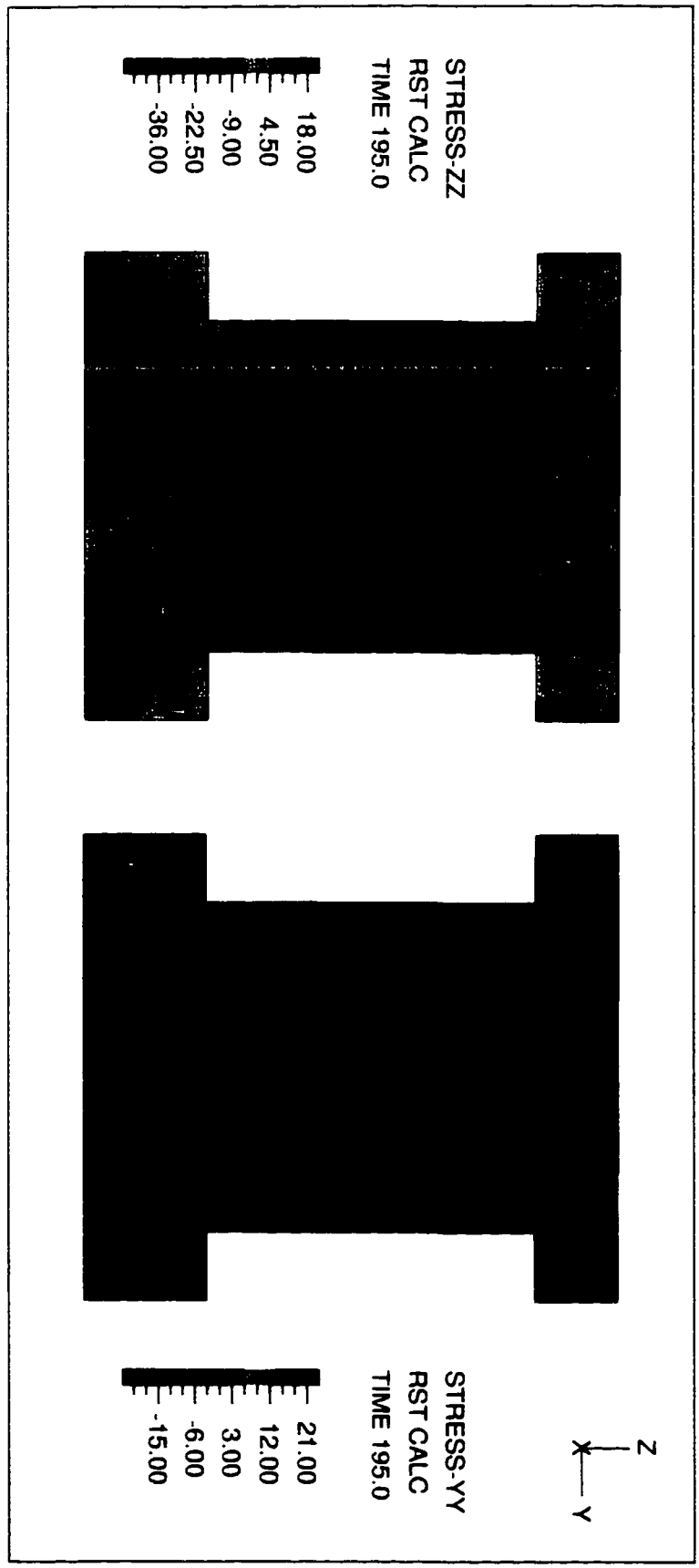

Fig. 5.58 Stress distribution of shear wall N15

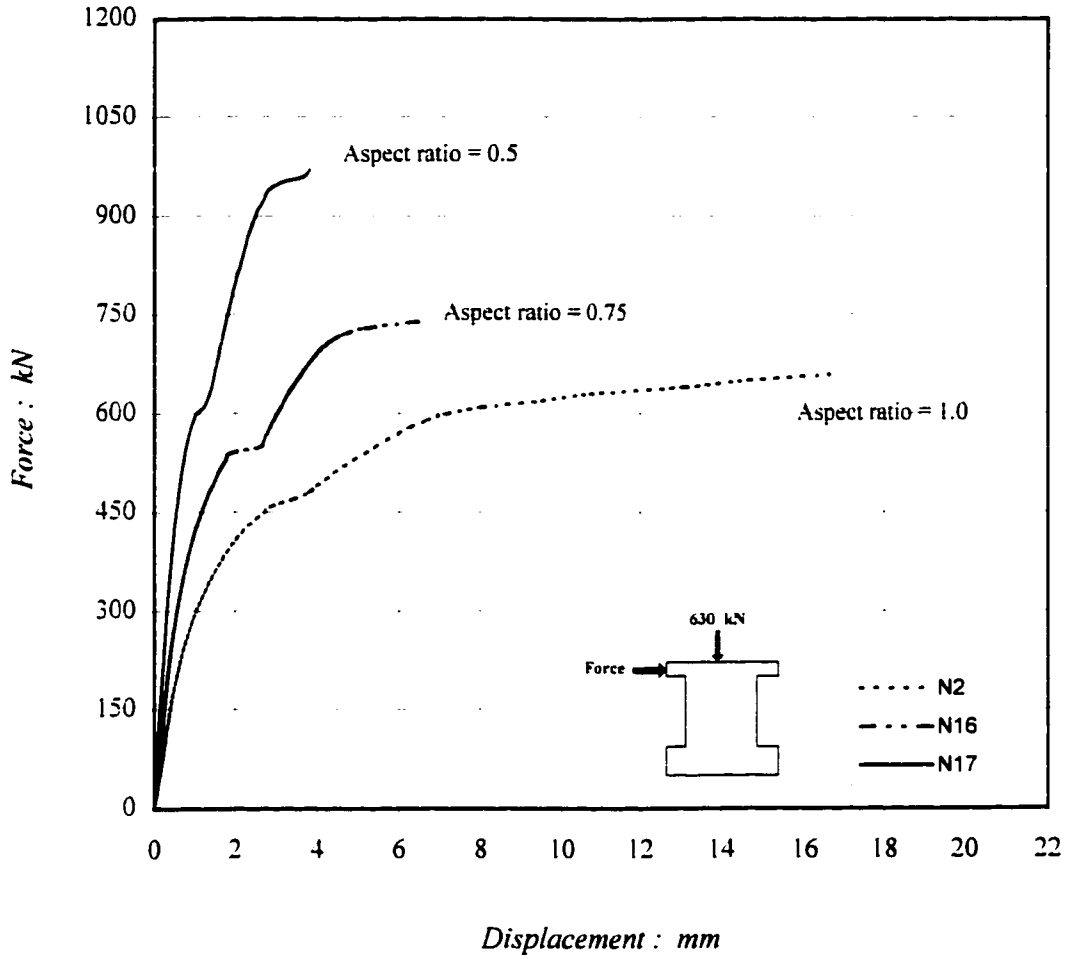

Fig. 5.59 Load-displacement response of shear walls N2, N16 and N17

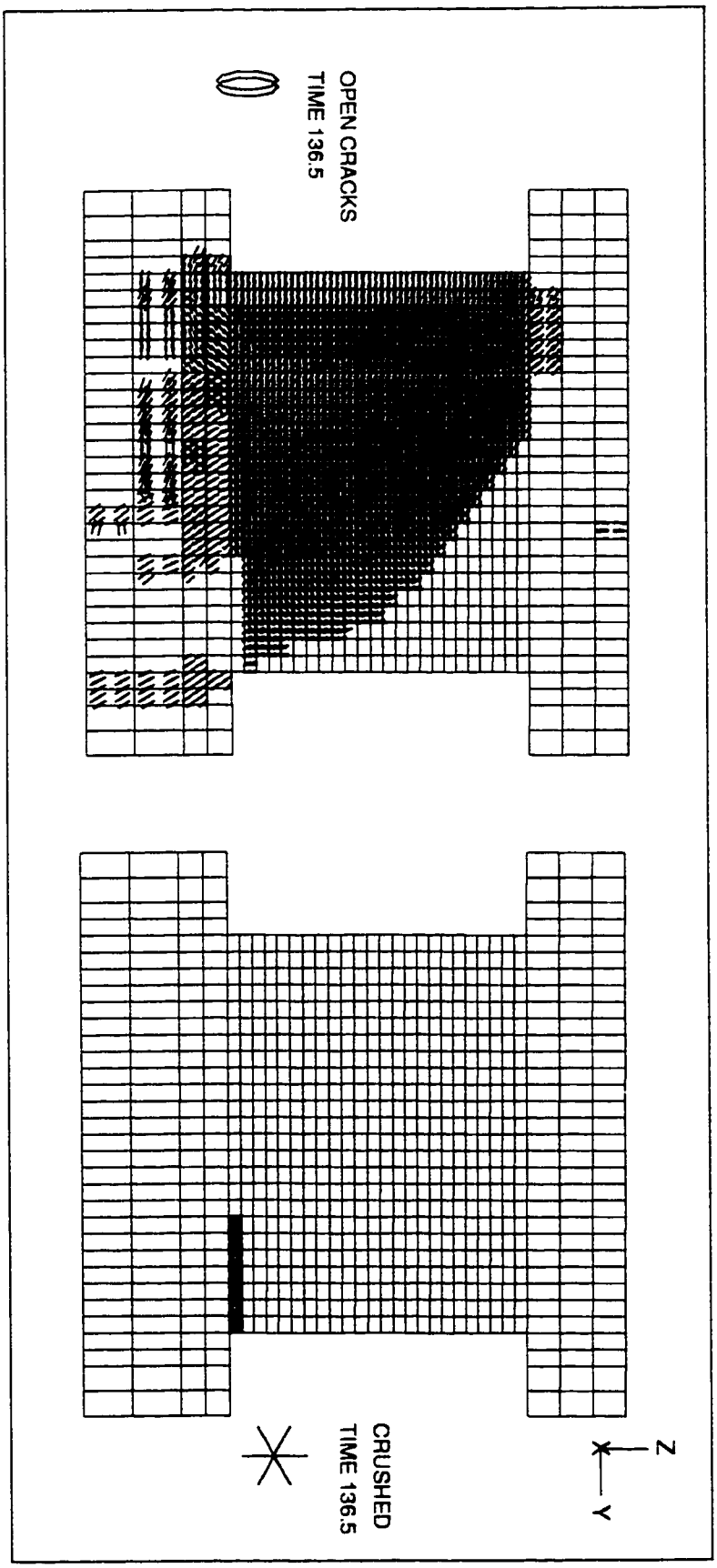

Fig. 5.60 Cracking and crushing pattern of shear wall N16

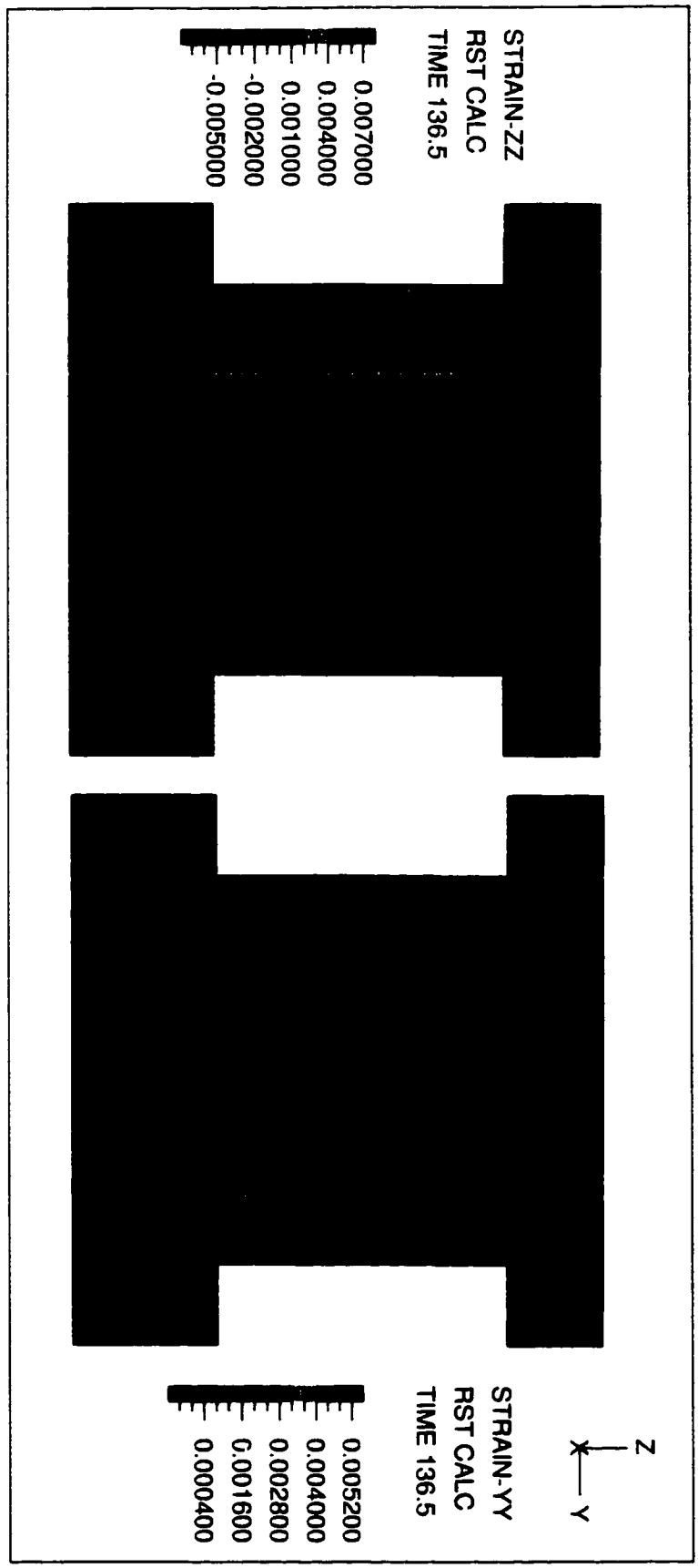

Fig. 5.61 Strain distribution of shear wall N16

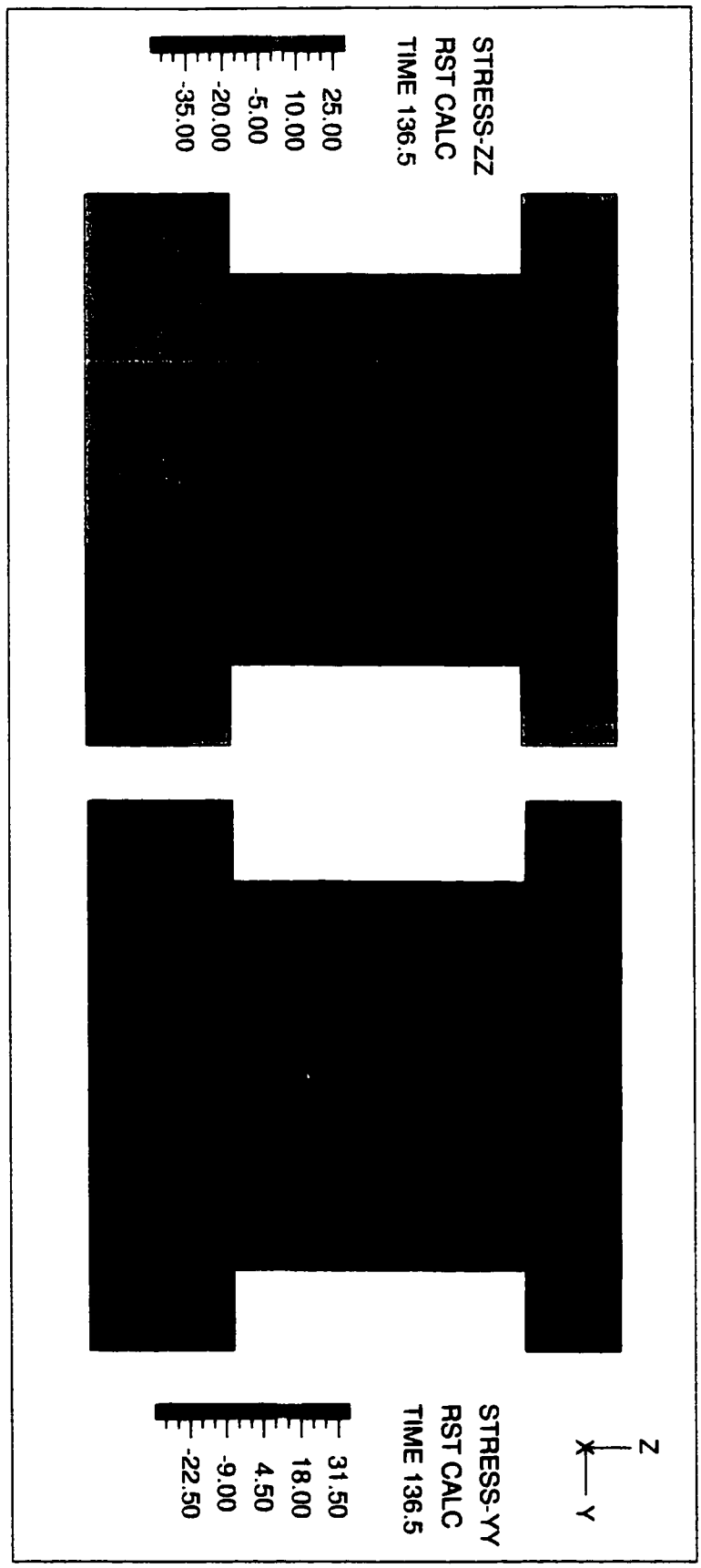

Fig. 5.62 Stress distribution of shear wall N16

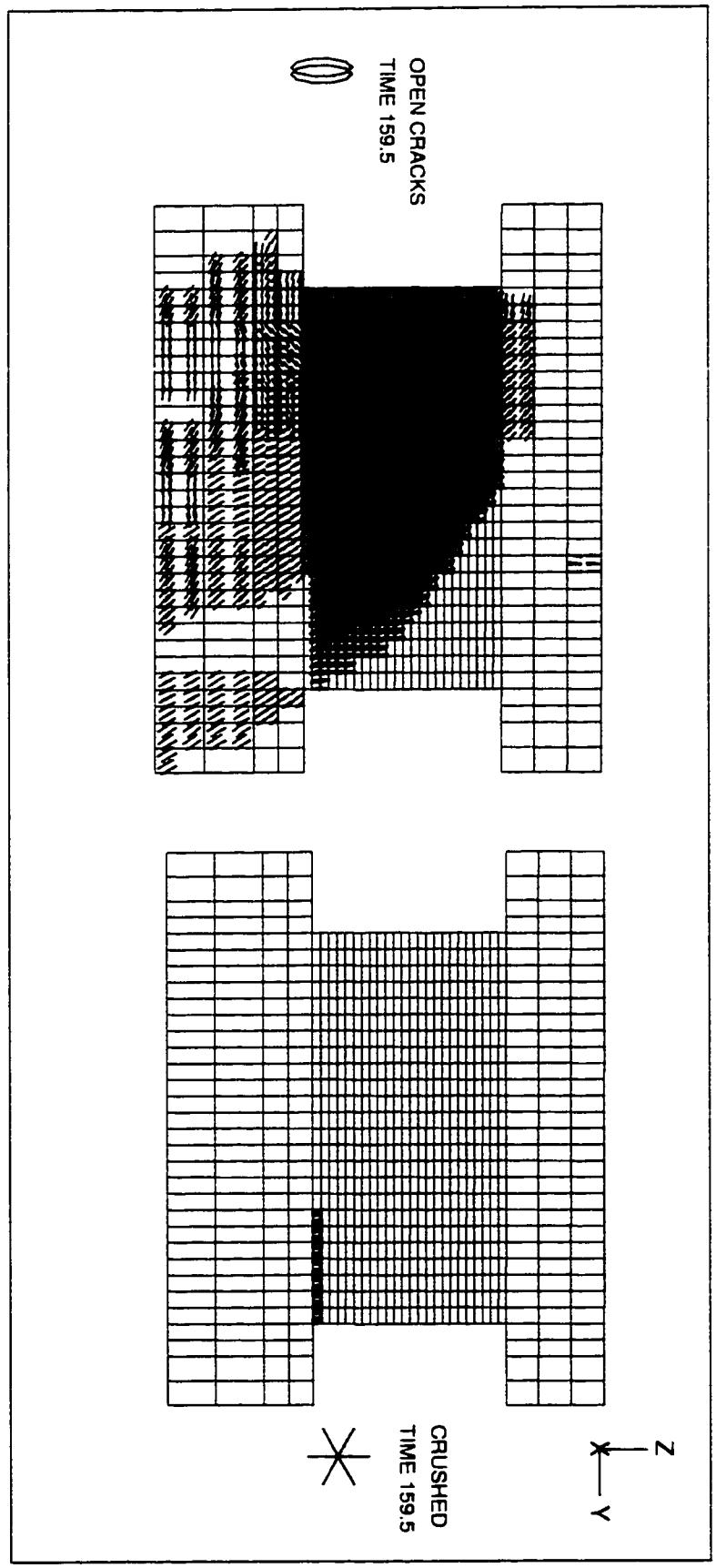

Fig. 5.63 Cracking and crushing pattern of shear wall N17

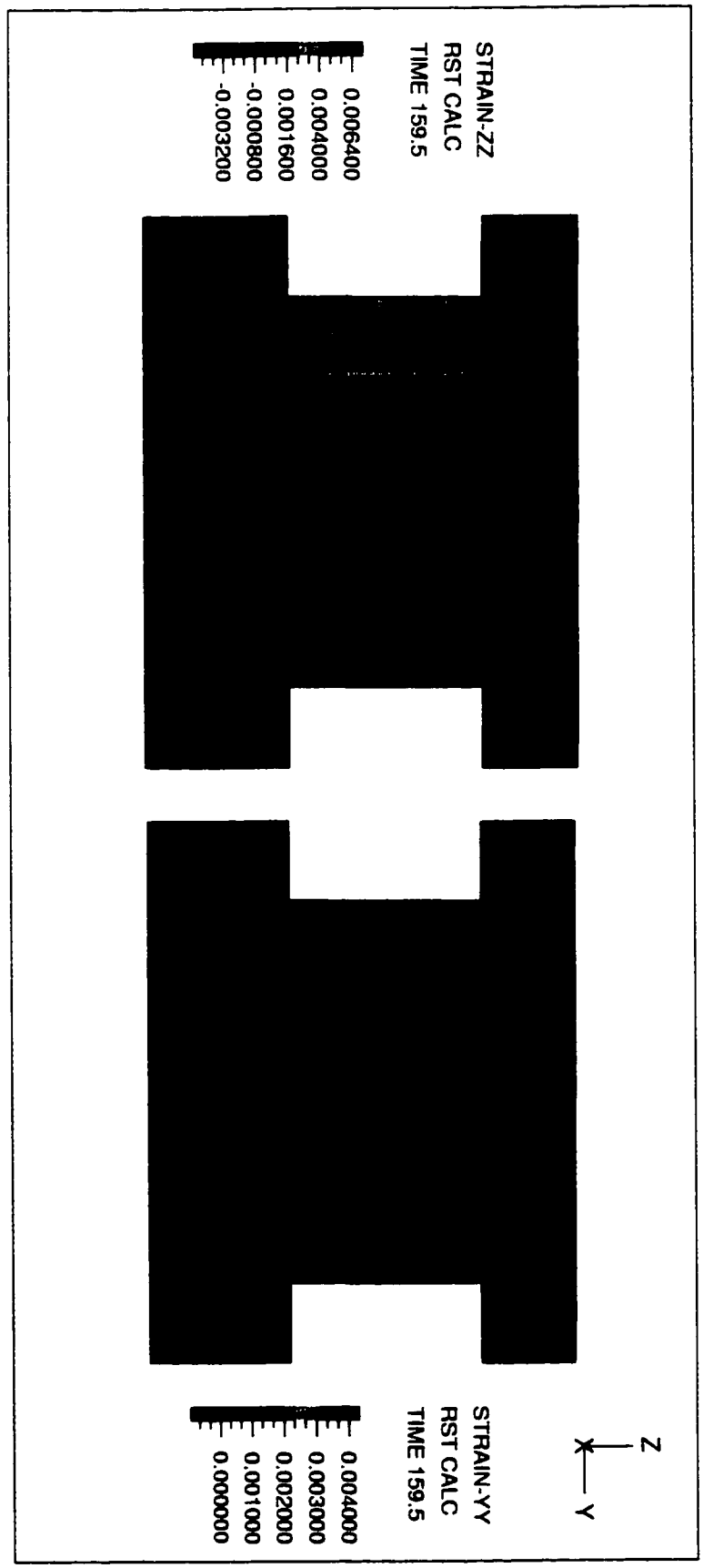

Fig. 5.64 Strain distribution of shear wall N17

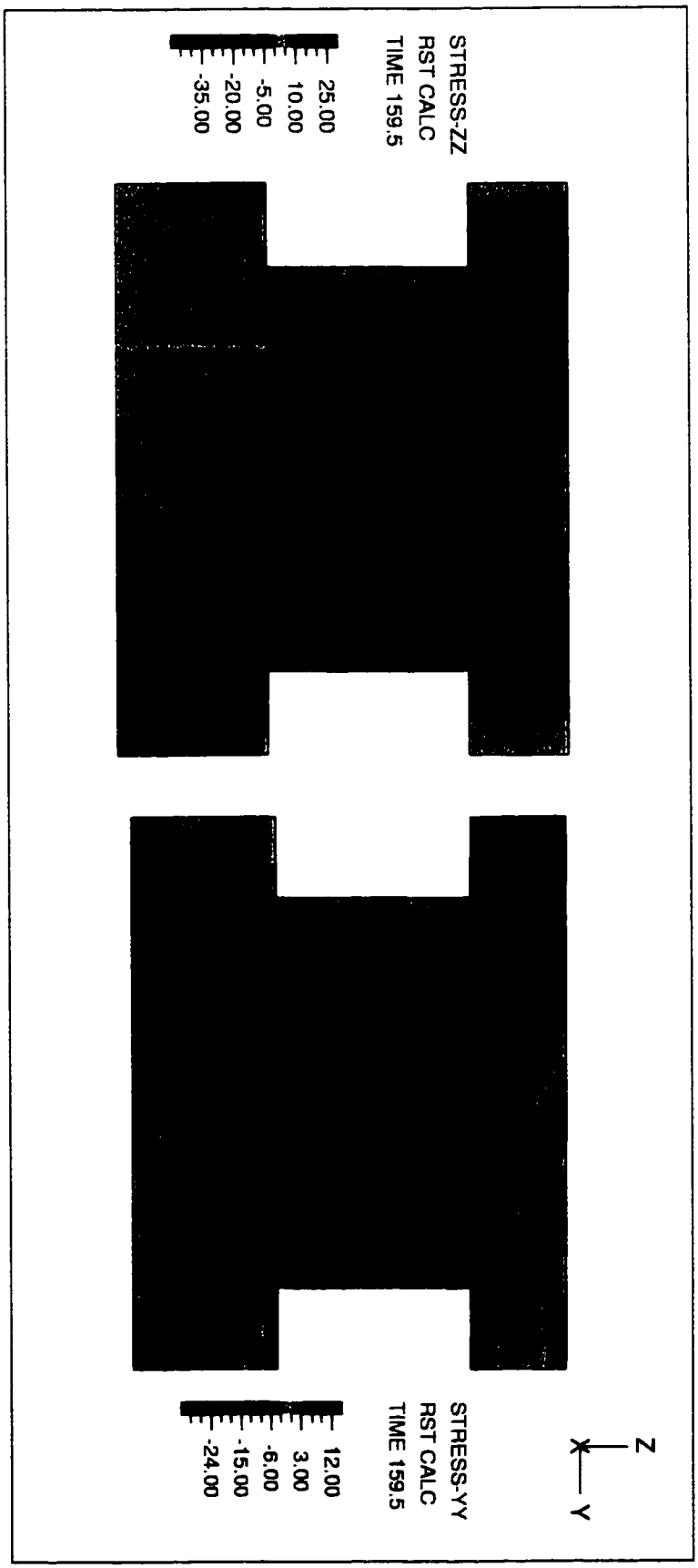

Fig. 5.65 Stress distribution of shear wall N17

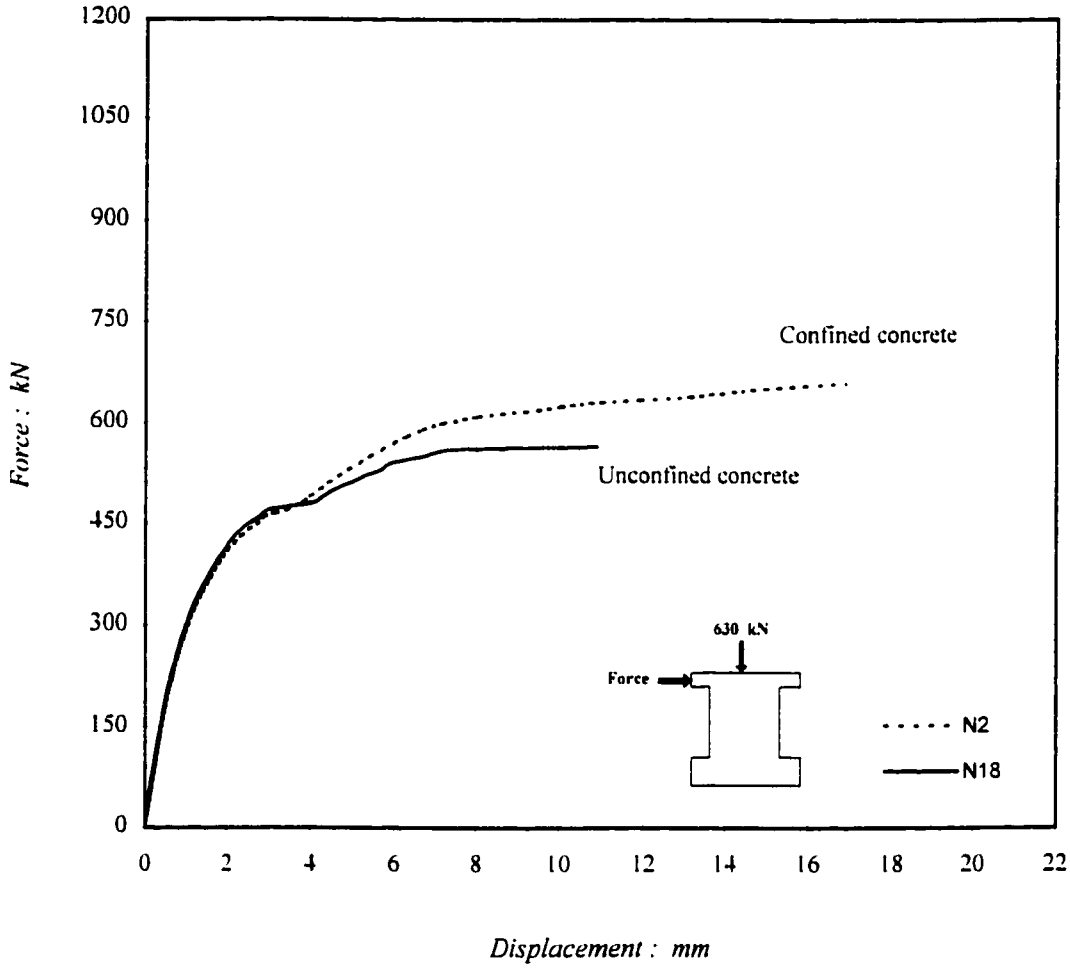

Fig. 5.66 Load-displacement response of shear walls N2 and N18

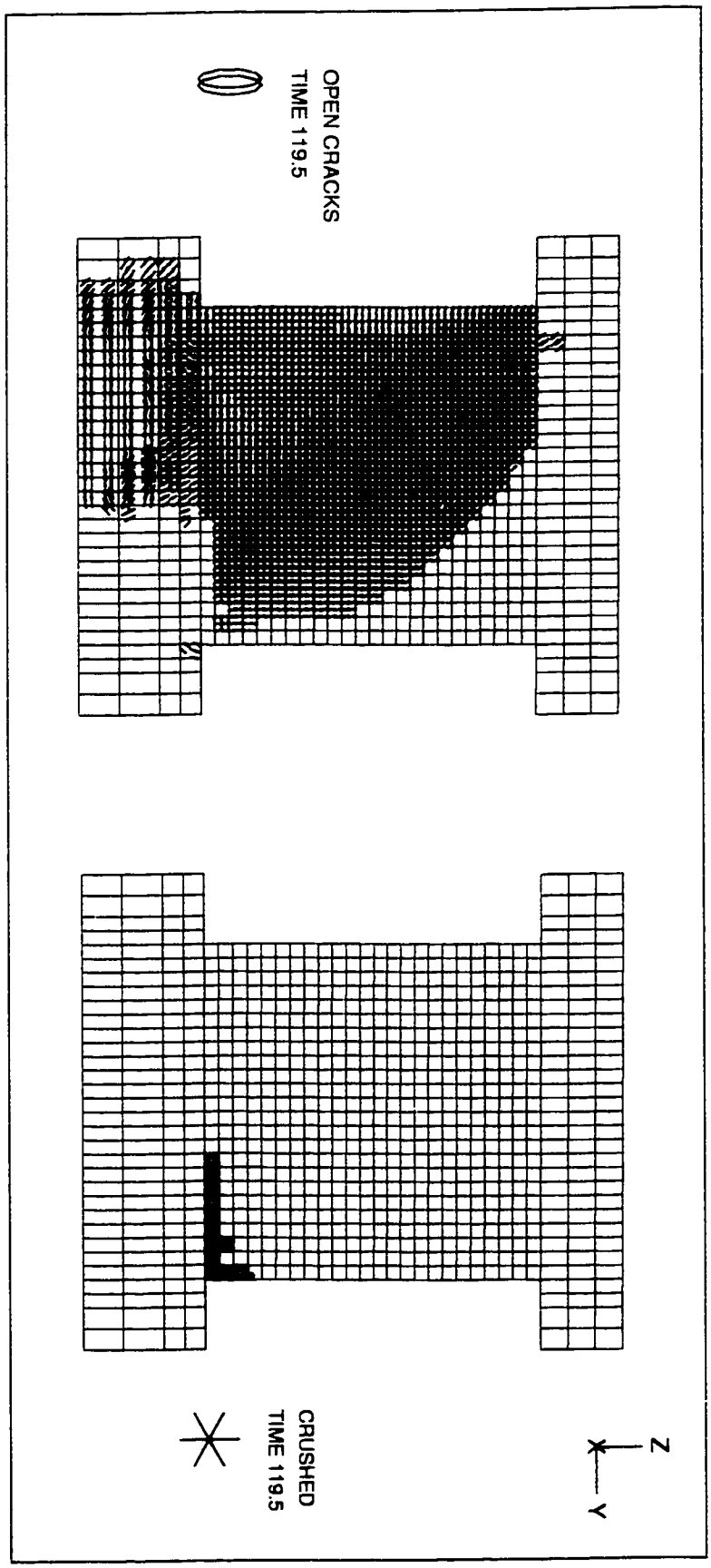

Fig. 5.67 Cracking and crushing pattern of shear wall N18

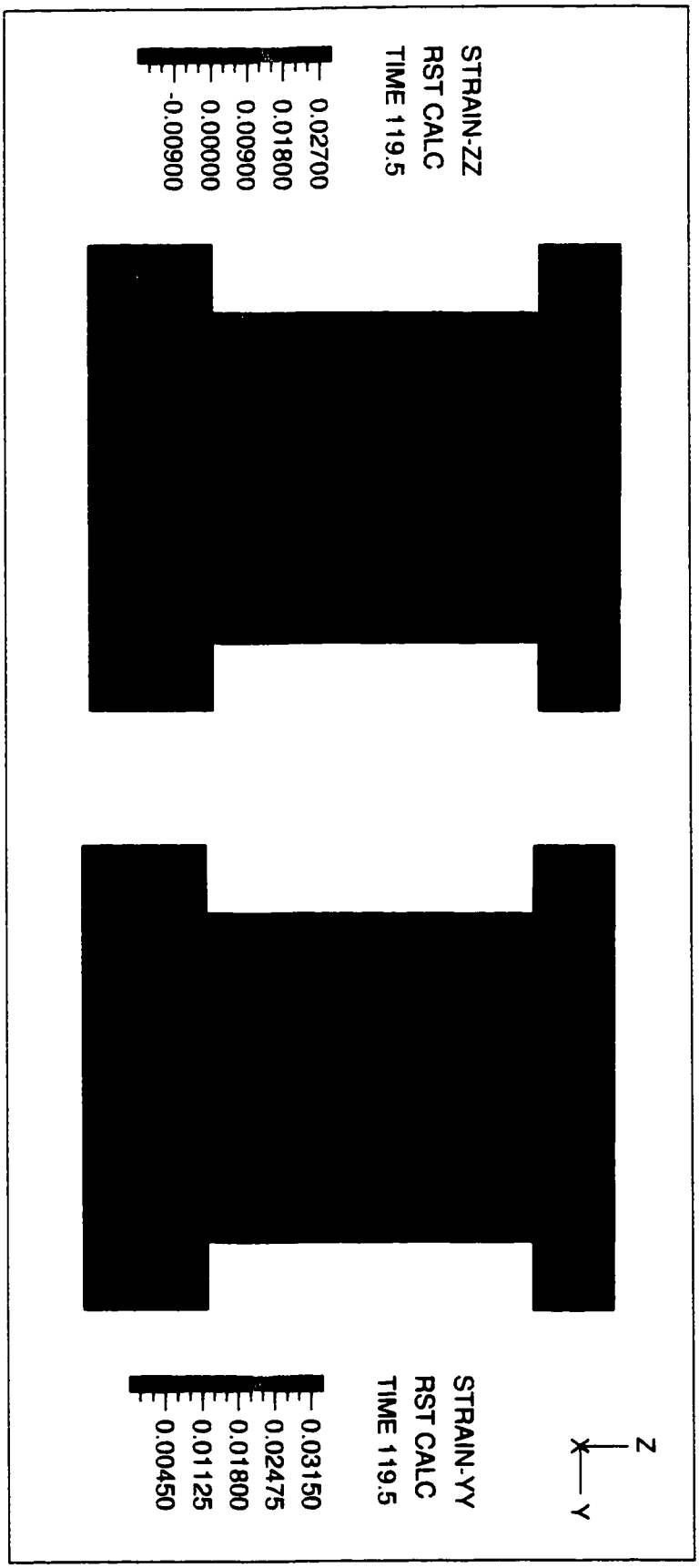

Fig. 5.68 Strain distribution of shear wall N18

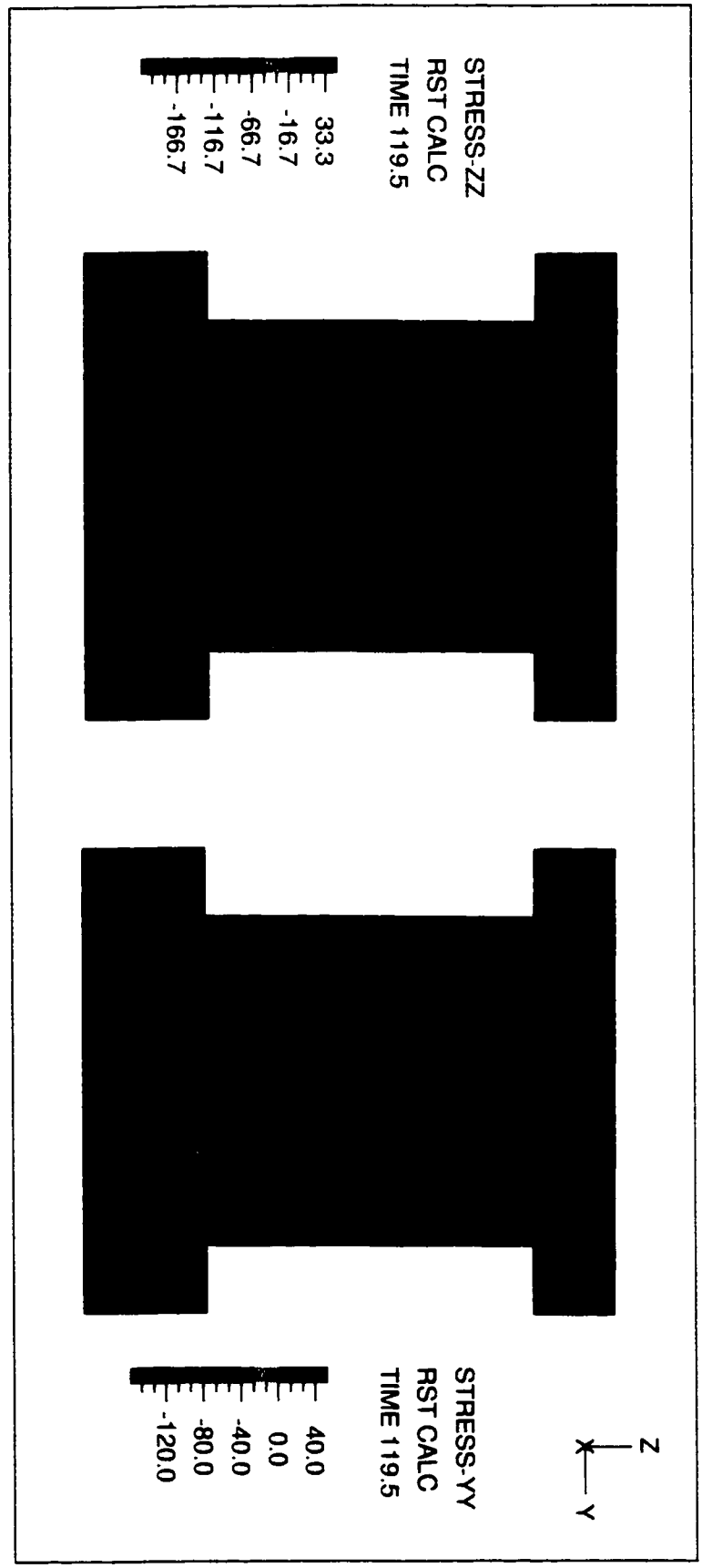

Fig. 5.69 Stress distribution of shear wall N18

Shear Wall	Hoop Spac. S (mm)	Normal Force F_v (kN)	Boundary ρ_{be}	Web ρ_{wx}	Web ρ_{wy}	Aspect Ratio h/l	Yield Str. f_y (MPa)	Compressive Str. f'_c (MPa)
N1	---	630	0.022	0.0056	0.0056	1	400	35
N2†	65	630	0.022	0.0056	0.0056	1	400	35
N3	130	630	0.022	0.0056	0.0056	1	400	35
N4	195	630	0.022	0.0056	0.0056	1	400	35
N5	65	630	0.011	0.0056	0.0056	1	400	35
N6	65	630	0.033	0.0056	0.0056	1	400	35
N7	65	630	0.022	0.0028	0.0056	1	400	35
N8	65	630	0.022	0.011	0.0056	1	400	35
N9	65	630	0.022	0.0056	0.0028	1	400	35
N10	65	630	0.022	0.0056	0.011	1	400	35
N11	65	630	0.022	0.0056	0.0056	1	400	50
N12	65	630	0.022	0.0056	0.0056	1	600	35
N13	65	630	0.022	0.0056	0.0056	1	800	35
N14	65	0	0.022	0.0056	0.0056	1	400	35
N15	65	1260	0.022	0.0056	0.0056	1	400	35
N16	65	630	0.022	0.0056	0.0056	0.75	400	35
N17	65	630	0.022	0.0056	0.0056	0.5	400	35
N18 *	65	630	0.022	0.0056	0.0056	1	400	35

† : Reference wall

* : Unconfined concrete material properties

Table 5.1 Specifications of shear walls N1 to N18

Shear Wall	Observed Failure	Ultimate Load (kN)	Ultimate Displ. (mm)
N1	Crushing of concrete started at 400 kN shear force and 3.2 mm top deflection. Yielding of reinforcement started at 330 kN shear force and 1.5 mm top deflection.	440	7.9
N2	Crushing of concrete started at 540 kN shear force and 5.1 mm top deflection. Yielding of reinforcement started at 450 kN shear force and 2.7 mm top deflection.	660	16.9
N3	Crushing of concrete started at 500 kN shear force and 4.2 mm top deflection. Yielding of reinforcement started at 450 kN shear force and 2.6 mm top deflection.	630	14.9
N4	Crushing of concrete started at 500 kN shear force and 4.2 mm top deflection. Yielding of reinforcement started at 450 kN shear force and 2.6 mm top deflection.	610	12.7
N5	Crushing of concrete started at 460 kN shear force and 5.0 mm top deflection. Yielding of reinforcement started at 360 kN shear force and 1.6 mm top deflection.	542.5	16.1
N6	Crushing of concrete started at 600 kN shear force and 5.3 mm top deflection. Yielding of reinforcement started at 540 kN shear force and 4.2 mm top deflection.	692.5	13.6

Table 5.2 The observed failure modes of shear walls N1 to N6

Shear Wall	Observed Failure	Ultimate Load (kN)	Ultimate Displ. (mm)
N7	Crushing of concrete started at 540 kN shear force and 5.5 mm top deflection. Yielding of reinforcement started at 450 kN shear force and 2.7 mm top deflection.	600	11.5
N8	Crushing of concrete started at 560 kN shear force and 5.2 mm top deflection. Yielding of reinforcement started at 450 kN shear force and 2.7 mm top deflection.	700	14.9
N9	Crushing of concrete started at 520 kN shear force and 5.4 mm top deflection. Yielding of reinforcement started at 430 kN shear force and 2.4 mm top deflection.	647.5	18.5
N10	Crushing of concrete started at 580 kN shear force and 5.0 mm top deflection. Yielding of reinforcement started at 480 kN shear force and 3.1 mm top deflection.	701.25	15.3
N11	Crushing of concrete started at 560 kN shear force and 5.2 mm top deflection. Yielding of reinforcement started at 460 kN shear force and 2.7 mm top deflection.	750	20.5
N12	Crushing of concrete started at 580 kN shear force and 5.4 mm top deflection. Yielding of reinforcement started at 590 kN shear force and 5.5 mm top deflection.	731.25	14.3

Table 5.2 The observed failure modes of shear walls N7 to N12

Shear Wall	Observed Failure	Ultimate Load (kN)	Ultimate Displ. (mm)
N13	Crushing of concrete started at 600 kN shear force and 5.7 mm top deflection. Yielding of reinforcement started at 680 kN shear force and 7.0 mm top deflection.	770	13.4
N14	Crushing of concrete started at 290 kN shear force and 3.5 mm top deflection. Yielding of reinforcement started at 220 kN shear force and 1.8 mm top deflection.	555	18.9
N15	Crushing of concrete started at 640 kN shear force and 4.2 mm top deflection. Yielding of reinforcement started at 650 kN shear force and 4.4 mm top deflection.	690	6.1
N16	Crushing of concrete started at 620 kN shear force and 3.2 mm top deflection. Yielding of reinforcement started at 600 kN shear force and 3.0 mm top deflection.	740	6.5
N17	Crushing of concrete started at 800 kN shear force and 2.0 mm top deflection. Yielding of reinforcement started at 800 kN shear force and 2.0 mm top deflection.	970	3.8
N18	Crushing of concrete started at 460 kN shear force and 2.8 mm top deflection. Yielding of reinforcement started at 450 kN shear force and 2.5 mm top deflection.	565	10.9

Table 5.2 The observed failure modes of shear walls N13 to N18

Chapter 6

Discussion and conclusion

6.1 General

The output obtained from the finite element program ADINA contains a variety of results expressed in terms of nodal and element characteristics. The program includes the capability of displaying the results in a graphical manner, including crack patterns, and stress and strain distributions, as illustrated in the previous chapter. The finite element analysis provides an inexpensive way of investigating the behavior of shear walls with different configurations, enabling parametric investigation. Such a parametric investigation forms part of the scope of this thesis. The results of the parametric study are presented in Chapter 5 for the 18 cases considered. The following are the conclusions drawn from this investigation, which are based on analyses of walls with an aspect ratio of 1.0.

1) Finite element analysis conducted by program ADINA provides a good correlation of non-linear force-displacement relationship of low-rise shear walls relative to

experimentally obtained results. However, inelastic modeling remains to be a crucial aspect of finite element analysis, especially in terms of material modeling.

2) The effect of boundary elements is to increase strength and ductility of walls. Shear wall N2, with boundary elements showed ductile response. When the boundary elements were not provided, as in shear wall N1, the wall resisted 33% lower force, developing 53% lower displacement ductility. These results underline the importance of boundary elements in dissipating inelastic energy.

3) The effect of hoop spacing in boundary elements is to confine concrete. Increasing the hoop spacing from 65 mm in shear wall N2 to 130 mm in shear wall N3 resulted in 5% and 12% reductions in lateral load resistance and displacement ductility ratio, respectively. Further increase in hoop spacing to 195 mm in shear wall N4 produced further decreases in force and ductility capacities of 8% and 25%, respectively. However, this parameter did not play a significant role on the overall behavior, possibly because of the low wall aspect ratio of 1.0, which promoted shear dominant response.

4) The ratio of longitudinal reinforcement in boundary elements produces effects on both wall strength and ductility. When the reinforcement ratio was reduced to 1.1% in shear wall N5, relative to wall N2 with 2.2% reinforcement ratio, the load carrying capacity decreased to 82%, and the ductility ratio decreased to 95%. When shear wall N6 was analyzed with a higher reinforcement ratio of 3.3%, the load resistance improved by 5%. However, the ductility decreased by 19%, possibly because of increased shear force and its effect on the web, in terms of reduced deformability.

5) The effect of horizontal web reinforcement in walls with an aspect ratio of 1.0 may be insignificant. Shear walls N7 and N8 had 0.28% and 1.1% horizontal reinforcement ratios in the web, respectively. Shear wall N7 failed with 9% lower lateral load

capacity and 32% lower top displacement. Shear wall N8, however, resisted 6% more shear force with 12% lower top displacement, compared to the reference shear wall N2. These results indicate that even when the horizontal reinforcement ratio was increased by a factor of 2.0, as in shear wall N8, the load capacity was increased only by 6%. Therefore, it is concluded that the horizontal reinforcing ratio does not play an important role in the load carrying capacity of low-rise shear walls.

6) The influence of vertical reinforcement ratio in the web was studied in shear walls N9 and N10. Shear wall N9, with a vertical web reinforcement ratio of 0.28%, which corresponded to one half of the reinforcement in wall N2, showed only a 2% reduction in load capacity, while the ductility ratio increased by about 9%. Shear wall N10 with a higher reinforcement ratio of 1.1% was able to resist only 6% higher load with an accompanying reduction of 9% in displacement ductility. It should be noted, however, that all of these walls had boundary elements, which dominated flexural behavior. Therefore, the relatively small effect of vertical web reinforcement on wall response is understandable. Although only limited analyses were carried out in this research, it can be concluded that the vertical reinforcement ratio did not have an important impact on wall response.

7) The sensitivity of wall response to concrete strength was studied in shear wall N11. When the compressive strength of concrete was increased by 43%, relative to wall N2 (from 35 MPa to 50 MPa) the ultimate load capacity was increased by 14%. The corresponding top displacement was also increased by 21%. This limited comparison indicated that the compressive strength of concrete could have significant impact on strength and ductility of low-rise shear walls.

8) The yield strength of reinforcing steel has considerable influence on ultimate capacity of low-rise shear walls. Shear wall N12, with 600 MPa reinforcing steel, resisted 11% higher shear force than the reference shear wall with 400 MPa reinforcement. On the other hand, top displacement was reduced by 16 % when higher-grade steel was used.

Further increase in steel grade showed a continued trend. Shear wall N13, with 800 MPa grade reinforcement, failed after 17% increase in ultimate load capacity, but developed 21% lower ductility. It may therefore be concluded that the effect of increased steel grade is to improve load resistance, but reduce wall deformability.

9) The axial load has a substantial effect on force-displacement characteristics of low-rise shear walls. Under zero axial load the tensile cracks form at a low force level, accompanied by reduced strength, contrary to wall N15 with high level of axial load (1260 kN), where the wall capacity was increased by about 5% with a 64% reduction in deformability. In the latter case (N15) the excessive compressive stress caused crushing of concrete in a brittle manner. In the former case (N14) the load resistance dropped by 16% while the deflection increased by 12%, as compared to the reference shear wall N2 with 630 kN of axial force. It may then be concluded that the effect of axial compression is to increase strength but decrease wall ductility very substantially.

10) Wall aspect ratio plays an important role on ductility. When the aspect ratio decreased from 1.0 to 0.75, as in the case of N16, the lateral force resistance increased by about 12% though the displacement capacity decreased by 62%. Further reduction in the aspect ratio to 0.5, as in the case of wall N17, resulted in a 47% increase in lateral load capacity. However, the reduction in deformability was drastic, showing 78% decrease in displacement ductility ratio, relative to shear wall N2 with an aspect ratio of 1.0.

11) The effect of concrete confinement is to increase strength and deformability of walls. When concrete confinement was ignored in the boundary elements of shear wall N18, the reductions in strength and ductility were 14% and 36%, respectively, relative to the reference shear wall N2.

References

[1] Barda, F., Hanson J. M., and Corley, W. G., 'Shear Strength of Low-Rise Walls with Boundary Elements', Reinforced Concrete Structures in Seismic Zones, Publication SP-53, American Concrete Institute, Detroit, 1977, pp. 149-202.

[2] Bathe, K. J., and Cimento, A. P., 'Some Practical Procedure for the Solution of Nonlinear Finite Element Equations', Computer Methods in Applied Mechanics and Engineering, 1980, Vol. 22, pp. 59-85.

[3] Bathe, K. J., Finite Element Procedures, Prentice-Hall, 1982.

[4] Bazant, Z. P., and Bhat, P. D., 'Endochronic theory of Inelasticity and Failure of Concrete', Journal of the Engineering Mechanics Division, ASCE, Vol. 102, No. EM4, Proceeding Paper 12360, August 1976, pp. 701-721.

[5] Bazant, Z. P., and Kim, S. S., 'Plastic-Fracturing Theory of Concrete', Journal of the Engineering Mechanics Division, ASCE, Vol. 105, No. EM3, Proceeding Paper 14653, June 1979, pp. 407-428.

[6] Bremer, H. H. J., 'Seismic Analysis of a Shear Wall', Technical Report 96-NM-R0984, TNO Building and Construction Research, Rijswijk, 1996.

[7] Canadian Portland Cement Association, CSA Standard A23.3-94, Concrete Design Handbook, August 1995, Ottawa, Ontario, Canada.

[8] Cardenas, A. E., Hanson, J. M., Corley, W. G., and Hognestead E., 'Design Provisions for Shear Walls', ACI Journal, Proceedings, Vol. 70, March 1973, pp. 221-230

[9] Carreina, D. J. and Chu, K. H., ' Stress-Strain Relationship for Plain Concrete in Compression', ACI Journal, 82(6), 1985, pp. 797-804.

[10] Cervenka, V. and Gerstle, K. H., 'Inelastic Analysis of Reinforced Concrete Panels', IABSE Publications, V. 31-11, Zurich, 1971.

[11] Chen, A. C. T. and Chen, W. F., ' Constitutive Relations for Concrete', Journal of the Engineering Mechanics Division, ASCE, Vol. 101, No. EM4, August 1975, pp. 465-481.

[12] Chen, W. F., ' Concrete Plasticity: Macro and Micro Approaches', 1992, Structural Engineering Report, No. CE-STR-92-25, School of Civil Engineering, Purdue University, West Lafayette, IN, 63 pp.

[13] Chen, W. F. and Cohen, M. D., ' Micromechanical Consideration in Concrete Constitutive Modeling', 1992, Proceeding of 10th ASCE Structures Congress, San Antonio, TX, J. Morgan, Ed., May 13-15, 1992, pp. 270-273.

[14] 'Command Reference Manual', Volume I: ADINA Model Definition, and 'Theory and Modeling Guide', Volume I: ADINA, Report ARD 97-2, September 1997.

[15] Crisfield, M. A., 'A Fast Incremental/Iterative Solution Procedure That Handels "Snap-Through" ', Computer & Structures Journal, Vol. 13, pp. 55-62.

[16] Darwin, D. and Pecknold, D. A. W., 'Inelastic Model for Cyclic Biaxial Loading of Reinforced Concrete', University of Illinois at Urbana-Champaign, SRS No. 409, Urbana, Illinois, 1974.

[17] 'Finite Element Analyses for Seismic Shear Wall, International Standard Problem', By Y.J. Park and C. H. Hofmayer, Department of Advanced Technology, Brookhaven National Laboratory, April 1998.

[18] Franklin, H. A., 'Nonlinear Analysis of Reinforced Concrete Frames and Panels', Ph.D. Thesis, University of California, Berkeley, California, March 1970.

[19] Hasegawa T., Kumagai H., Irino K., Rots J. G., Feenstra P. H., 'Seismic Analysis of RC Shear Wall', Transactions of the 14th International Conference on Structural Mechanics in reactor Technology (SMiRT 14), Lyon, France, August 17-22, 1997.

[20] Khatri, D. and Anderson, J. C., 'Analysis of Reinforced Concrete Shear Wall Components Using the ADINA Nonlinear Concrete Model', Computers & Structures, Vol. 56, No. 2/3, 1995, pp. 485-504.

[21] Kupfer. H. B. and Gerstle, K. H., 'Behavior of Concrete under Biaxial Stresses', ASCE, Journal of the Engineering Mechanics Division, Vol. 99, No. EM4, August 1973, pp. 852-866.

[22] Kwak, H. G. and Filippou, F., 'Nonlinear FE Analysis of R/C Structures Under Monotonic Loads', Computers and Structures, Vol. 65, No. 1, 1997, pp. 1-16.

[23] Lefas, I. D., Kotsovos, M. D., and Ambraseys, N. N., 'Behavior of reinforced concrete structural walls: Strength, Deformation Characteristics and Failure Mechanism', ACI Journal, Vol. 87, No.1, 1990, pp. 23-31.

[24] Machida A. and Mutsuyoshi H., ' Evaluation of Ductility of R/C Members and Influence of Ductility on Inelastic Response Behavior of R/C Frame Structure', International Workshop on Concrete Shear in Earthquake, University of Houston, Texas, 13-16 January 1991.

[25] Maier, J., 'Shear Wall Tests', The Swiss Federal Institute of Technology, Zurich, Switzerland.

[26] Mehta P. K., and Monteiro P. J. M., 'Concrete: Structure, Properties, and Materials', Prentice-Hall, 1993.

[27] Mirza, M. S., and Houde, J., 'Study of Bond Stress-Slip Relationship in Reinforced Concrete', ACI Journal, Proceedings, Vol. 76, No. 1, January 1979, pp. 19-46.

[28] Mohammadi-Doostdar, H., 'Behavior and Design of Earthquake Resistant Low-rise Shear Walls', Ph.D. Thesis, Department of Civil Engineering, University of Ottawa, 1994.

[29] Monti, G. and Filippou, F., 'Finite Element for Anchored Bars under Cyclic Load Reversal', Journal of Structural Engineering, ASCE, Vol. 123, No. 5, May 1997.

[30] Ngo, D., and Scordelis, A. C., 'Finite Element Analysis of Reinforced Concrete Beams', ACI Journal, Vol. 64, No. 3, March 1967, pp. 152-163.

[31] Nilson, A. H., 'Nonlinear Analysis of Reinforced Concrete by the Finite Element Method', ACI Journal, Vol. 65, No. 9, September 1968, pp. 757-766.

[32] Nilson, A. H. and Winter, G., Design of Concrete structures, Tenth edition, McGraw-Hill, 1986.

[33] Park, R. and Paulay, T., 'Reinforced Concrete Structures', John Wiley, NY, 1975.

[34] Paulay, T., Priestley, M. J. N., and Synge, A. J., 'Ductility in Earthquake Resistant Squat Shear Walls', Journal ACI, No. 79-26, July-August 1982, pp. 257-269.

[35] Pilette, C. F., 'Behavior of Earthquake Resistant Squat Shear Wall', M. A. Sc. Thesis, Department of Civil Engineering, University of Ottawa, 1987.

[36] Popovics, S., ' A Numerical Approach to the Complete Stress-Strain Curve of Concrete', Cement Concrete Research, 3(5), 1973, pp. 583-599.

[37] Rashid, Y. R., 'Analysis of Prestressed Concrete Pressure Vesseles', Nuclear Engineering and desighn, Vol. 7, No. 4, April 1968, pp. 334-344.

[38] Saatcioglu, M., 'Hysteretic Shear Response of Low-Rise Walls', The International Workshop on Concrete Shear in Earthquake, University of Houston, January 14-16, 1991.

[39] Saatcioglu, M., and Razvi, S. R., 'Strength and Ductility of Confined Concrete', Journal of Structural Engineering, Vol. 118, No. 6, June 1992.

[40] Saenz, L. P., Discussion of ' Equation for the Stress-Strain Curve of Concrete' by P. Desai and S. Krishman, ACI Journal, 61(9) ,1964, pp. 1229-1235.

[41] Sittipunt, C. and Wood, S. L., 'Finite Element Analysis of Reinforced Concrete Shear Walls', Department of Civil Engineering, University of Illinois at Urbana-Champain, Urbana, Illinois, December 1993.

[42] Specification Report of Seismic Shear Wall ISP on NUPEC's Seismic Ultimate Dynamic Response Test. Committee on the safety of Nuclear Installations, Nuclear Power Engineering Corporation. Nr. NU-SSWISP-D009. Japan. 1994.

[43] Taghdi, M., 'Seismic Retrofit of low-rise Masonry and Concrete Walls by Steel Strips', Ph.D. Thesis, Department of Civil Engineering, University of Ottawa, 1998.

[44] Users Guide, ADINA User Interface, Report ARD 97-1, November 1997.

[45] Vecchio, F. J., and Collins, M. P., (1986), ' The Modified Compression Field Theory for Reinforced Concrete Element Subjected to Shear', J. of the Amer. Conc. Inst., Vol. 83, No. 2, pp. 219-231.

[46] Wasiewicz, Z., 'Sliding Shear in Squat Shear Wall', M.A.Sc. Thesis, Department of Civil Engineering, University of Ottawa, 1987.

[47] Working Group on Stiffness of Concrete Shear Wall Structures, 'Stiffness of Low Rise Reinforced Concrete Shear Wall', American Society of Civil Engineers, 1994.

[48] Yuzugullu, D., 'Finite Element Approach for the Prediction of Inelastic Behavior of Shear Wall-Frame System', Ph.D. Dissertation, Department of Civil Engineering, University of Illinois at Urbana-Champain, Urbana, Illinois, 1972.